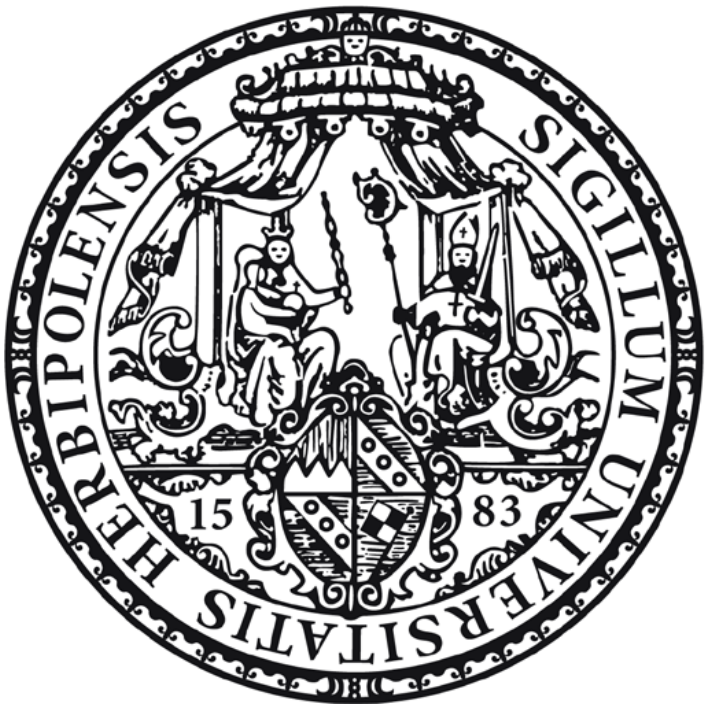

TPC1 mutants provide insight into SV channel function

(TPC1-Mutanten geben Einblick in die SV-Kanalfunktion)

Dissertation on the attainment of a doctorate in natural sciences
Julius-Maximilians-Universität Würzburg,
submitted by

DAWID ARTUR JAŚLAN

from

Ostrowiec Świętokrzyski

Würzburg 2017

Submitted on: ……..……..

Office stamp

Members of the *Promotions committee*:

Chairperson: ……..…...

Primary referee: Prof. Dr. Rainer Hedrich

Second referee: Prof. Dr. Erhard Wischmeyer

Date of Public Defence: ……

Date of Receipt of Certificates: …….

“ If you can’t explain it simply, you don’t understand it well enough”

Albert Einstein

Table of content

1. Introduction

1.1. Plant vacuole - subcellular compartment with multiple functions

Plant vacuoles are important, subcellular organelles playing a role in many physiological processes, which are fulfilled by two types of them: lytic vacuoles (LV) and protein storage vacuoles (PSV) (Fig. 1). The inherence of distinct types of vacuoles with different cellular functions in one cell is easily observed in plant seeds (Robinson et al., 2005). LVs and PSVs can be distinguished via the presence of certain soluble proteins in the vacuolar lumen and tonoplast intrinsic proteins (TIPs) in the membrane (Martinoia et al., 2006). Often PSVs primarily contain α-TIPs. δ-TIP are additionally localized in the tonoplast when seed-type storage proteins are accumulated in the vacuolar lumen (Jauh et al., 1999; Frigerio et al., 2008). Instead, δ-TIP and γ-TIP are localized in the vacuolar membrane when pigments and vegetative storage proteins are directed to this compartment (Martinoia et al., 2006). As the name “PSV” already implies, the major function of PSV relates to the storage of proteins in vegetative tissues and seeds (Herman et al., 1999; Jauh et al., 1999; Frigerio et al., 2008). For example, PSVs appearing in seeds contain protein complexes in crystalline form and salt complexes as phytates. Storage proteins and minerals are consumed by the developing plant embryo during the process of seed germination (Otegui et al., 2002). Potassium, calcium and phosphoric ions are released from the phytate salts and distributed in the embryo, whereas reduced carbon and nitrogen compounds are provided to the embryo upon starch and protein metabolism (Loewus and Murthy., 2000; Yan et al., 2014)

LVs harbour particularly γ-TIPs in the membrane and fill up to 90% of the volume of mature cells (Martinoia et al., 2012). LVs are the plant equivalents of animal lysosomes and vacuoles in yeasts. They share an acidic environment and contain many hydrolases for degradation of different cellular substances. Depending on the cell type, organ and developmental stage, lytic vacuoles play distinct roles. They control turgor pressure determining cell stiffness important for the general cell shape, plant growth and development. Vacuoles are involved in cell homoeostasis, stress response, pathogen defence and detoxification by degrading cellular substances and accumulating not only ions, primary and secondary metabolites but also xenobiotics or toxic substances (Echeverria et al., 1989). Carbohydrates and proteins as well

as ions and nutrients can be accumulated in the vacuole and released under demand (Maathuis et al., 1999). Among these compounds, the vacuole represents a large subcellular reservoir for Ca^{2+} ions; the total concentration can be more than 60 mM (Conn et al., 2006; Schonknecht, 2013). Some portion of vacuolar Ca^{2+} ions are chelated with organic acids or are available in a free form. With a free Ca^{2+} concentration between 0.2 and 2 mM in the vacuole and of about 200 nM in the cytosol at rest, a strong Ca^{2+} gradient directed into the cytosol exists (Schonknecht, 2013; Hedrich and Marten, 2011). Thus, when Ca^{2+}-permeable channels are open, vacuolar Ca^{2+} ions will be released into the cytosol and will lead to countless cytosolic Ca^{2+} signal trails triggering cellular responses (Sanders et al., 2002).

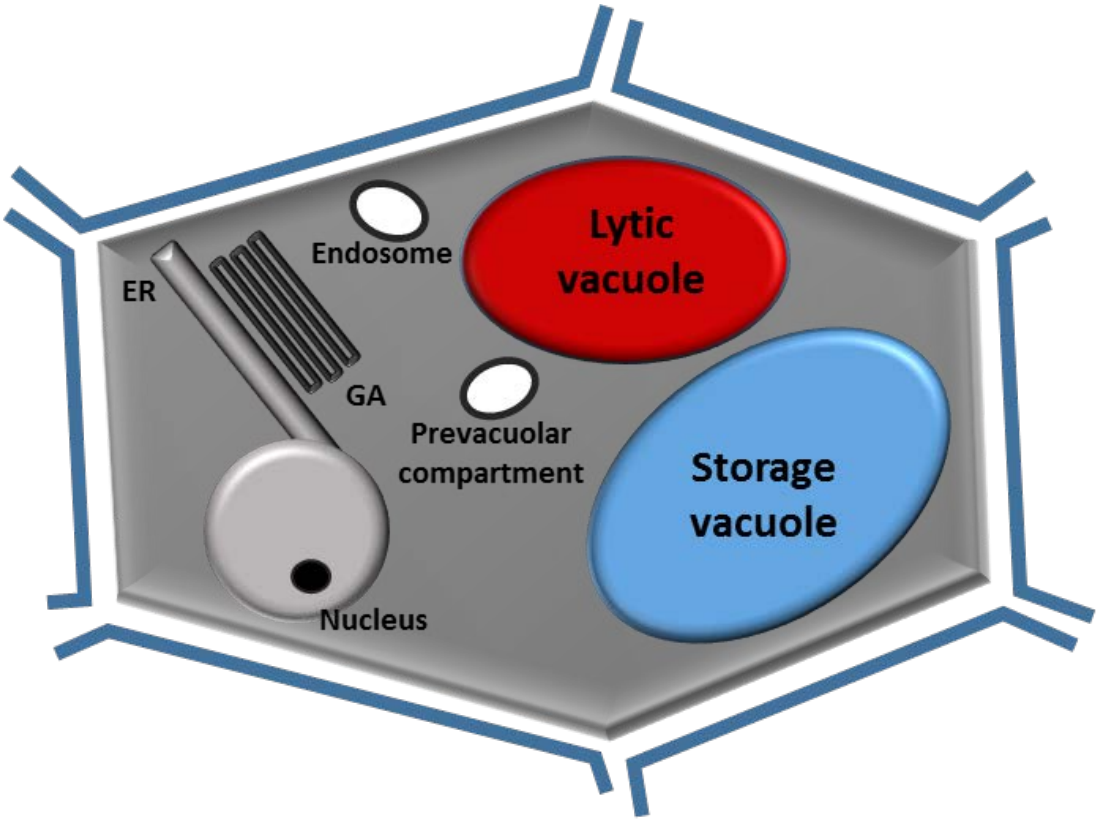

Figure 1. Model of plant cell with different plant organelles. GA - Golgi apparatus, ER - endoplasmic reticulum. Illustration is traced according to Becker, 2007.

All the different vacuolar functions require the transport of solutes across the vacuolar membrane. For this, various transport proteins are embedded in the vacuolar membrane like e.g. ABC transporters, pumps, carriers and ion channels (Isayenkow et al., 2010). Among them, three types of electrogenic transport proteins such as the prominent proton pumps and the K^+-permeable TPK and SV/TPC1 channels (Fig. 2) are described in more detail in the following sections.

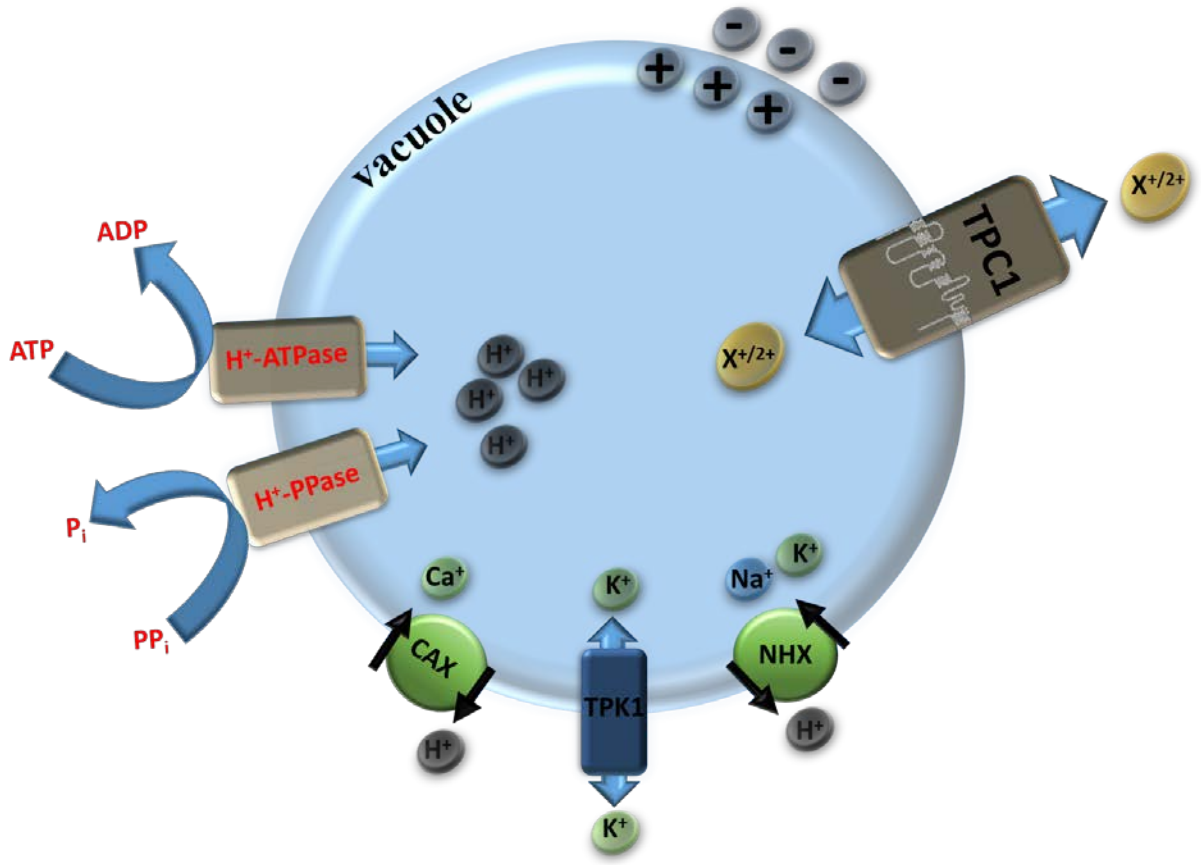

Figure 2. Selected proteins involved in vacuole membrane transport.

Illustration shows transport proteins in the vacuole membrane with their respective conductivities. Passive transport: cation channel TPC1 (X^+, X^{2+}), K^+ channel TPK1. Active proton transport: H^+-ATPase and H^+-PPase. Secondary-active transport: the antiporter CAX (Ca^{2+}/H^+), NHX (K^+-Na^+/H^+),

1.2. Proton pumps for energization of electrogenic solute transport

The activity of H^+-translocating pumps is a prerequisite for energizing the electrogenic solute membrane transport. The high impact of these electromotor enzymes for vacuolar transport processes is reflected by their high abundance in the vacuolar membrane (Carter et al., 2004; Jaquinod et al., 2007). The tonoplast usually harbour two types of proton pumps: the V-ATPase and the V-PPase (Fig. 2) (Schumacher, 2014). In vacuoles of certain plant tissues, e.g. in lemon fruit cells, a proton pump of the P3A/B type was also identified in the vacuolar membrane (Müller et al., 1996; Faraco et al., 2014; Aprile et al., 2011). Until this discovery it was believed that P-type ATPase only localizes to the plasma membrane (Schumacher, 2014; Hedrich et al., 2015). V-ATPase is broadly widespread in distinct organelles of eukaryotic cells, having an acidic lumen (Martinoia et al., 2006). It is a multi-heteromeric enzyme. V-ATPase is built from two main subcomplexes, the ATP-hydrolysing peripheral V_1 motor and H^+-translocating V_0 turbine, which are connected by a central shaft. In contrast to V-ATPase, the second plant H^+ pump protein, V-PPase, do not appear in fungi and animal cells (Martinoia et al., 2006). However, its presence in intracellular structures, as an active form, is not limited only to vacuolar membrane. PPases were also found in plasma membrane, TGN (*trans*-Golgi network) and multi-vesicular bodies (Ratajczak et al., 1999). In comparison to V-ATPase, the structure of V-PPase is much simpler: It represents a homo-dimer composed of a hydrophobic polypeptide with an atomic weight of about 70-80 kDa (Drozdowicz et al., 2001; Maeshima, 2000).

The proton pumps use and mobilize the metabolic energy stored in energy-rich compounds. Upon hydrolysis of either ATP (V-type and P-type -ATPase) or PP_i (V-PPase) they are able to translocate protons from the cytosol into the vacuole. As a result of this uphill transport, a proton motif force (PMF) composed of a steep proton and a weak electrical gradient is established across the vacuolar membrane. Usually, a luminal pH of about 5-6 is set up, leading to a difference of about 2 pH units between cytosol and vacuole (Krebs et al., 2010; Schumacher, 2014). In some specific tissues the luminal pH can be even much lower and in turn the pH gradient is much higher; e.g. a luminal pH < 3 was found in lemon fruit sac cells (Faraco et al., 2014). At rest the difference in the electrical potential reaches about -30 mV, being more negatively charged in the cytosol relative to the vacuolar lumen (Bethman et al., 1995; Wang et al., 2015). The generated PMF is used as driving force for secondary active and

passive solute fluxes (e.g. sugars, cations, organic and inorganic anions, like citrate, malate, chloride and nitrogen ions) mediated by carrier and ion channel proteins. For example, AtClC was shown to function as a $2NO_3^-/1H^+$ exchanger that is able to accumulate specifically nitrate into the vacuole (De Angeli et al., 2006). AtALMT6 and AtALMT9 represent vacuolar ion channels which conduct malate and chloride (Mayer et al., 2011; Kovermann et al., 2007; De Angeli et al., 2013). Likewise, the vacuolar cation transport also affects ion homoeostasis, mainly of sodium, potassium, magnesium and calcium, and – in case of potassium - may even feedback on the membrane potential of the vacuole (Hedrich and Marten, 2011). Uptake of cations like sodium/potassium, magnesium and calcium into the vacuole proceed with H^+-coupled cation antiporters. Additionally, several cation channel types such as the TPK1/FV channel or the SV/TPC1 channel are able to mediate K^+ fluxes across the vacuolar membrane (Fig. 2).

1.3. TPK1/VK, voltage-independent K^+-selective channel

First recordings of the vacuolar K^+ (VK) channel activity were performed in *Vicia faba* guard cells (Ward and Schroeder, 1994). It was demonstrated that this voltage-independent channel type is highly selective for K^+ and activated by cytosolic Ca^{2+} ions and protons (Ward and Schroeder, 1994; Allen and Sanders, 1996). A slow process followed to provide evidences that the *TPK1* (tandem pore K^+ 1) gene encodes the VK channel, and not an outward-rectifying K^+ channel (Czempiński et al., 1997) or a portion of the slow activating vacuolar SV channel (Schonknecht et al., 2002). Finally, results obtained from TPK1-expressing yeast and from plant mutants lacking functional TPK1 channels, verified that TPK1-encoded channels give rise to the vacuolar FK-type K^+ currents (Fig. 2) (Bihler et al., 2005; Gobert et al., 2007). TPK1 is not only expressed in guard cells, but also in other plant tissues, like shoots, roots and flowers (Deeken et al., 2003). The *TPK1* gene belongs to a small gene family, called tandem pore K^+ channel family, which consists of five members in *Arabidopsis thaliana* (TPK1-5). Among them four TPKs (TPK1/2/3/5) are localised in the membrane of lytic vacuoles (Voelker et al., 2006; Latz et al., 2007). Only TPK4 is targeted to the plasma membrane (Becker et al., 2004; Dunkel et al., 2008). A diacidic (DLE) sequence was identified in the C-terminus that is responsible for releasing TPK1 from ER and targeting to the vacuolar membrane (Dunkel et al., 2008). The

TPKs are composed of four transmembrane segments with two pore regions. Upon assembly into functional dimeric channels, four pore regions are finally present creating together the characteristic GYGD motif, that provides for the K^+ selectivity. As regulatory domains, the C-terminus contains EF-hands for putative cytosolic Ca^{2+} binding and the N-terminus an interaction site for 14-3-3 proteins (Czempiński et al., 1999). Likewise to cytosolic Ca^{2+}, binding of 14-3-3 proteins was shown to stimulate the TPK1 activity (Latz et al., 2007). Transgenic plants (knockout and overexpression plants) indicate that TPK1 contributes to intracellular potassium homeostasis (Gobert et al., 2007). Additionally, TPK1 activity is important for the process of germination, seedling growth and stomatal closure (Gobert et al., 2007).

1.4. SV/TPC1, voltage-dependent non-selective cation channel

1.4.1. General SV/TPC1 channel characteristics

SV/TPC1 channel, a highly regulated vacuolar non-selective cation channel type. The SV/TPC1 channel represents a very prominent non-selective cation channel type in the vacuolar membrane which is strongly and ubiquitously expressed in all terrestrial plants (Fig. 2) (Schultz-Lessdorf and Hedrich, 1995). This channel type was for the first time discovered in 1986 by Rainer Hedrich, Ulf-Ingo Fluegge und Jose M. Fernandez. One year later Rainer Hedrich and Ernst Neher showed in barley mesophyll vacuoles that voltage-dependent cation channels slowly activated upon membrane depolarization providing for a large cation conductance (Hedrich and Neher, 1987). Thus, the SV/TPC1 (slow vacuolar) channel owes its original name “SV” to its slow activation kinetics and its targeting to the vacuolar membrane. In addition to the membrane voltage, the SV/TPC1 channel activity is modulated by many other factors, underpinning the complex structure of the TPC1/SV channel and its regulatory network. For instance, the SV/TPC1 channel was shown to be also regulated by calmodulin (Weiser et al., 1991), 14-3-3 proteins (Latz et al., 2007), kinases and phosphatases (Allen and Sanders 1995; Bethke and Jones 1997), pH (Schultz-Lessdorf and Hedrich, 1995; Beyhl et al., 2009), redox state (Carpaneto et al., 1999), Mg^{2+} and Ca^{2+} (Carpaneto et al., 2001; Hedrich and Neher, 1987). In addition, natural polyamines (like e.g. spermidine; Dobrovinskya et al.,

1999a,b) and heavy metals (Carpaneto, 2003) have been reported to inhibit ion passage through open SV channels in red beet and radish. Upon activation the SV/TPC1 channel can serve as an ion-conducting pathway for various cations, mainly potassium and sodium (Schulz-Lessdorf and Hedrich, 1995). The selectivity and ion transport capacity of SV/TPC1 channels, however, can differ between plant species (Schulz-Lessdorf and Hedrich, 1995). For instance, TPC1/SV channels from barley mesophyll cells are characterized by a 6-fold higher permeability for K^+ over Na^+ while those from *Allium cepa* are slightly better permeable for Na^+ over K^+ (Kolb et al., 1987, Amodeo and Zeiger, 1994). Furthermore, the unitary conductance of SV/TPC1 from *Vicia faba* was about twice of those from red beet (Schulz-Lessdorf and Hedrich, 1995). The SV/TPC1 channel features can even vary between cell types. In *Arabidopsis thaliana* it was demonstrated that the SV/TPC1 channels of guard cells were more sensitive towards cytosolic Ca^{2+} than those of mesophyll cells (Rienmüller et al., 2010).

SV channel represents a Two-Pore-Channel encoded by the TPC1 gene. After the *TPC1* gene was first described in 2001 (Furuichi et al., 2001), four years later it was proven in *Arabidopsis thaliana* that this single gene encodes the SV channel (Peiter et al.,2005). The SV/TPC1 protein consists of 733 amino acids with a total of 12 transmembrane domains (S1-S12) and short N- and C-termini (Fig. 3). The SV/TPC1 polypeptide can be structurally subdivided into two Shaker-like segments (DI and DII), with each of them containing six transmembrane domains (S1-S6 and S7-S12). These Shaker modules are connected via a cytoplasmic linker region carrying two EF-hand motifs that are responsible for cytosolic calcium binding (Schulze et al., 2011; chapter 1.4.2). Due to its voltage-dependent activation, TPC1 belongs to the *Superfamily* of voltage-gated channels. In this superfamily voltage dependence is conditioned by the voltage sensor, which is mostly structurally provided by the first four transmembrane segments within one Shaker module; i.e. with the TPC1 channel this would be equivalent to S1-S4 in domain DI and to S7-S10 in domain DII (Fig. 3). The core region of a typical voltage sensor is constructed of four up to seven positively charged amino acids (usually arginine) where each of them is separated by two hydrophobic amino acids (Catteral, 2010). These positively charged amino acids are usually present in the fourth transmembrane domain within the voltage sensor cassette. During evolution plant TPC1s were formed by two separate Shaker-like domains. However, the transmembrane domain S4 in the first Shaker half (DI) of the SV/TPC1 channel was recently revealed as a degenerated voltage sensor, i.e. the

contribution of helix S4 to voltage sensing was found to be negligible (Guo et al., 2016; Jaslan et al., 2016).

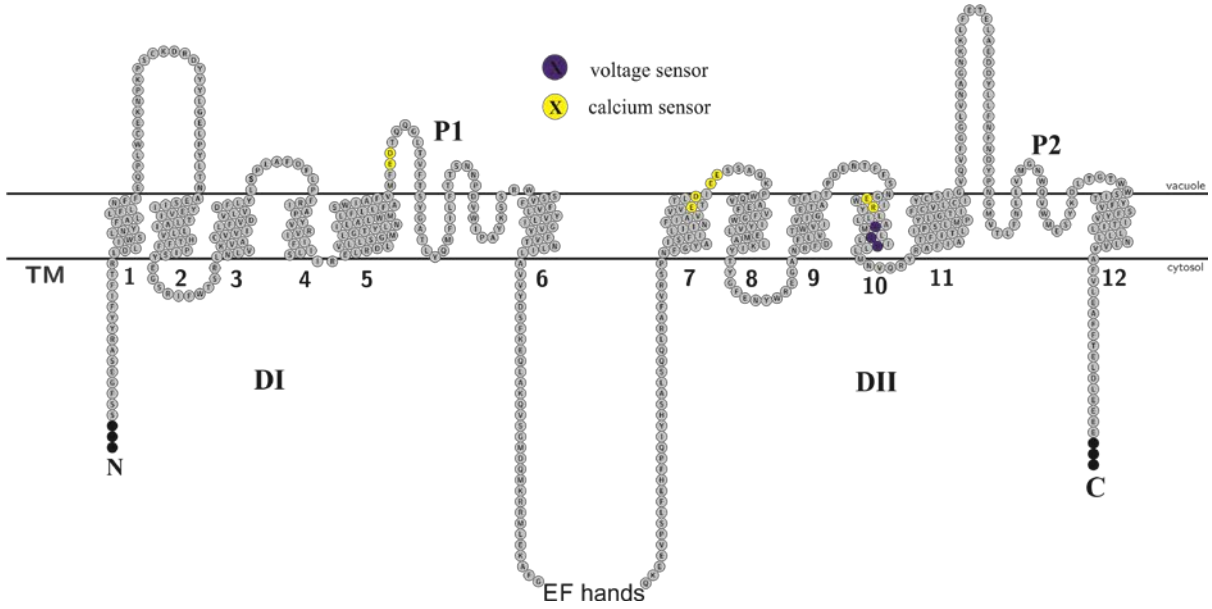

Figure 3.Two-dimensional model of the TPC1 topology.

EF indicates the cytosolic EF-hands. Yellow-marked amino acids are involved in vacuolar calcium (E239,D240,E450,D454,E456,E457,E528,R531) sensing while violet-labelled amino acids (R537,R540,R543) in S10 are responsible for voltage sensing in TPC1 channel. TM = transmembrane domain; P1/P2 = pore region 1 and 2 DI, DII = Shaker-like subdomain I and II

Instead, the major voltage-sensing function was attributed to the transmembrane domain S10 in DII, where we and other researchers identified voltage-sensing arginine residues at positions 537, 540 and 543 (Fig. 3) in the transmembrane region S10 (Guo et al., 2016; Jaslan et al., 2016). Structure-function analysis of the Arabidopsis TPC1 channel in its native membrane revealed that Glu450 and Glu478 are possible ion-pair partners for voltage-sensing Arg537 (Jaslan et al., 2016). When the TPC1 channel is open, the channel pore provides for a hydrophilic pathway for the cation flux through the vacuolar membrane. The pore region is related to the last two transmembrane segments within one Shaker module. Thus, SV/TPC1 channel harbors two pore domains, P1 and P2 (P1 in domain DI: S5-S6, and P2 in domain DII: S11-S12). It is worth noting, that amino acids are not identical in the pore region P1 and P2, but still they are highly conserved among plant species (White et al., 2002). Due to its particular structure, the SV/TPC channel belongs to the class of "Two Pore Channels". As confirmed by the recently published crystal structure (Guo et al., 2016; Kintzer et al., 2016),

the functional SV/TPC1 channel protein represents an assembly of two polypeptides giving rise to the dimeric channel structure (Larisch et al., 2016).

Regulatory effect of SV/TPC1 N- and C-terminal tails. Both, the N- and the C-terminus of SV/TPC1 are localized in the cytosol. The group of Petra Dietrich (University Erlangen-Nürnberg) unequivocally showed that targeting of the SV/TPC1 channel to the vacuolar membrane is guided by the N-terminus (Larisch et al., 2012). The N-terminal tail contains a dileucine motif (EDPLI) that represents a crucial sorting signal for TPC1 protein trafficking to the vacuolar membrane. When this motif is deleted, TPC1 targeting is altered. Instead being localized to the vacuolar membrane, the mutated TPC1 channel protein is directed to the plasma membrane (Larisch et al.,2012). Besides this motif, the N-terminus further contains a conserved so-called KAAAL domain that appears to be required to establish a certain α-helical secondary structure of the N-terminus, which supports efficient vacuolar trafficking and was essential for TPC1 function (Larisch et al.,2012). In contrast, the C-terminus of TPC1 is not involved in the SV/TPC1 targeting process to the vacuolar membrane (Larisch et al.,2012). Nevertheless, the C-terminus has also a considerable impact for SV/TPC1 channel function. The regulation of ion channel activity via the hydrophilic protein endings is a widespread phenomenon (Gustina et al., 2011; Bagneris et al., 2013). Often, voltage-gated channels are altered in their voltage dependency when the C-terminus is mutated or parts are deleted (Marten et al., 1997; Hatano et al., 2004). Instead, the major function of the SV/TPC1 C-terminus seems to provide secondary structures as prerequisite for dimerization of the channel protein (Larisch et al., 2016). Using different approaches (e.g. site-directed mutagenesis, bimolecular fluorescence complementation or microscale thermophoresis experiments), the group of Petra Dietrich demonstrated that a highly conserved α-helical region in the C-terminus (aa707- aa723) is required for building an antiparallel coiled-coil structure during assembly of two polypeptides to a functional TPC1 channel protein (Larisch et al., 2016).

Animal counterparts of SV/TPC1 channel. In analogy to SV/TPC1 in the vacuole membrane, the animal TPC channels also reside in the membrane of an acidic compartment, the lysosomes. A SV/TPC1-channel orthologue represents the animal lysosomal TPC2 channel (Calcraft et al., 2009). Targeting of TPC2 to the endosomal membrane is also under the control of a N-terminal dileucine motif (Brailoiu et al., 2010). TPC2 belongs to the NAADP-gated

calcium release channels and is part of a signaling pathway, that leads to the release of calcium ions from lysosomes to the cytosol (Ruas et al., 2010). Both loss- and gain-of-function experiments including electrophysiological recordings of TPC2 (Brailoiu et al., 2010; Schieder et al., 2010; Pitt et al., 2010) support the idea that TPC2s function as NAADP targets (Hooper and Patel, 2012). But a series of studies have challenged this assumption, suggesting instead that TPC2s are Na^+ channels activated either by $PI(3,5)P_2$ (TPC2) or NAADP (Wang et al., 2012). Thus, both the activating ligand and the ion permeability is unclear (Marchant and Patel, 2013)

For many years up to now, it is intensively discussed, whether the SV/TPC1 channel might be also involved in Ca^{2+} signaling pathways in plants. This debate originates from the fact that Ca^{2+} ions can pass the SV/TPC1 channel under artificial experimental conditions (Ward and Schroeder 1994; Pottosin et al.,2001) and that SV/TPC1 activity is stimulated with increasing cytosolic Ca^{2+} (Hedrich and Neher, 1987; Hedrich and Kurkdjian, 1988; chapter 1.4.2). In this context, the Calcium-Induced Calcium Release (CICR) hypothesis was proposed in which cytosolic Ca^{2+} signals may cause the activation of SV/TPC1 and in turn SV/TPC1-mediated Ca^{2+} release in planta (Ward and Schroeder, 1994). This hypothesis has still its opponents as well as supporters in the plant community.

1.4.2. Stimulatory effect of cytosolic divalent cations on TPC1 channel activity

Ca^{2+} and Mg^{2+} function as helper ions for channel activation. Beyond membrane depolarization, SV/TPC1 channel activation can be promoted via modulatory factors like cytosolic Ca^{2+} and Mg^{2+} ions. The dependency of the SV/TPC1 channel on the cytosolic Ca^{2+} concentration was first described and quantified with a K_m value of 1.5 µM in sugar beet vacuoles by Hedrich and Neher (1987). Increase in cytosolic calcium concentration shifted the energy barrier for channel activation to more physiological membrane voltages, therefore entailing more active SV channels. The same effect on voltage-dependent SV/TPC1 activation was observed with increasing cytosolic Mg^{2+} concentrations (Pei et al.,1999, Carpaneto et al., 2001). Interestingly, activation of TPC1 takes place after binding of at least three Mg^{2+} ions, and is further enhanced by nanomolar calcium concentration (Carpaneto et al., 2001). It seems that calcium and magnesium ions influence TPC1 channel gating in a synergistic manner

(Pei et al., 1999). However, calcium ions may have the predominant physiological impact on TPC1 (Hedrich and Marten, 2011).

Two EF-hand domains in TPC1. The two Shaker-like domains of the TPC1 channel are separated via a cytoplasmic linker region which contain two EF-hands motifs (Fig. 3) for putative calcium binding and one putative interaction site with 14-3-3 protein (Latz et al., 2007; Furuichi et al., 2001; Peiter et al., 2005; Larisch et al., 2016). A typical EF-hand motif resulted in (E-helix)-loop-(F-helix) secondary structures where the loop between the two helices enables calcium or magnesium ion binding (Marchler-Bauer et al., 2009). Thereby, coordination of the centered Ca^{2+} ion is often exerted by seven oxygen atoms arranged in a pentagonal bipyramid (Grabarek, 2006). Various proteins with paired EF-hands domains differing in the amino acidic sequence are known which can dramatically alter their ability of calcium and magnesium binding (Grabarek, 2006). Functional analysis of the two EF-hands in the TPC1 channel indicated that EF-hand 1 and EF-hand 2 have different impact on regulation of TPC1 channel activity (Schulze et al., 2011). EF-hand 2 provides for a high affinity binding site for Ca^{2+} ions, enabling SV/TPC1 channel responses to physiological changes in the cytosolic Ca^{2+} concentration. When the crucial amino acid Glu376 in the loop of EF-hand 2 was mutated, Ca^{2+} binding was impaired leading to silent TPC1 channels. In contrast, EF-hand 1 has a low ability for binding of calcium and magnesium ions and therefore plays a rather modulatory role in affecting the Ca^{2+} sensitivity of the TPC1 channel (Schulze et al., 2011).

1.4.3. Inhibitory effect of vacuolar divalent ions on SV/TPC1 channel activity

SV/TPC1 conductance is additionally regulated upon vacuolar Ca^{2+} ions (Pottosin et al., 1997, 2004). In contrast to the cytosolic stimulatory Ca^{2+} effect (chapter 1.4.2), SV/TPC1 currents are reduced with increasing luminal free Ca^{2+} concentrations. A similar inhibitory effect on the SV/TPC1 currents of sugar beet vacuoles has been reported for luminal Mg^{2+}, even though this divalent cation appeared to be less effective than luminal Ca^{2+} (Pottosin et al., 2004). Based on their patch-clamp experiments, Pottosin and coworkers (2004) concluded that two independent binding sites for luminal divalent cations might exist at the SV/TPC1 channel protein. One less cation-selective interaction site may be localized within or nearby the pore

region, and another high Ca^{2+}-selective one at a channel domain outside of the membrane. Thus, calcium and magnesium cations may block the flow of potassium ions, by entering the ion pathway and interacting there with a binding site.

The kinetical studies of voltage gating suggested that the SV/TPC1 can probably reside in at least three conformational states (Pottosin et al., 2004). The delayed SV channel activation kinetics pointed to at least two closed non-conducting channel states (C_1 and C_2), and the single exponential deactivation kinetics proposed one open ion-conducting state (O). The opening of SV/TPC1 channel probably requires the sequential transition from closed state C_2 to closed state C_1, and then to open state O ($C_2 \leftrightarrow C_1 \leftrightarrow O$). Binding of luminal Ca^{2+} to the peripheral Ca^{2+} interaction site of SV/TPC1 channel protein seems to affect channel gating because the activation time was found to be slow down and the deactivation time accelerated (Pottosin et al., 1997). The energy barrier for SV/TPC1 activation was shifted towards more positive voltages and in turn the number of open channels finally reduced upon high luminal Ca^{2+} loads (Pottosin et al., 2004). Thus, luminal Ca^{2+} ions specifically modulates the TPC1 channel activation and deactivation process via a high affinity binding site.

First insights into the structure of the luminal peripheral Ca^{2+} sensor of TPC1 provided the TPC1 mutant channel *fou2* (Bonaventura et al., 2007a). The *fou2* channel harbors the mutation D454N localised in the luminal loop between S7 and S8. Due to the *fou2* mutation, the energy barrier for channel activation was shifted towards more negative membrane potentials, even at high luminal Ca^{2+} concentrations (Beyhl et al. 2009). As a result, the SV/TPC1 channels became hyperactive (Bonaventura et al., 2007a; Beyhl et al., 2009). When the underlying mechanisms of this effect on TPC1 channel activity were electrophysiologically studied, the *fou2* channel sensitivity to cytosolic stimulatory Ca^{2+} was found to be unaltered (Beyhl et al., 2009). However, the sensitivity of the *fou2* channel to inhibitory luminal Ca^{2+} ions were largely reduced leading to more open channels at the resting voltage of the tonoplast. Therefore, it was proposed that Asp454 is part of the luminal Ca^{2+} sensor (Beyhl et al., 2009). Further studies, including analyses of amino acid polymorphism in TPC1 from many species, structural modelling, site-directed mutagenesis, electrophysiological experiments with different TPC1 channel variants and the crystal structure (Dadacz-Narloch et al., 2011; Guo et al., 2016; Kinzer et al., 2016), revealed additional negatively charged amino acids which are involved in luminal Ca^{2+} sensing. Two luminal Ca^{2+} coordination sites are provided by Asp454, Glu528, Asp240

(site I) on one hand and Glu239, Glu457, Asp240 (site II) on the other (Fig. 3). Thus, these sites share Asp240 for Ca^{2+} binding. However, it is thought that only site I has an impact in Ca^{2+} coordination *in vivo* to stabilize the closed state of TPC1 (Guo et al., 2016). Beyond of these residues, Glu450 and Glu456 and Arg531 (Fig. 3) additionally play a role in luminal Ca^{2+} sensing (Dadacz-Narloch et al., 2011; Jaslan et al., 2016). It was proposed that Glu456 and Asp531 may connect the luminal Ca^{2+} sensor to the voltage sensor helix S10 mediating the inhibitory effect of Ca^{2+} binding to the voltage gate (Dadacz-Narloch et al., 2011, Jaslan et al., 2016). Replacing these charged residues by neutral ones resulted in the loss of the inhibitory influence of vacuolar Ca^{2+} on SV/TPC1 channels.

Considering this luminal high-affinity Ca^{2+} binding site at the periphery of the channel protein together with the comparable free concentrations of Mg^{2+} and Ca^{2+} in the vacuolar lumen (Shaul, 2002), one can conclude that luminal Mg^{2+} most likely does not play a crucial role in TPC1 regulation (Pottosin et al., 2004). Instead, cytosolic Mg^{2+} might be additionally involved in SV/TPC1 regulation because the cytosolic free concentration of Mg^{2+} is much higher than that of Ca^{2+}. Interestingly, the affinity of the endosomal TPC2 channel, the orthologue of SV/TPC1 in animals (Calcraft et al., 2009), to cytoplasmic activating ligands are increased with a rise in the luminal Ca^{2+} concentration (Pitt et al., 2010).

1.4.4. Physiological impact of SV/TPC1 channel

TPC1 is one of the main plant vacuolar channel broadly expressed in terrestrial and marine plants (Carpaneto et al., 1997). Since loss of TPC1 channel function does not fully impair plant growth (Peiter et al., 2005), scientists already debate its physiological function for a long time. Due to a T-DNA insertion, TPC1 channel protein was not functionally expressed in the *tpc1-2* null mutant. Lack of TPC1 protein resulted in ineffective ABA-dependent suppression of germination and reduced stomatal closure in response to high external Ca^{2+} loads, but not to abscisic acid (ABA) (Peiter et al., 2005). In the opposite situation, overexpression of TaTPC1 in *Arabidopsis thaliana* promoted external Ca^{2+}-induced stomatal closure (Wang et al., 2005). We can observe lack of differences between *Arabidopsis thaliana* WT and *tpc1-2* loss-of-function mutants plants in responses to ABA (Peiter et al., 2005). This is in line with the *Attpc1-2* seedlings and adult mutant plants behaviour challenged with different effectors (cold,

hyperosmotic, salt, and oxidative stress or pathogenic factors) causing cytosolic calcium to rise (Ranf et al., 2008; Hedrich and Marten, 2011). When roots of seedlings were exposed to salt treatment, growth of the *tpc1-2* null mutant was more impaired than that of WT plants (Choi et al., 2014). In comparison, TPC1 overexpressor showed a higher salt tolerance (Choi et al., 2014). Interestingly, salt-triggered Ca^{2+} propagating signals in the root were attenuated in *tpc1-2* but increased in TPC1 overexpressor lines (Choi et al., 2014). Furthermore, it was shown that systemic Ca^{2+} signals, generated upon wounding, was gone with the loss of TPC1 function. This observation points to a role of TPC1 in systemic Ca^{2+} signals (Kiep et al., 2015). The *fou2* point mutation D454N (from fatty acids oxygenation upregulated 2) led to an increased production of the stress hormone jasmonate, even under non-stressed conditions. The *fou2* plants also showed a strong retarded growth phenotype (Bonaventure et al., 2007a,b), probably originating from the increased ability of releasing potassium from the vacuole due to the hyperactive TPC1 channels (Bonaventure et al., 2007b). TPC1 channel and its hyperactive version *fou2* seem to be a good tool to evaluate initial stages of jasmonic acid production and wounding responses.

1.5. Jasmonate, a wounding signal

Plant tissues are highly susceptible to damages, caused for example by pathogens, herbivorous animals and various environmental factors. These factors induce complex responses in the plant organism, manifested by metabolic, growth and developmental changes. Phytohormones play a key role in the regulation of these dynamic processes (Pieterse et. al., 2009; Koo and Howe., 2009). It is well known that oxylipins (oxygenated fatty acid derivatives) regulate many important functions under biotic and abiotic stress conditions (Browse, 2009). Thereby, the phytohormone jasmonate (JA) is one crucial oxylipin that is involved in plant response to wounding. JA is produced from glycerolipids of the chloroplast membrane. After linolenic acid is released by phospholipases, several reaction steps, catalysed by e.g. lipoxygenases (LOXs) and allene oxide synthase (AOS), are needed to finally synthesize JA and biological active JA derivatives, like JA-Isoleucine (JA-Ile) (Howe GA et al., 2000; Blee, 2002; Gfeler et al., 2010; Ahmad et al., 2016). Among the six LOXs, the action of LOX2 particularly causes the accumulation of high JA levels proximal to the injury site (Glauser

et al., 2009). LOX6 activity is needed for a rise in the JA level in the wounded and the distal unwounded leaf tissue (Savatin et al.,2014; Wasternack et al., 2013). Under natural environmental conditions plant cells have low JA levels. Then, transcription factors (TFs) responsible for JA-responsive gene expression are blocked by interaction with repressor proteins belonging to the JASMONATE ZIM-domain family (JAZ) (Chini et al.,2007; Thines et al.,2007; Yan et al.,2007). When JA synthesis is trigged upon wounding, JA starts to accumulate logarithmically nearby the injury site, even within 30 seconds after wounding (Glauser et al., 2008). The increase in JA concentration stimulates the binding of JAZ suppressor to the F-box protein CORONATIVE INSENSITIVE1 (COI1), which is a component of the E_3 ubiquitin ligase SCF^{COI1} (Balbi and Devoto, 2008; Thines et al., 2007). The COI1-JAZ interaction leads to the ubiquitination of the JAZ repressor and in turn, to its proteasomal degradation. Consequently, TFs are released, and JA signalling pathway genes are expressed (Fig. 4). Regulation of JA biosynthesis is adjusted by JA itself. Thereby, a positive regulatory feedback loop reinforces JA production, but also availability of substrates and tissue specificity (Wasternack et al., 2013). Turning off the JA signalling pathway can take place by hydroxylation, carboxylation or epimerization of JA/Ja-Ile leading to biologically inactive JA forms (Wasternack et al.,2013; Farmer, 1994; Fonesca et al., 2009). Additionally, it was shown that JAZ repressor is stabilized and its degradation pathway turned off. It enables the regulation by negative feedback (Chung and Howe, 2009). The mechanisms underlying the initiation of JA synthesis in the first phase of JA signalling are not well known. The fast onset of JA synthesis suggest that all enzymes required for JA biosynthesis are already available prior to the stressed condition (Koo and Howe, 2009). Electrical signals such as changes in the plant surface potential, depolarization of the plasma membrane represent early responses to wounding (Maffei et al., 2007). Recently, electrical signals have been implicated in the stimulation of JA biosynthesis in leaves distal to the damaged sites (Mousavi et al., 2013). In comparison, the subsequent activation of the JA signalling pathway in the second phase is better understood. There are several reports suggesting that cytosolic Ca^{2+} might be involved in this process. The application of calcium channel blockers was shown to negatively affect JA-triggered gene expression (Sun et al., 2006). Furthermore, this Ca^{2+}-induced signalling cascade depended on the activity of Ca^{2+}-sensing proteins. In *Zea mays* leaves wounding resulted in an increased activity of the Ca^{2+}-dependent protein kinase ZmCPK11 and its gene expression level (Szczegielniak et al., 2005),

and in Arabidopsis the calmodulin-like protein CML37 was stimulated by mechanical wounding (Scholz et al., 2014).

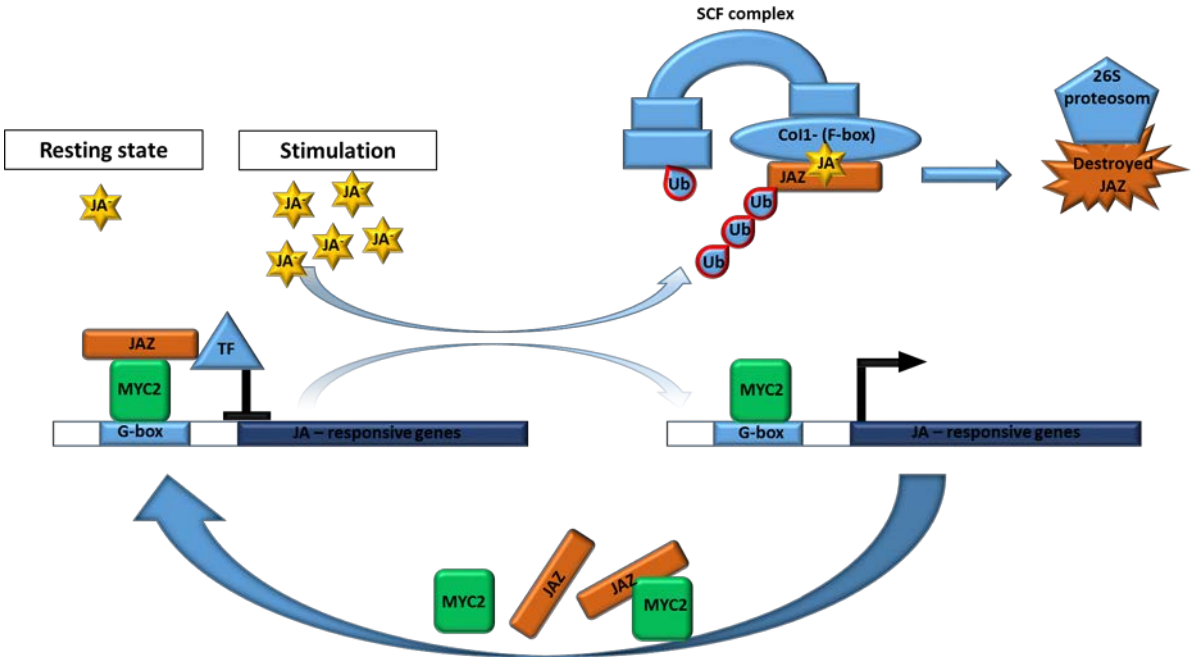

Figure 4.COI1–JAZ co-receptor complex participation in jasmonic acid (JA) perception.

In the resting state (left, low JA-Ile level), the binding of the transcription factor MYC2 to a G-box within the promoter of a JA-responsive gene does not activate transcription due to binding of the JA repressor ZIM domain protein (JAZ) to MYC2 and other repressors (TF). Upon stimulation (right, high JA-Ile level), JAZs are recruited by COI1. As a result, JAZs are ubiquitinated and subsequently degraded by the 26S proteasome releasing MYC2. Accordingly, MYC2 can activate transcription of early JA-responsive genes such as those encoding JAZ and MYC2. F-box protein is a part of SCF complex; Ub, ubiquitin. (Illustration is traced according to Wasternack & Hause, 2013)

Using a genetically encoded Ca^{2+} reporter, the generation of local and systemic cytosolic Ca^{2+} signals were monitored upon wounding (Kiep et al., 2015). Stress caused by biotic factors often entails systemic gene expression, to initiate host defence responses for protection of healthy tissue against another attack (Heil and Ton, 2008; Vlot et al., 2008). The role of biologically active JA forms in systemic plant responses to injury is unquestionable, and it was verified by studies of mutants with disorders in JA production or perception (Wasternack et al., 2006; Browse, 2009). JA-dependent plant systemic responses may vary in intensity, time of occurrence and spatial scale. Fast changes in gene expression and hormone level take place within less than a minute after the tissue injury. Other responses, including toxins, repellents

and volatiles production involved in tri-trophic interactions, last a little longer (Matsui, 2006; Heil and Silva Bueno, 2007; Pauwels et al., 2009). There are two models depicting JA-dependent plant systemic response (Koo and Howe, 2009). In the first model JA and its derivatives are synthesized at the site of injury and serve as a mobile activation signal in tissues distal to the injury site. The second model presumes the existence of other mobile signals induced by injury, activating JA and its derivative production in plants. Both models consider a rise in JA/JA-Ile concentration as well as JAZ repressor ubiquitination and its proteolytic degradation. Thus, the two models differ in the source of JA and its derivatives used for tissue protection, and the type of mobile signal activating plant defence (Koo and Howe, 2000)

2. Aim of the study

Plant vacuoles play an important role in many physiological processes (Robinson et al., 2005). Many of these activities require solute transport across the vacuolar membrane. For this purpose, various proteins are embedded in the vacuolar membrane (Isayenkow et al., 2010). One of the most prominent vacuolar transport protein, is the ubiquitously expressed nonselective, cation channel TPC1/SV (Hedrich and Marten, 2011). The TPC1 channel activity is strictly regulated via many factors (i.e. vacuolar and cytosolic Ca^{2+}, membrane voltage, phosphorylation) emphasizing its complex structure and function. Nevertheless, scientists still debate about the physiological role of TPC1 channels. In this aspect, the *fou2* plant harboring a hyperactive TPC1 channel version (D454N), that is almost insensitive to vacuolar calcium provided the chance to gain more insights (Dadach-Narloch et al., 2011; Beyhl et al., 2009). Due to the missense D454N mutation, the *fou2* plants exhibit a retarded growth phenotype characterized by an overproduction of jasmonate acid (JA) (Beyhl et al., 2009; Bonaventure et al., 2007a). After EMS-based secondary mutagenesis of *fou2* plants, these *fou2* characteristics, interestingly, disappeared in eight mutants, named *ouf1-8.* In order to better understand now the role of the TPC1 channel activity in JA signalling pathway, the function of the TPC1 channels in the *ouf* mutants should be electrophysiologically studied in this thesis. For this, the patch-clamp technique should be applied to mesophyll vacuoles isolated from *Arabidopsis thaliana* WT, *fou2* and *ouf* mutant plants to quantify different TPC1 channel features such as current density, single channel conductance, luminal calcium dependency and voltage-dependent gating behaviour (i.e. relative voltage-dependent open-channel probability, activation kinetics). Thereby, my aim was to elucidate the most crucial TPC1 channel feature possibly present in all *ouf mutants*, leading to the reversion of the characteristic *fou2* phenotype, and to specifically link the reverting mutations with the channel structure. These studies should link jasmonate signalling with TPC1 and bring us closer to achieve further insights in the physiological role of this dominant vacuolar cation channel.

3. Material and methods

3.1. Plant cultivation and preparation of plant tissue

3.1.1. *Arabidopsis thaliana*

3.1.1.1. Growth condition

Arabidopsis thaliana plants of the ecotype Columbia-0 (Col-0) were cultivated on soil in plastic pots of 7 cm diameter under controlled short-day conditions in a climate chamber. Plants were illuminated for 8 hours with a light intensity of 150 µmol s^{-1} m^{-2} using fluorescent lamps from Osram (L58W / 77 FLUORA; Munich, Germany) and Philips (TLD 58W / 840; Hamburg, Germany). The temperature was constantly hold at 22°C and 16°C during the light and dark period, respectively. Air humidity was maintained at 60%. All *Arabidopsis thaliana* mutants were grown under identical environmental conditions as WT plants. The experiments were carried out with plants which were 5 to 7 weeks old. Seeds of the different stable *ouf* lines were kindly provided by Prof. E. Farmer (University of Lausanne, Switzerland).

3.1.1.2. Mesophyll protoplast isolation and osmotic release of vacuoles

For protoplast generation an enzymatic method was used (Beyhl et al. 2009). 3-4 mature leaves of average size were selected from *Arabidopsis thaliana* plant. The lower leaf epidermis was gently removed with sandpaper of P500 grain size. The prepared leaf was immediately placed into a petri dish (Ø = 3,5 cm with cams; Sarstedt AG & Co., Nümbrecht, Germany) filled with enzyme solution (see below). Thereby, the lower leaf surface was in direct contact with the enzyme solution which contained the following components:

- 0.05% Pectolyase Y-23 (Kyowa Chemical Products CO., LTD, Japan)
- 0.5% Cellulase R-10 (Yakult, Tokyo, Japan)
- 0.5% Mazerozyme R-10 (Yakult, Tokyo, Japan)
- 1 mM $CaCl_2$
- 1% BSA (bovine serum albumine)
- 10 mM Mes adjusted to pH 5,6 with Tris
- π = 500 mosmol kg^{-1} adjusted with D-Sorbitol

The leaf material was incubated for 45-60 minutes at room temperature. To stop the enzyme reaction and to eliminate leaf debris, the sample was then filtered through a moistened nylon mesh with a size of 50 µm into a 50 ml plastic tube using about 50 ml wash solution (1 mM $CaCl_2$, π = 500 mosmol kg^{-1} adjusted with D-Sorbitol). The filtrate was centrifuged for 7 minutes (Eppendorf 5810R Eppendorf AG, Hamburg, Germany) at 60 x *g* and 4°C (with no acceleration and deceleration). After the supernatant was decanted, the protoplast-enriched precipitate was re-suspended in 0.5-1.0 ml wash solution, depending on the protoplast density which was visually estimated. The protoplast suspension was stored at ice until the electrophysiological measurements were carried out. Under consideration of the protoplast density, a sample of the protoplast suspension (usually 50-100 µl) was then transferred to the patch-clamp measuring chamber. To exploit the phenomenon of a hypoosmotic shock, 250 µl lysis buffer (10 mM EGTA, 10 mM Hepes/Tris pH 7,5, π=200 mosmol kg^{-1} with D-Sorbitol) was added. As a result of the lower osmotic potential of the lysis buffer, water flowed into the protoplasts and the hydrostatic internal pressure increased. The plasma membrane finally burst releasing the vacuoles from the protoplast. After about two minutes of incubation, the lysis buffer was slowly washed out for at least 8 minutes by perfusion of the patch-clamp bath solution at a speed of 0.5 to 0.7 ml/min.

3.1.2. *Vicia faba* and *Lotus japonicus*

3.1.2.1. Growth condition

Vicia faba [Kleine (französische) Weißkeimige] and *Lotus japonicus* [MG-20; kindly provided by Prof. Martin Parniske, Ludwig-Maximilians-University München] plants were cultivated in the greenhouse under long-day conditions. The light period with a light intensity around 150 µmol s^{-1} m^{-2} lasted 16 hours, and the temperature was hold at 16°C. During the 8-hours dark phase, the temperature was adjusted to 14°C. Air humidity was hold at 55%. For patch clamp experiments two-week-old *Vicia faba* plants were used, while *Lotus japonicus* plants were 8-10 weeks old.

3.1.2.2. Mesophyll protoplast isolation and osmotic release of vacuoles

With some exceptions, the procedure for the protoplast isolation and osmotic-induced release of vacuoles from protoplasts of *Lotus japonicus* and *Vicia faba* was essentially the same as used for *Arabidopsis thaliana* protoplasts/vacuoles (chapter 3.1.1.2). With respect to *L. japonicus,* leaves were incubated in enzyme solution (chapter 3.1.1.2) for three hours and were subjected to continuous gentle shaking (GFL, Burgwedel, Germany). For isolation of *Vicia faba* protoplasts leaves were incubated in an enzyme solution composed of:

- 2% Cellulose R-10 (Yakult, Tokyo, Japan)
- 1% Mazerozyme R-10 (Yakult, Tokyo, Japan)
- 1 mM $CaCl_2$
- 0.5% BSA (bovine serum albumin)
- 10 mM Na-ascorbic adjusted to pH 5,5 with HCl
- π = 500 mosmol kg^{-1} adjusted with D-Sorbitol

3.2. Patch-Clamp technique

The patch-clamp technique allows the recording of ionic currents through the membrane mediated by either individual ion channels or an entity of ion channels, ion pumps or electrogenic carriers. The method uses one measuring glass microelectrode (Neher and Sakmann, 1976; Hamill et al., 1981) which is sealed to the target membrane in a way that a high electrical resistance between membrane and electrode in the Giga-ohmic range is established. As a result the signal-to-noise ratio is highly improved, and ion fluxes through even individual ion channels - as low as about 1 pA - can be resolved and measured. Since the development of this sophisticated electrophysiological method provided the basis to verify the existence of ion channels and to study their function in many cells, Erwin Neher and Bert Sakmann were honoured for establishing this method with a Noble prize in Physiology/Medicine in 1991. Since the patch-clamp technique was first applied to plant cells in 1984 (Moran et al. 1984; Schroeder et al. 1984), many researchers have used this method to characterise active and passive membrane ion transport processes in plants (Hedrich and Neher, 1987; Hedrich et al, 1989; Schulz et al, 2011;. Hedrich, 2012; Rienmüller et al, 2012).

3.2.1. Measuring configurations of the patch-clamp technique

In principle, when the patch-clamp technique is applied, one can measure in four different configurations: *cell attached, inside-out, whole-cell and outside-out*, with the possibility of a smooth transition between some of them. Among them the *cell-attached* mode is first established, being the prerequisite for the generation of all the other three configurations. To achieve this configuration, the glass microelectrode (patch electrode) with a tip diameter of about 1 µm (may vary depending on the used patch clamp configuration) is placed on the target membrane of a single cell or a released protoplast or internal compartment such as the vacuole. When gentle suction is then applied to the membrane via the patch pipette, the resistance of the measuring pipette eventually rises to the GΩ range. This formation is known as the so-called „*gigaseal*", whereas the configuration that is stabilised is called „*cell-attached*" or - when vacuoles are used – "vacuole-attached". In this mode, the patched single cell or internal compartment (i.e. vacuole) will not be damaged, and all internal regulators as

well as ion concentrations remain unchanged. The small membrane area that tightly covers the patch pipette tip is electrically isolated from the rest of the membrane. Accordingly, the fluctuation of single ion channels can be measured in this membrane patch. When in the *cell-* or *vacuole-attached* mode the patch pipette is slowly pulled away from the patched cell or vacuole, the membrane will rupture leaving a small excised membrane patch in the pipette tip. In this „*inside-out*" (Fig. 5) configuration the internal side of the membrane patch is exposed towards the bath solution in the measuring chamber. In order to gain electrical access to the entire membrane surface of the cell or vacuole, in the cell/vacuole attached mode the membrane patch in the pipette tip will be destabilized and finally destroyed via applying a short and strong voltage pulse (700-900 mV) and/or a controlled negative pressure to the membrane via the patch pipette. As a result, the patch pipette achieves access to the interior of the cell or vacuole leading to the equilibration of the solutes in the lumen of the patched cell/vacuole with the patch pipette solution. Since the electrogenic transport proteins of the entire membrane can be studied, this configuration is called „*whole-cell*" or "*whole vacuole*" mode. When in this configuration the patch pipette will be carefully withdrawn from the patched cell/vacuole, the membrane attached to the glass pipette will rupture and immediately re-fuse and form a tight membrane patch in the tip of the patch electrode. This measuring configuration is known as „*outside-out*" mode suitable to measure single ion channel currents.

In this work, the patch clamp technique was applied to mesophyll vacuoles. In these experiments either the *whole vacuole* or the *outside-out* mode was established. In both cases the cytosolic side of the tonoplast was exposed towards the bath solution in the measuring patch-clamp chamber, while the luminal side of the vacuole membrane was facing the patch pipette solution.

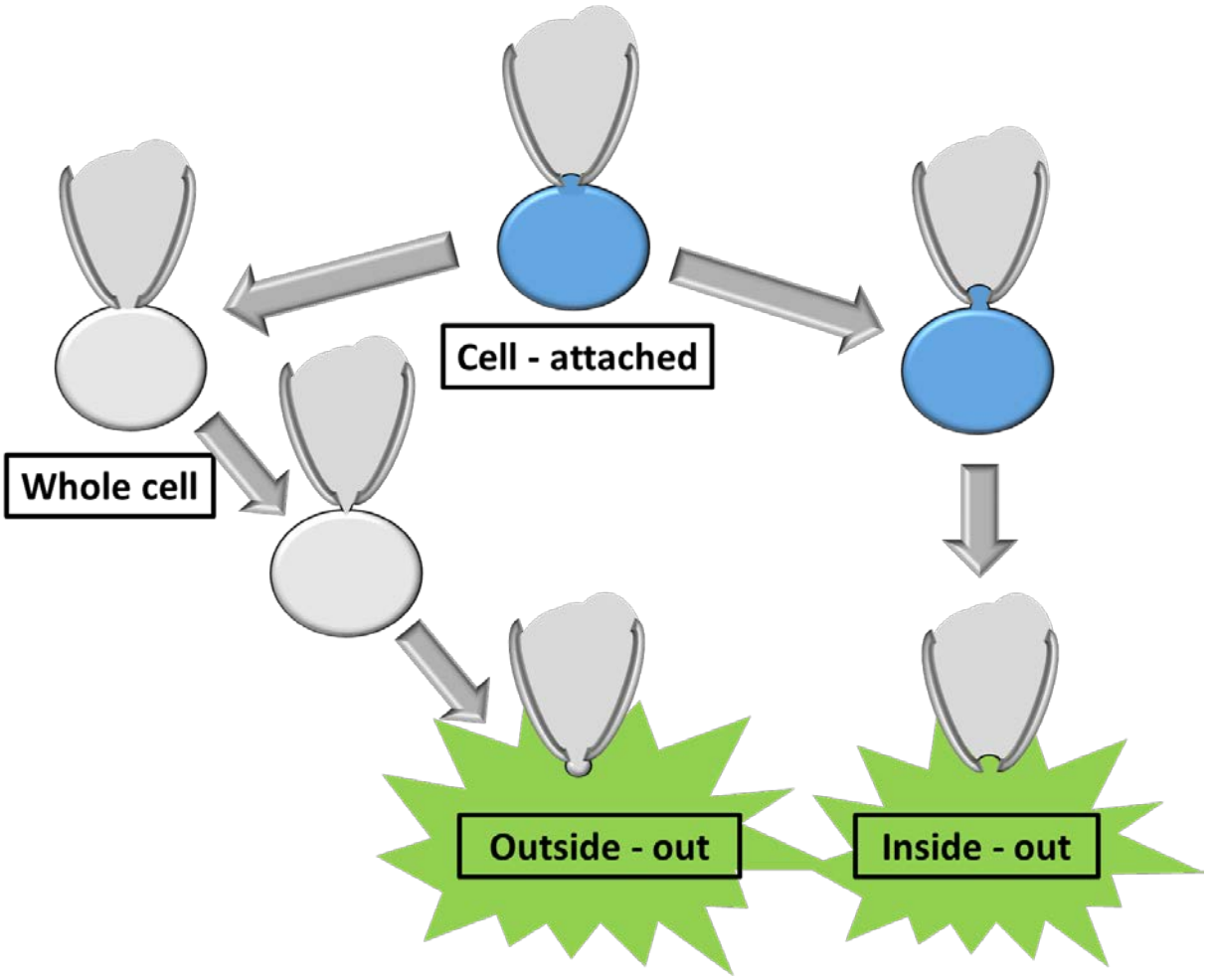

Figure 5. Measuring configurations of the patch-clamp technique.

The establishment of the different patch clamp configurations such as Cell-attached, Whole-Cell, Outside-out and Inside-out mode in practice are illustrated according to Hamill et al. 1981. The designation of the configurations presented here refer to the plasma membrane and must be converted to e.g. Whole Vacuole when working with endomembrane's such as the tonoplast. For details, please see the main text.

3.2.2. Components of the patch-clamp set-up

The patch-clamp set-ups used for the structure-function studies of the vacuolar AtTPC1 channel in this thesis was composed of the following elements. For shielding the measuring advices, i.e. the electrodes, from external electromagnetic interference and electrostatic discharge, a self-made Faraday cage surrounded the internal pneumatic table (Technical Manufacturing Corporation, Peabody, Massachusetts, USA). The table itself was necessary to remove or at least to minimize eventual vibrations transmitted from the ground to the inverted microscope (Axiovert 10, Carl Zeiss, Jena, Germany; IX50, Olympus, Hamburg, Germany). The measuring chamber containing the vacuoles in the bath medium was placed in

the centre of the microscope stage (Inverted movable top plate, Scientifica, Uckfield, England). Additionally, a micromanipulator (Patch Star Mikromanipulator, Scientifica, Uckfield, England) placed on the right side of the measuring chamber was mounted on the microscope table. The patch clamp preamplifier (EPC10; Elektronik Dr. Schulze GmbH, Lambrecht, Germany) was fixed to the holder of the micromanipulator, thus enabling the precise manual control of the patch-electrode position in the measuring chamber. Besides the patch electrode, the reference electrode was also connected to the preamplifier. In order to maintain homogeneous solute conditions (ion concentration) in the patch clamp chamber, two peristaltic pumps (Pharmacia LKB Pump P-1, Pfizer, Berlin) were connected via polyethylene tubes to the patch clamp chamber allowing the continuous influx and efflux of bath solution. The solution flowed through glass olives, covered from inside with Sigmacote® (Sigma, Munich, Germany), to avoid electrical connection between pumps and measuring chamber. The peristaltic pumps were placed outside of the Faraday cage, in order to avoid additional sources of electromagnetic interference. Application and acquisition of electrical signals were performed with the EPC10 patch clamp amplifier, which contained a built-in analogue-digital AD/DA converter interface, allowing communication and recording of data between the patch electrode and the computer. The patch clamp amplifier was operated with a special software (HEKA Patchmaster Version 2x73.2, Elektronik Dr. Schulze GmbH, Lambrecht, Germany) installed on the computer. Additionally, single channel data acquisition was done with an amplifier EPC7 (HEKA, Lambrecht, Germany) under the control of the software PULSE (HEKA, Lambrecht, Germany). The signal was moved to an AD/DA converter (ITC-16, Instrutech Corp., Elmont, NY, USA), digitalized and saved on a computer. Any signal recorded In the whole-vacuole or excised patch configuration passed first a 10 kHz filter and subsequently in series a second filter of either 5, 2.9 kHz or 1.3 kHz , respectively. Filtering was enabled, by either built-in components of the EPC10 amplifier or an external low-pass filter (npi electronic GmbH, Tamm, Germany) when the EPC7 amplifier was used. Data points were collected in intervals from 10 µs to 100 µs in whole-vacuole and 1 ms in excised patch configuration. The patch clamp amplifiers, the control unit and power supply of the micromanipulators, the peristaltic pumps and the computer were mounted outside of the Faraday cage.

3.2.3. Performing whole-vacuole experiments

For patch clamp experiments the patch pipette was moved with the micromanipulator under visual control into the bath medium. After compensation of the *Offset potential* (the difference in the electrical potential of the measuring and reference electrode), a test pulse of +10 mV (hold for 10 ms) was continuously applied from a holding voltage of 0 mV to the patch pipette (Fig. 6). Accordingly, changes in the patch pipette resistance could be observed enabling to determine whether a Giga-ohmic seal resistance has been established and to differentiate between different patch clamp modes. When the tip of the glass microelectrode was directed towards the vacuole membrane, its touching of the membrane caused a delicate membrane invagination into the patch pipette. At this point the resistance of the patch electrode already slightly increased. Gentle suction finally resulted in the required Giga-ohmic patch-pipette resistance indicating the successful establishment of the *vacuole-attached* configuration. Fast relaxing capacitive current responses to the +10 mV test pulse arising from electrostatic charging of the components within the measuring chamber were compensated via the patch clamp amplifier. When then a 10-ms lasting voltage pulse of ±900 mV were simultaneously applied with slight suction, and in turn the membrane patch in the patch pipette only but not the Gigaseal was destroyed, large slowly relaxing capacitive current responses (C_{slow}) to the test pulse were recorded. The appearance of these capacitive current transients indicated the successful transition from the *vacuole-attached* into the *whole-vacuole* mode because they resulted from the fact that the membrane acts not only as a resistor but also as a capacitor. Therefore, compensation of these capacitive spikes (C_{slow}) via built-in components of the amplifier specified the membrane capacitance (C_m). As soon as the whole-vacuole mode was established, access of the patch pipette to the much smaller vacuole lumen was achieved, resulting in an equilibration of the vacuole sap with the patch pipette solution (Schulz et al. 2011). Usually, it was waited for about eight minutes to accomplish this equilibration process and in turn to allow patch-clamp recordings under controlled solute conditions on both sides of the membrane. Before the patch clamp experiments were started, the serial resistance (R_s) was controlled, giving a feedback information about the quality of the electrical access of the patch pipette to the vacuole lumen. The serial resistance were usually less than 12 Mohm. Higher R_s values in combination with high membrane current amplitudes can lead to strong errors in the clamp voltage. For data acquisition adequate pulse protocols

were applied either in the voltage-clamp or current-clamp mode (chapter 3.2.7). The resulting electrical responses were recorded and stored on a personal computer for off-line analysis. Under the solute conditions of the patch clamp experiments, liquid junction potentials (Neher, 1992) did not appear and therefore the clamped voltages had not to be corrected.

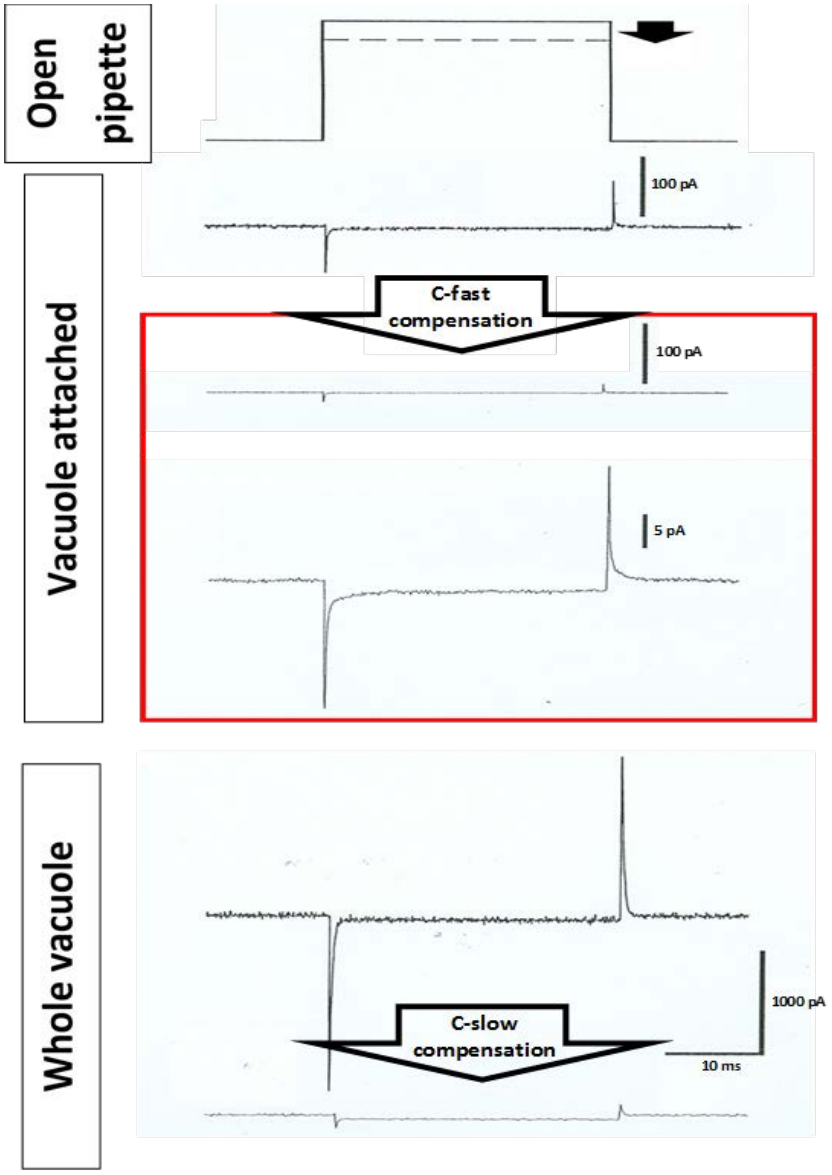

Figure 6. Establishment of the whole vacuole configuration.

Change in the current responses to a +10 mV voltage pulse when the patch pipette was open and just immersed in the bath solution or already attached to the vacuole membrane in the vacuole-attached or whole-vacuole configuration. Steps are illustrated according to Hamill et al. 1981. For details, please see the main text.

3.2.4. Reference and patch electrode

Patch clamp experiments were carried out with two silver/silver chloride electrodes: the reference electrode and the measuring patch electrode. The silver wires (WPI, Sarasota, USA) of both electrodes were electrolytically coated with a silver chloride layer. For this, the silver wire was immersed in 1 M KCl and connected to the negative pole of a 6 V alkaline battery as a direct voltage source. Another silver wire was fixed at the cathode of the power supply. As a result of this electrical circuit, AgCl layer was formed at the silver wire of the anode while electrons were transferred to the cathode (Numberger and Draguhn 1996).

$$Ag^0 + Cl^- \leftrightarrow AgCl + e^-$$

The silver/silver chloride wire of the reference electrode was placed in a polyethylene tube which was filled with 3 M KCl solution and sealed at its opening with 2% agarose gel prepared again on the basis of 3 M KCl. The agar bridge prevented the leakage of 3 M KCl and cytotoxic silver ions into the bath medium, while at the same time the electrical conductivity with the bath solution was maintained. The silver wire of the measuring patch electrode covered with a dark layer of silver chloride was placed in the holder, that connected the patch pipette to the preamplifier. Another core of the patch pipette was a tapered glass capillary (tempered borosilicate glass; 1,05 mm inner diameter, 1.5 mm outer diameter, 80 mm length, GB150T-8P, Science Product, Hofheim, Germany). The glass capillaries were internally coated with a hydrophobic reagent Sigmacote® (Sigma, Munich, Germany) which facilitated the stabilization of a *gigaseal* with vacuole membranes as known from experience. The tapered shaping of one end of the glass capillary was obtained by several stages of preparation. Initially, capillaries were placed in a vertical pipette puller (Narishige PP-83, Narishige Scientific Instruments, Tokio, Japan). Due to applied high temperature and gravity, glass pipettes with a more or less tapered tip were formed in two pulling steps. The form and diameter of the tip opening was specified by the applied temperature. Using a Microforge (Zeiss ID03, Carl Zeiss, Jena, Germany), the surface of glass pipette was then coated close to the tip - without plugging it - with a hydrophobic silicone material (Sylgard 184 silicon elastomer kit, Dow Corning Corporation, Midland, MI, USA). This outer layer reduced the amount of electrostatic charging of the glass pipette in the bath medium and, in turn, the background noise. In a last step, the glass pipette tip was polished with a heated platinum-iridium wire. Thereby, the geometry of

the pipette tip was optimized and sharp edges of the glass pipette were eliminated, supporting the formation of a *gigaseal*. Such a prepared glass pipette was filled free of air bubbles with pipette solution to 2/3 of its length and pulled over the silver/silver chloride wire of the patch electrode placed at the preamplifiers holder. Patch pipettes prepared for *whole-vacuole* experiments had a pipette resistance of 3 to 6 MΩ, and those used for single channel recordings had a pipette resistance of 8 to 24 MΩ.

3.2.5. Sign convention of electric potentials

Voltages and ion currents are presented in accordance with the sign convention proposed for endomembrane's by Bertl et al. (1992). It unifies that the electrical potential is always given for the cytoplasmic side of the endomembrane, while the electrical potential at the luminal side of the membrane is set to 0 mV. Then, a negative ionic current corresponds to the influx of cations into the cytosol, or the efflux of anions out of the cytosol. Vice versa, a positive ionic current can be caused by cation efflux out of the cytosol, or the influx of anions into the cytosol. Thus, the vacuole lumen can be practically considered as an extra-cytosolic space.

3.2.6. Standard pipette and bath solution for patch clamp experiments

All chemical substances used in this thesis were derived from the following companies: AppliChem GmbH (Darmstadt, Germany), Sigma-Aldrich Chemie GmbH (Steinheim, Germany), Merck KGaA (Darmstadt, Germany) and Carl Roth GmbH (Karlsruhe, Germany). The pH in the solutions was adjusted by titration with appropriate buffers using a digital pH meter 646 Calimatic (Knick Elektronische Messgeräte GmbH & Co.KG Berlin, Germany). The final step in preparation of all patch clamp solutions was the adjustment to a suitable osmolality with D-sorbitol under the control of a Vapor Pressure Osmometer 5520 (Wescor, Utah, USA).

Table 1. Solutions for whole-vacuole measurements

Pipette solution 0 mM Ca^{2+}	**Pipette solution 10 mM Ca^{2+}**	**Bath solution 1 mM Ca^{2+}**
150 mM KCl	150 mM KCl	150 mM KCl
0 mM $CaCl_2$	10 mM $CaCl_2$	1 mM $CaCl_2$
2 mM $MgCl_2$	2 mM $MgCl_2$	-
0.1 mM EGTA	-	-
10 mM HEPES	10 mM HEPES	10 mM HEPES
pH 7.5 adjusted with Tris	pH 7.5 adjusted with Tris	pH 7.5 adjusted with Tris
π= 500 adjusted with D-sorbitol	π= 500 adjusted with D-sorbitol	π= 500 adjusted with D-sorbitol

Table 2. Solutions for single channel measurements

Pipette solution pH=5.5	**Pipette solution pH=7.5**	**Bath solution**
100 mM KCl	100 mM KCl	100 mM KCl
0 mM $CaCl_2$	0 mM $CaCl_2$	0.5 mM $CaCl_2$
2 mM $MgCl_2$	2 mM $MgCl_2$	-
2 mM EGTA	2 mM EGTA	-
10 mM MES	10 mM HEPES	10 mM HEPES
pH 5.5 adjusted with Tris	pH 7.5 adjusted with Tris	pH 7.5 adjusted with Tris
π= 400 adjusted with D-sorbitol	π= 400 adjusted with D-sorbitol	π= 400 adjusted with D-sorbitol

Table 3. Pipette solutions for current clamp measurements.

Pipette solution 0 mM Ca^{2+}	**Pipette solution 1 mM Ca^{2+}**	**Pipette solution Cs^{+}**
150 mM KCl	150 mM KCl	150 mM CsCl
0 mM $CaCl_2$	1 mM $CaCl_2$	0 mM $CaCl_2$
2 mM $MgCl_2$	2 mM $MgCl_2$	2 mM $MgCl_2$
0.1 mM EGTA	-	0.1 mM EGTA
10 mM HEPES	10 mM HEPES	10 mM HEPES
pH 7.5 adjusted with Tris	pH 7.5 adjusted with Tris	pH 7.5 adjusted with Tris
π= 500 adjusted with D-sorbitol	π= 500 adjusted with D-sorbitol	π= 500 adjusted with D-sorbitol

Table 4. Bath solutions for current clamp measurements.

Bath solution 1 mM Ca^{2+}	**Bath solution 2 mM Mg^{2+}**	**Bath solution Cs^{+}**
150 mM KCl	150 mM KCl	150 mM CsCl
1 mM $CaCl_2$	1 mM $CaCl_2$	1 mM $CaCl_2$
-	2 mM Mg Cl_2	2 mM $MgCl_2$
10 mM HEPES	10 mM HEPES	10 mM HEPES
pH 7.5 adjusted with Tris	pH 7.5 adjusted with Tris	pH 7.5 adjusted with Tris
π= 500 adjusted with D-sorbitol	π= 500 adjusted with D-sorbitol	π= 500 adjusted with D-sorbitol

3.2.7. Pulse protocols

3.2.7.1. Whole-vacuole measurements

For voltage-clamp experiments in the whole-vacuole mode a voltage pulse protocol was applied that consisted of three segments, and the corresponding current responses were recorded (Fig. 7). In the first segment the vacuolar membrane was clamped to a membrane voltage of -60 mV for 300 ms, maintaining the population of vacuolar TPC1 channels in a closed non-conducting channel state. Then, the clamp voltage was instantaneously varied to voltages in the range of -80 mV to +110 mV in 10-mV steps. These voltages pulses lasted 1 s and were applied essentially to observe the voltage-dependent activation of TPC1 currents. In the last segment the membrane was instantaneously clamped to -60 mV for 300 ms to induce deactivation of TPC1 channels and to record the relaxing tail currents. Before the 3-segment voltage pulse was started again, the holding voltage of -60 mV was kept for further 3.4 s without recording the membrane currents. Thus, one total pulse interval lasted 5 seconds.

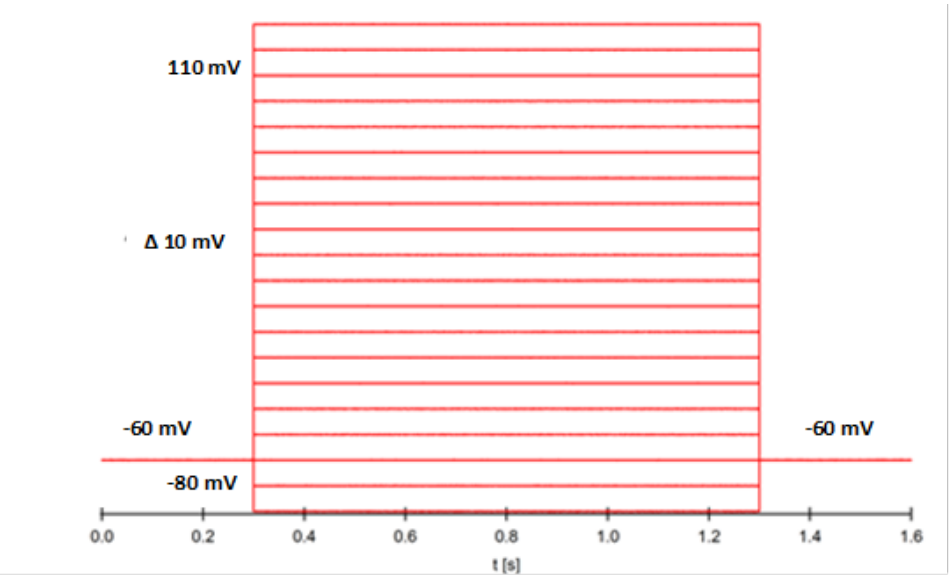

Figure 7. Pulse protocol 1 used for whole-vacuole current recordings.

3.2.7.2. Single channel measurements

After stabilizing the excised patch configuration with the luminal side of the vacuolar membrane facing the patch pipette solution, a two-pulse voltage protocol was applied to the membrane patch (Fig. 8). First, the membrane was clamped to -60 mV for 300 ms, to deactivate the channels and thereby to standardize the initial TPC1 channel state. Then, a 60-s-lasting activation pulse to either +35 mV, +40 mV, +45 mV or +50 mV was applied.

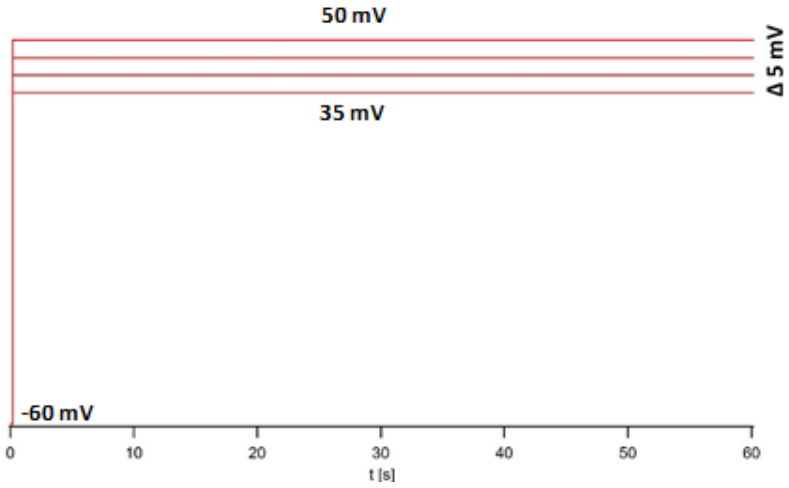

Figure 8. Pulse protocol 2 used for single channel measurements.

3.2.7.3. Current clamp measurements

In the current-clamp mode, current was injected to set the membrane potential to a certain value as indicated in the respective experiments (chapter 4.4). After residing for 1 s at this polarized membrane state, currents of different amplitudes (10, 30, 70, 150, 300 pA) were injected for 200 ms (Fig. 9). The corresponding current-induced changes in the membrane voltage were recorded for a total duration of 12.2 s after each current injection pulse.

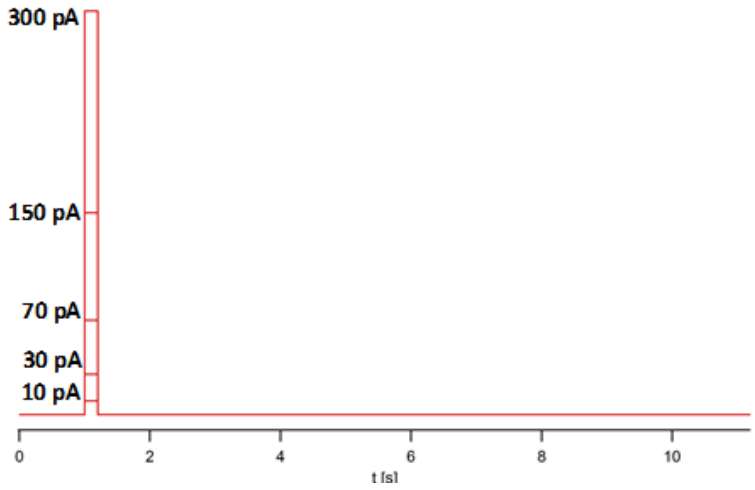

Figure 9. Pulse protocol 3 used for current clamp measurements.

3.2.8. Data analysis

Raw data were exported from the stored Patchmaster or Pulse data file as an IGOR text data format for off-line analysis with the software program IGOR Pro 6 (Wave Metrics Inc., Lake Oswego, USA). To compensate differences in current responses due to different vacuole sizes, the macroscopic membrane currents were normalized to the membrane capacity determined via compensation of the capacity currents (chapter 3.2.3). The membrane capacity can be used as a measure for the vacuole size, because the membrane behaves as a plate capacitor and therefore the membrane capacitance is proportional to the membrane surface (Hille, 1992). The figures were prepared using the software programs IGOR Pro 6 (Wave Metrics Inc., Lake Oswego, USA) and Corel DRAW X7 (Corel Corporation., Ottawa, Canada)

3.2.8.1. Determination of the steady-state current density, the relative channel open probability and half-activation time

In the steady-state the number of activated channels and in turn the corresponding current amplitudes remain unaltered. However, the macroscopic current amplitude (I_{ss}) recorded in the steady-state at a certain membrane voltage depends on (i) the number of channels present in the membrane (N), (ii) single-channel current amplitude (i ($V-E_N$)) which is defined

by the applied membrane voltage (V) and Nernst potential of the transported ion (E_N), and (iii) the voltage-dependent channel open probability P_o (V) as followed:

$$I_{ss}\,(V) = N \bullet i\,(V\text{-}E_N) \bullet P_o\,(V)$$

To determine the steady-state current amplitude at each clamped voltage in the range of -80 mV and +110 mV, the mean current amplitude was determined for the last 10 ms of the 1-s-lasting voltage pulse (Fig. 7, Fig 10A, chapter 3.2.7.1). Since the membrane capacitance is proportional to the membrane surface, for each whole-vacuole experiment the obtained I_{ss} values were normalized to the membrane capacity of the individual vacuole (I_{ss}/C_m) (chapter 3.2.7.1). Subsequently presented as a function of the membrane voltage in a current/voltage (I/V) graph (Fig. 10B).

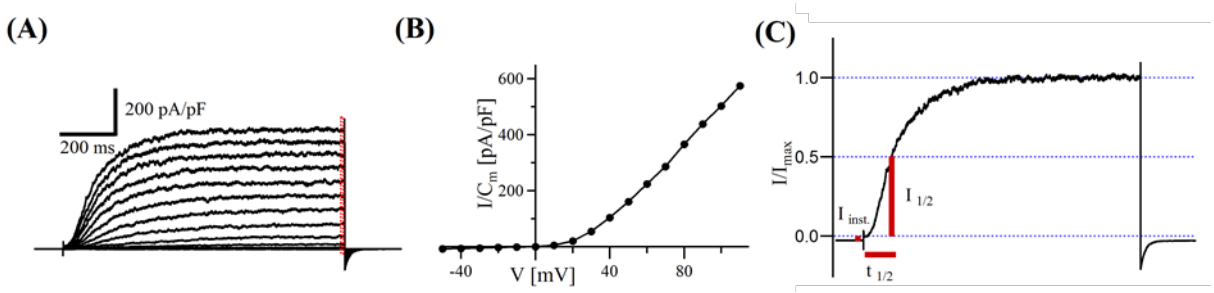

Figure 10. Data analysis 1 of whole-vacuole recordings: steady-state current density.

(A) Current traces recorded in response to different voltage pulses in the range of -60 mV to 110 mV in 10 mV steps. Holding voltage was -60 mV. Red dotted region indicates the current responses to the voltage pulses in the last 10 ms used to determine the mean steady-state current amplitude. (B) Current-voltage characteristic of the SV/TPC1 channel. Averaged current amplitude at equilibrium (Iss; red marked region in A) normalized to the size of the vacuole (I_{ss}/C_m) were plotted against the respective applied membrane voltage. (C) Current trace evoked upon +110 mV stimulation, was normalized to maximal steady-state current amplitude and the instantaneous currents (I_{inst}) were subtracted. Red line indicates half-maximal current amplitude ($I_{1/2}$) with the half-activation time $t_{1/2}$.

Activation half-times $t_{1/2}$ of the TPC1 channel is the time, at which the time-dependent currents evoked upon a certain voltage pulse reached 50% of the maximum steady-state current amplitudes. To determine half-activation time, first the instantaneous ($I_{inst.}$) current amplitude was subtracted. Subsequently, the current response elicited upon a certain voltage was normalized to maximum current amplitude (I_{max}), and the time required to reach 50% of I_{max}, which is defined by the difference in the two time points $t(I_0)$ and $t(I_{1/2})$, was determined (Fig. 10C).

To determine the relative probability of channel opening (rel. P_o) at each applied membrane voltage, tail currents were analysed. For this, after prepulse-voltages in the range of -80 to +110 mV were applied, tail currents were recorded at -60 mV (Fig. 7, chapter 3.2.7.1). Due to the identical driving force ($V-E_N$) for the ion movement through open TPC1 channels at the tail pulse voltage of -60 mV, the instantaneous tail current amplitude only depends on the number of channels which were open at the end of the prepulse-voltage. The number of open channels is defined at each voltage by the voltage-dependent channel open probability ($N*P_o(V)$). Assuming a constant number of channel proteins present in the membrane, therefore the instantaneous tail current amplitude is a measure for the relative voltage-dependent channel open probability (rel. P_o (V)). The instantaneous tail current density was determined (Fig. 11), plotted against the corresponding membrane voltage and normalized to the maximum likelihood of the opening. According to Pottosin et al. (2004) and Dadacz-Narloch et al. (2011), a three step model ($C_2 \leftrightarrow C_1 \leftrightarrow O$) for TPC1 channel gating consisting of two closed and one open state was assumed. Therefore, the slope of the data points were fitted with a two-phase Boltzmann equation as followed:

$$rel.P_o(V) = P_{max}/(1+\exp(-z_1 \bullet (x-V_1)/25.26)\bullet(1+\exp(-z_2 \bullet (x-V_2)/25.26)))$$

with two midpoint voltages for activation (V_1 and V_2) and fixed z1 (0.77) and z2 (2.9) values for equivalent gating charges, which correspond with the movement of charge(s) during channel opening.

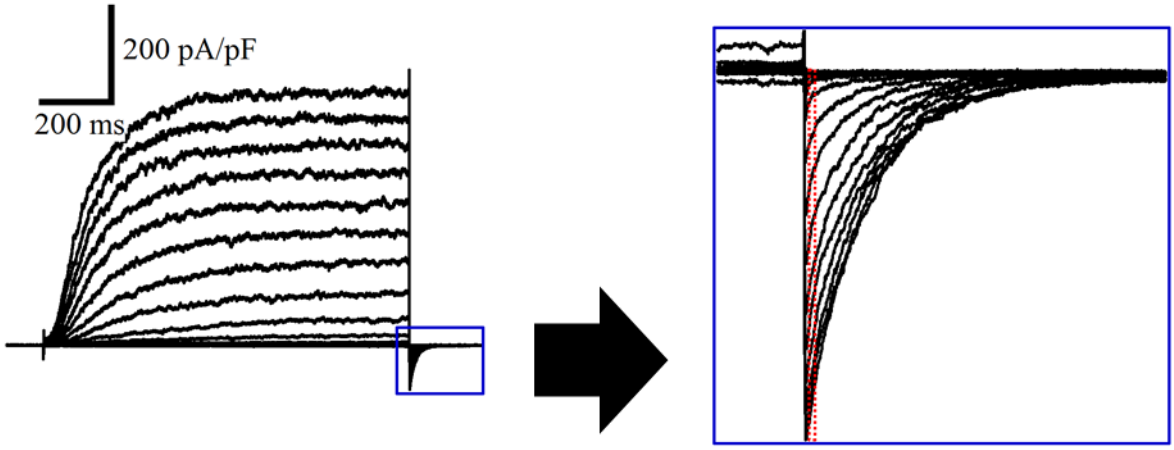

Figure 11. Data analysis 2 of whole-vacuole recordings: tail currents.

The macroscopic current responses to several depolarizing voltage pulses are shown in the range from -80 to +110 mV. The voltage pulses were increased in 10 mV steps. After these prepulse-voltages tail currents I_{tail} (magnified at the right) were induced by jumping to the deactivating holding voltage of -60 mV. The instantaneous tail current amplitudes were determined at the red marked spot and shown as a function of the respective prepulse-voltage.

3.2.8.2. Determination of the single channel conductance

To determine the single-channel conductance, the single-channel current amplitude was determined for voltages in the range of +30 mV to +55 mV (Fig. 12A). For this, *all-point* histograms were created from the recorded single-channel current traces, giving the number how often distinct current levels were monitored. The derived peaks reflect the prominent current levels at which (i) the channels were closed and (ii) one or more channels were simultaneously in the open state. To calculate the single channel amplitude from the averaged difference between the peak maxima, the peak maxima were determined by fitting the histogram with a Gaussian equation (Fig. 12B). The single channel amplitudes deduced for several experiments were then plotted as a function of the corresponding membrane voltages. The total data set was subjected to global fitting with a linear function ($y = ax + b$), to derive the channel conductivity from the slope a of the linear function (Fig. 12C).

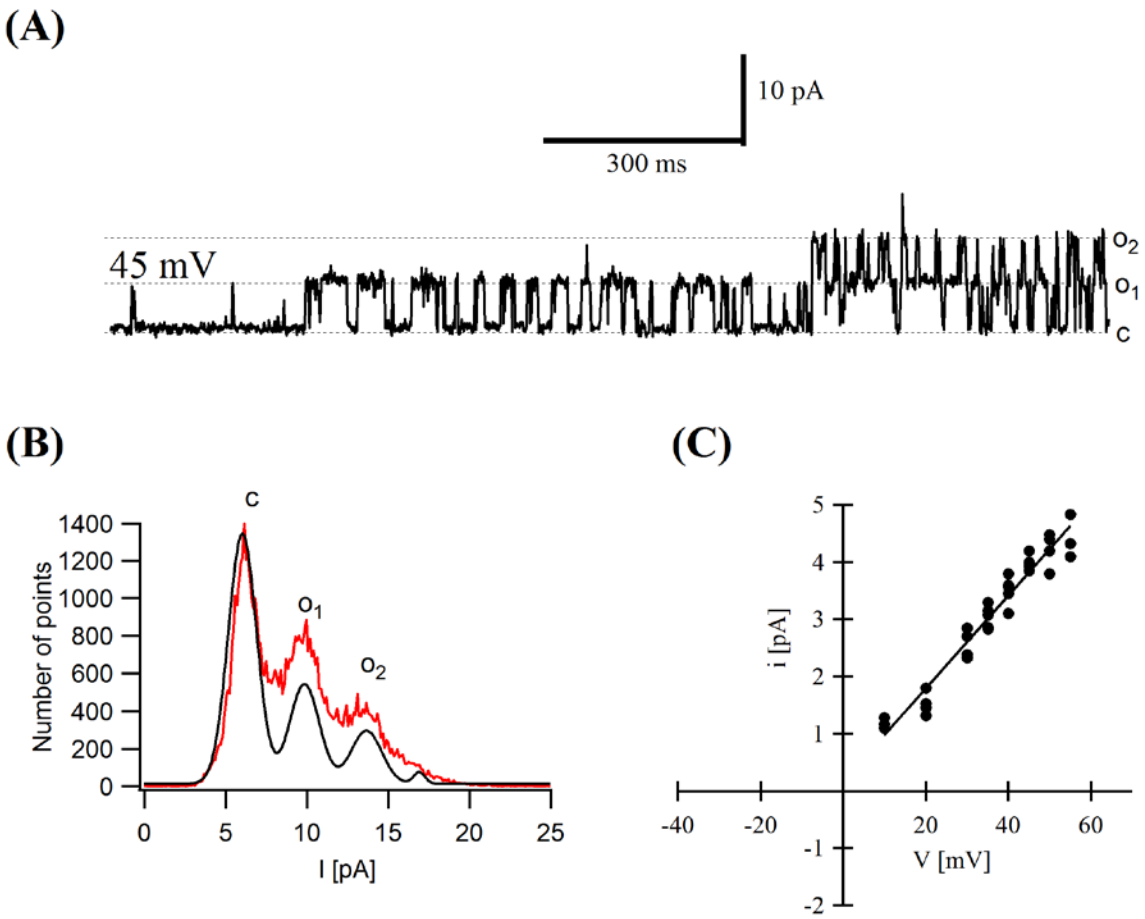

Figure 12. Data analysis for determination of single channel conductance.

(A) Single channel current trace evoked upon +45 mV voltage stimulation were analyzed for distinct current levels such as C, O_1, O_2 indicting closed channels, 1 or 2 simultaneously open channels, respectively. (B) All-Point current amplitude histogram (red) derived for the single channel current trace shown in (A) were fitted with a Multi-Gauss equation (black). Peak maxima represent current levels where the channels were closed (C) or 1 or 2 channels (O_1, O_2) open. (C) i/V graph with single channel currents of several experiments determined for different voltages via All-point histograms as shown in B. Red line gives the global fit of the total data points.

3.3. Plant protoplast transformation

3.3.1. User reaction

Point mutation into cDNA of TPC1 was introduced, according to a modified USER fusion method (Norholm, 2010). *TPC1*/pSAT1365 was used as a template for USER mutagenesis. Overlapping primer pairs – covering 8-11 bp of the mutagenesis site – carrying the desired mutation at their respective 5'-end were designed (chapter 3.3.1.2). The requirement for

USER-based mutagenesis was an adenosine (A) at the 5'-end and a thymidine (T) 8-11 bp downstream of the desired fusion product. This T residue in the tail region of the desired USER primers was replaced by an uracil (U). The site of mutagenesis was located within this tail region (Dadacz-Narloch et al., 2011)

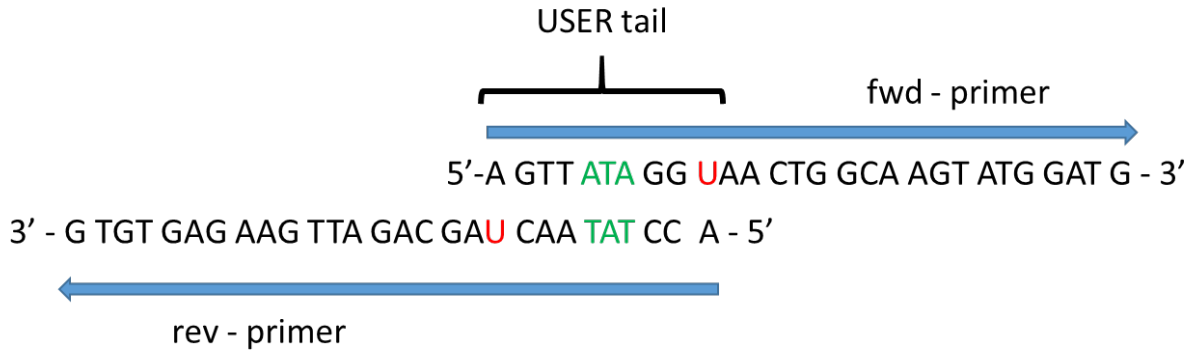

Figure 13. Principle of generation of point mutation with overlapping USER primers

The localization of uracil (red) and adenine at the beginning and end of the USER-tail is shown. To introduce a certain point mutation, corresponding base pairs must lie within the USER-tail, as highlighted here in green as an example, and have to be exchanged in an appropriate manner.

3.3.1.1. PCR reaction

By means of the polymerase chain reaction, specific DNA fragments can be amplified *in vitro*. It was based on three reaction steps, which were repeated several times. A reaction mix, which contained a mixture of G, A, T, C – deoxyribonucleotide, short primers and the DNA template, to be amplified firstly was denatured at 94°C. After cooling to the primer hybridization temperature, the primers hybridized with the complementary sequences of the starting DNA. In the third reaction step, the DNA polymerase (*PfuX*, Stratagene, CA, USA) filled the missing strands with free nucleotides, beginning with the 3'-end of the attached primer. This step is referred to elongation or amplification. Finally, an exponential amplification of the starting DNA was obtained. In this work the following standard reaction approach was used:

Reaction mix (total volume 50 µl adjusted with H_2O) (RM):

- 1 µl DNA-Template (~10 ng)
- 10 µl Reactions buffer (5x)
- 1 µl dNTPs (10 mM)
- 1 µl sense Primer (10 µM)
- 1 µl antisense Primer (10 µM)
- 1 µl 0.25 U DNA-Polymerase

Table 5. PCR program for TPC1/pSAT1365 plasmid multiplication.

Initial Denaturation	98°C	90 s	
Denaturation	98°C	10 s	x 30
Annealing	55°C	30 s	
Elongation	72°C	60 s	
Final Elongation	72°C	180 s	

Following primer pairs were used in the reaction mix to generate the M629I, M629T and M629S channel mutants:

Table 6. Primers for USER reaction.

TPC1 USER	fwd 5'-GGC TTA AUA TGG AAG ACC CGT TGA TTG G-3' rev 5'-GGT TTA AUT CAT GTG TCA GAA GTG GAA CAC TC-3'
M629I	fwd 5'- AGT TAT AGG UAA CTG GCA AGT ATG GAT G-3' rev 5'- ACC TAT AAC UAG CAG ATT GAA GAG TGT G-3'
M629T	fwd 5'- AGT TAC GGG UAA CTG GCA AGT ATG GAT G-3' rev 5'- ACC CGT AAC UAG CAG ATT GAA GAG TGT G-3'
M629S	fwd 5'- AGT TTC GGG UAA CTG GCA AGT ATG GAT G-3' rev 5'- ACC CGA AAC UAG CAG ATT GAA GAG TGT G-3'

3.3.1.2. Sequencing and sequence analysis

Sequencing of mutated TPC1 genes (Met629 mutants) was carried out by an external company (GATC Biotech AG, Constance, Germany). The sequencing reactions were based on the dideoxy-method according to Sanger (Sanger et al., 1977). For non-radioactive sequencing, the DNA was labelled with fluorescent dyes, excited and measured by a laser. Previously, constructed primers were used for the sequencing, which were complementary to the respective DNA (Table 7). All sequencing was performed with purified DNA. The derived DNA sequence data were analysed using the VectorNTI program (Invitrogen, InforMax, Karlsruhe).

Table 7. Sequencing primers.

TPC1 USER	fwd 5'-GGC TTA AUA TGG AAG ACC CGT TGA TTG G-3'
(1-594)	rev 5'- CCA AAA GAT TCG GGA ACC TTC A-3'
(496-1089)	fwd 5'-GTT GAT GTG CTG GTT GAC TTT CTG-3'
(1090-1683)	Fwd 5'-AGA CTC AGA CAA AAA CGG GGA GAT TG-3'
(1684-2218)	Fwd 5'-GCC ATA TTT AGG GAC CAT TTT CTG CG-3'

3.3.2. Bacteria transformation and growth

Aliquots (50 µl) of *E. coli* bacteria (*MRF* strain) were stored at -80°C. Plasmid DNA containing the coding sequence of the TPC1 channel variant as eGFP-fusion construct (2 µl) was added to one thawed aliquot, mixed and heated at 42°C for 50 s. In the following, the sample was incubated for 3 min on ice and then plated an ampicillin-containing agar plates. As result, only bacteria harbouring the TPC1-eGFP plasmid with an ampicillin resistance were grown. Single transformed bacterial colonies were selected and transferred from agar plate to 5 ml tubes filled with LB medium (Lucia broth: 10 g trypton, 5 g yeast extract, 10 g of sodium chloride, 1 l of de-ionized H_2O) for overnight incubation. Next day 1 ml of overnight bacterial culture was added to approximately 150 ml LB medium in sterile Erlenmeyer flask. The LB medium of both incubation steps (bacteria grown in 5 ml tubes and 150 ml Erlenmeyer flask) was supplemented with 50 µg/ml ampicillin antibiotic as selective substance. The suspension was incubated at 37°C for about 16 h overnight on a shaker (New Brunswick Scientific Innova 4230 Incubator).

3.3.3. Isolation of plasmid-DNA and determination of DNA concentration

Isolation of plasmid DNA from *E. coli* (chapter 9.2) was carried out using QIAGEN Plasmid Midi Plus Kit (QIAGEN, Hilden, Germany) according to the manufacturers protocol. The obtained DNA was dissolved in deionized water, and the concentration of the nucleic acids was specified by measuring the absorbance (OD) of the sample at wavelengths around 260 nm and 280 nm with a spectrophotometer (NanoDrop Products, Wilmington, USA). DNA concentration was calculated by light absorbance at 260 nm, while the ratio of OD260 nm and OD280 nm allowed to determine the purity of the isolated DNA. Samples were used for transient transformation of plant protoplasts.

3.3.4. Transient SV/TPC1 channel expression in protoplasts

Transient transformation of mesophyll protoplasts from the TPC1 loss-of-function *A. thaliana* mutant *tpc1-2* was performed according to the protocol of (Yoo et al., 2007). For protoplast transformation about 20-30 leaves were detached from plants grown under conditions as described in section 3.1.1.1. Leaves were cut with a razor blade into thin strips of about 1 mm width and immediately transferred to a petri dish filled with filtered (50 µm sterile disposable filter, Minisart, Hartenstein, Germany) enzyme solution (section 3.3.5). To infiltrate the plant material with the digestive enzymes, the petri dish wrapped with an aluminium foil was then kept in a desiccator under vacuum for a period of 10 min. The following enzyme incubation lasted 3 hours at room temperature and allowed degradation of cell walls and the release of the mesophyll protoplasts. Then, the suspension was filtered through a nylon mesh (mesh size: 50 µm) by washing with buffer W5 (section 3.3.5). The obtained filtrate (about 50 ml) was centrifuged at 4°C for 2 min at 100 x *g* (no acceleration or deceleration) (Eppendorf 5810R Eppendorf AG, Hamburg, Germany). The supernatant was carefully decanted, while the precipitate was re-suspended in about 4 ml of W5 buffer and left for 30 minutes on ice. The supernatant was removed again, and the remaining protoplasts were re-suspended in MMg solution (section 3.3.5). The obtained suspension had a bright green colour due to the enriched mesophyll protoplasts (1-2 x 10^6). Then, 200 µl of protoplast-MMg suspension was mixed with 20 µg DNA plasmid which was dissolved in 200 µl water and carried the coding sequence of the TPC1-eGFP channel construct. After 220 µl PEG (polyethylene glycol) solution

(section 3.3.5) was additionally added and thoroughly mixed with the rest of the components, the sample was incubated for 15 minutes at room temperature. To stop the reaction, 880 µl W5 was added to the suspension which was then centrifuged for 1 min at 4°C, and 100 x *g*. The protoplast-containing precipitate was re-suspended in 1.5 ml of W5 and kept in a small petri dish (Ø = 3.5 cm) wrapped in aluminium foil for two-day incubation at room temperature. Afterwards patch clamp experiments were performed with transformed protoplasts. Efficiency of transformed protoplasts reached an amount of up to 90% of the total released protoplasts used for the transformation.

3.3.5. Solutions used for protoplast transformation

Enzyme solution

- 1.5% (w/v) Cellulose R-10 (Yakult, Tokyo, Japan)
- 0.4% (w/v) Mazerozyme R-10 (Yakult, Tokyo, Japan)
- 0.4 M mannitol
- 20 mM KCl
- 20 mM MES, adjusted to pH 5.7 with Tris
- 10 mM $CaCl_2$
- 0.1% BSA (w/v) (bovine serum albumin)

Before addition of $CaCl_2$ and BSA, the mixture was heated for 10 minutes at 55°C, and then discontinued to regain the room temperature.

W5-solution

- 154 mM NaCl
- 125 mM $CaCl_2$
- 5 mM KCl
- 2 mM MES adjusted to pH 5.7 with Tris

MMg-solution

- 0.4 M mannitol
- 15 mM $MgCl_2$
- 4 mM MES adjusted to pH 5.7 with Tris

PEG-solution

- 20-40% PEG 4000 (w/v) (Sigma-Aldrich GmbH, Munich, Germany)
- 0.2 M mannitol
- 100 mM $CaCl_2$

The solution was prepared 3-4 h prior to transformation. Mixing of the ingredients demanded around 4 h.

3.4. Gene expression analyses

In order to determine and to compare the expression level of different TPC1 channel variants, mRNA was isolated from *Arabidopsis thaliana* plants, cultivated in the climate chamber as described in chapter 1.1. Using a reversed transcriptase, cDNA was generated from the mRNA, which was then quantified by quantitative real-time polymerase chain reaction (qRT-PCR). The number of mRNA molecules of TPC1 channel was normalized to the amount of actin molecules 2 and 8.

3.4.1. Isolation of RNA

A single leaf from *Arabidopsis* WT or mutant plants were harvested. After removal of the major veins the plant material was placed in 1.5 ml Eppendorf tube. After sampling, material was

immediately frozen in liquid nitrogen. The plant material was teared by shaking at a high frequency (30 Hz) for 1 minute in the Tissuelyser II system (Qiagen). Total RNA was then isolated using the RNeasy Plant Mini Kit (www.quiagen.com) according to the manufacturer's protocol. An additional DNA digestion step followed before total RNA was extracted for cDNA synthesis by precipitation as described by Logemann *et al.* (1987). During work with ribonucleic acids only sterile materials and RNase-free solutions were used. The water contained 0.1% Diethylpyrocarbonate (DEPC) (v/v) and was autoclaved. For each mutant three to five replicates were generated.

3.4.2. Reverse transcription

Synthesis of cDNA (complementary DNA) from mRNA was performed according to the protocol described in Biemelt *et al.* (2004). For this purpose, RNA dissolved in 14 µl of RNAase-free water was mixed with 6.3 µl MASTERMIX (0.8 µl Oligo-dT-Primer (100 µM), 1 µl dNTPs (10 mM), 4 µl RT-Puffer (5x, Promega), 0.5 µl RNAase inhibitor). This mixture was incubated for about 2 minutes at 70°C, and then cooled on ice. In the following 0.8 µl MMLV-RT reverse transcriptase (100 U/µl, *Maloney Murine Leukaemia Virus Reverse Transcriptase*, Promega, Mannheim, Deutschland) was added to the sample, which was then incubated for 60 minutes at 42°C. Taking advantage of the 3´-poly(A) tail of the mRNA, the reverse transcriptase MMLV-RT used the Oligo-dT-Primer to synthesize a single-strand cDNA. After mRNA denaturation the reverse transcriptase MMLV-RT generated a double-strand cDNA which was used for either qRT-PCR reaction or stored at -80°C.

3.4.3. Quantitative real-time polymerase chain reaction (qRT-PCR)

Number of TPC1 channel transcripts was quantified with qPCR using the fluorescent dye SYBR®Green (Thermo Fisher Sci-Entific Inc., Waltham, Massachusetts, USA) according to the manufacturer's protocol. In principle, DNA amplification was monitored at each PCR cycle via the proportional increase in the amount of the fluorescent dye bound to the DNA (Rasmussen et al., 1998). Moreover, by analysing the curve of product melting, the PCR product of interest could be differentiated from side-products of the PCR reaction.

In order to avoid binding of the cDNA to the walls of measuring vessels and to adjust its concentration to the measuring buffers, the synthesized cDNA was diluted twenty-fold with H_20 tRNA, i.e. HPLC H_2O (Carl Roth GmbH, Karlsruhe, Germany) was supplemented with 10 ng/µl tRNA (Sigma-Aldrich Chemie GmbH, Steinheim, Germany). The number of TPC1 transcripts of the tested samples was then determined by using a standard curve that was generated from several standard concentrations of the target gene (i.e. 10, 1, 0.1 and 0.01 fg/ml). Two actins (ACT2/8) from *Arabidopsis thaliana* were used as reference genes: actin2 (AT3g18780)/ and actin8 (AT1g49240), and their amount in the tested samples was also estimated on the basis of a separately generated standard curve for these genes. The mixture of the examined respective samples and standard reaction mix (RM) was placed in 96-pit plates (Twin-TEC, Eppendorf) to duplicate and estimate the number of transcripts in real time by using Real-Time-Thermocycler Realplex-x4 (Eppendorf AG, Hamburg, Deutschland).

Table 8. qRT-PCR primers.

Primer	Sequence
TPC1fwd	5‘-CTGTGTATCTACTGCTC-3‘
TPC1rev	5‘-ACGAAATATGTAATGCTC-3‘
AtAct2/8fwd	5‘-GGTGATGGTGTGTCT-3‘
AtAct2/8rev	5‘-ACTGAGCACAATGTT-3‘

Table 9. Standard reaction mix (20 µl) (RM).

ABsolute QPCR SYBR® Green Capillary Mix	10.00 µl
Primer fwd (50 µM)	0.12 µl
Primer rev (50 µM)	0.12 µl
HPLC-H_2O	7.76 µl
Template	2.00 µl

Table 10. qRT-PCR program.

„Hot Start“	95°C	15 min	
Denaturation Annealing Elongation Detection	95°C 60°C 72°C 79°C	15 s 20 s 20 s 10 s 10 s	x 40-45
Melting point of product analysis	95°C 60°C ΔT_m (60°C→95°C) 95 °C	10 s 15 s [0,3 °C/s] 5 s	
End	40 °C	2 min	

3.5. Detection of eGFP fluorescence

Protoplasts were transformed with TPC1-eGFP (enhanced green fluorescent protein) fusion constructs (Cormack et al., 1996). Due to the eGFP label, the subcellular localization of the TPC1 channel variants could be monitored with a confocal laser scanning microscope (LSM 5 Pascal; Carl Zeiss). After vacuoles were released with deionized water, fluorescent images were immediately taken. The microscope was equipped with a lens Zeiss Plan Neofluar 20x / 0,5. The excitation wavelength was 488 nm, and excited fluorescence emission was measured with an emission filter of 505-530 nm. Corel PHOTO-PAINT X7 (Corel Corporation., Ottawa, Canada) was used to adjust the brightness and contrast of the LSM images.

In order to conduct patch clamp experiments on vacuoles released from successfully transformed protoplasts only, vacuoles were illuminated in the measuring patch-clamp chamber by a UV lamp (wavelength less than 400 nm) or diode laser (CNI Optoelectronics, Changchun, China) (wavelength 473 nm) to induce eGFP fluorescence. A transformed vacuole was then identified via detection of the eGFP fluorescent signal by using an emission filter of 490-560 nm.

4. Results

4.1. Identification of intragenic *ouf's* mutants

The single D454N mutation in the TPC1 channel *fou2* is localized at the luminal end of 7th transmembrane domain of the TPC1 channel protein. As a result the channel sensitivity to inhibitory luminal Ca^{2+} ions is strongly reduced leading to hyperactive TPC1 channels (Beyhl et al., 2009). When the plant phenotype of the *fou2* mutant was examined, a strong retarded growth phenotype became visible (Fig. 14; Bonaventura et al. 2007a). Under short-day conditions they manifested a reduced rosette diameter and epinastic leaves with short petioles in the adult stage (Fig. 14; Bonaventura et al. 2007a). Since the *fou2* plants additionally showed an increased production of jasmonate in response to wounding (Bonaventura et al. 2007a), the group of Prof. E.E. Farmer from the University of Lausanne (Switzerland) performed EMS-based secondary mutagenesis with *fou2* plants to gain further insights in the jasmonate signalling pathway (A. Lenglet and Prof. Farmer, pers. communication; Lenglet, Jaslan et al. 2017). Screening of the plants resulted in the selection of eight mutants which were named *ouf1-8* (A. Lenglet and Prof. Farmer, pers. communication; Lenglet, Jaslan et al. 2017). Under short-day conditions all these mutants showed a more wild-type-like growth performance again (Fig. 14). With respect to the size of the rosettes, the length of the petioles and the leaf shape established after growth for 6.5 weeks, the mutant plants could be divided into two major groups. The first one included the mutant lines *ouf1, ouf2, ouf6, ouf7* and *ouf8* which were looking very similar to WT and *tpc1-2* plants. The second group comprised the *ouf4* mutant showing still a smaller rosette size than WT and *tpc1-2* null mutant under short-day condition but the leaf form and length of petioles were similar to WT and *tpc1-2* (Fig. 14; Lenglet, Jaslan et al. 2017).

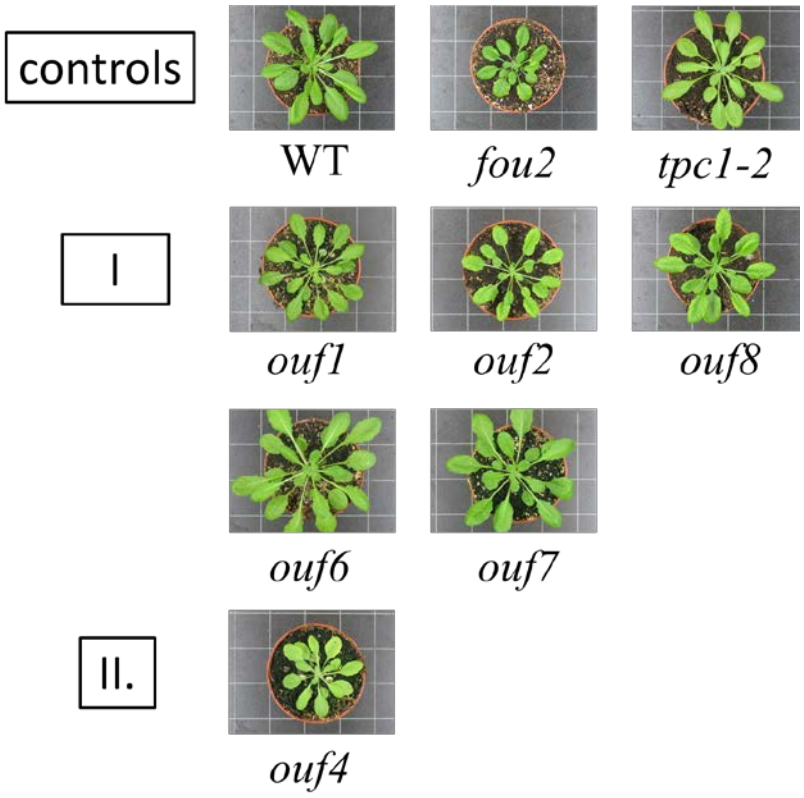

Figure 14. Phenotype of rosette morphology of WT, fou2, tpc1-2 null mutant and ouf mutant plants after growth for 6.5 weeks under short day conditions. Scaling of each square in the background = 3 cm.

Sequencing of the TPC1 gene revealed that in addition to the *fou2* mutation six of these eight *ouf* mutants have a second mutation in the TPC1 gene (Fig. 15) (A. Lenglet and Prof. Farmer, pers. communication; Lenglet, Jaslan et al. 2017). In the *ouf1* mutant deletion of a single nucleotide (guanine) at position 1586 was detected in the TPC1 coding sequence. As a result the three-nucleotide codon (UGG) for tryptophan 529 was affected and changed to a stop codon (UGA). In the TPC1 channel protein structure (W529-) of the *ouf1* mutant this nonsense mutation is present in the luminal part of transmembrane domain S10 (Fig. 15). Similarly, at position 1476 of the TPC1 coding sequence in the *ouf7* mutant a guanine nucleotide was exchanged by adenine leading also to the introduction of a stop codon at position 492 of the amino acid sequence. This mutation was localised in the cytosolic loop between the eighth (S8) and ninth (S9) transmembrane domain of the channel protein (Fig. 15). Three other mutants identified in the intragenic TPC1 region carried one missense mutation, creating new alleles of TPC1 gene. In *ouf2* a substitution of glycine to aspartate at position 583 of the amino acid sequence was identified. This second point mutation in the o*uf2* mutant is localized in the

luminal part of transmembrane domain S11, so between the major voltage-sensing domain S10 and the pore-forming region (Fig. 15).

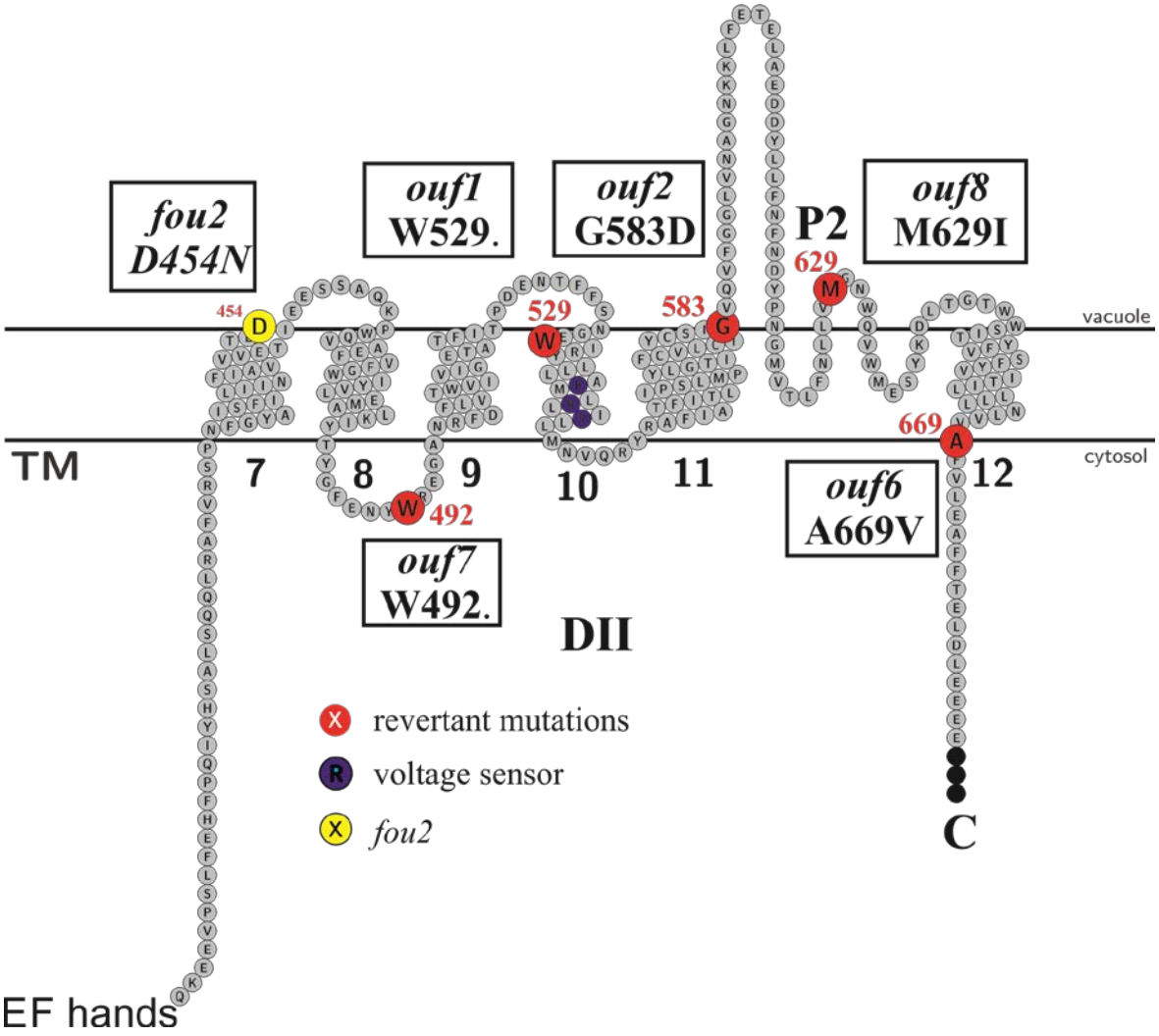

Figure 15. Localization of intragenic ouf mutations in TPC1.

Two-dimensional TPC1 model of second Shaker-like subdomain DII with six transmembrane domains (TM) including the second pore domain (P2). EF indicates the cytosolic calcium binding site within the cytosolic linker region between transmembrane domain 6 of the first Shaker-like subdomain DI (not shown, cf. Fig. 3 in chapter 1.4.1) and TM7 of the second Shaker-like subdomain DII.

Sequencing of the *TPC1* gene from the *ouf6* mutant revealed the replacement of alanine with valine at amino acid position 669, while the *ouf8* mutant contained a missense mutation at amino acid position 629 of the TPC1 channel, causing the insertion of isoleucine instead of methionine. The *ouf6* mutation (A669V) was localized at the C-terminal end of transmembrane domain S12, and the *ouf8* mutation (M629I) within the pore region of the *TPC1* channel protein (Fig. 15). Thus, like the *fou2* mutation, all these *ouf* mutations were

present in the second Shaker subdomain DII of the TPC1 protein (Figs.1, 15). In contrast, the other two *ouf* mutants 4 and 5 did not contain a second mutation in the *TPC1* gene. Except of that, it is not yet known at which position the *Arabidopsis thaliana* genome has been altered in the *ouf4* and *ouf5* mutant (A. Lenglet and Prof. Farmer, pers. communication).

4.2. Expression level in *ouf* mutants

Since the *tpc1-2* null mutant and the *ouf* mutants *ouf*1, *ouf*2, *ouf6* and *ouf8* exhibited a very similar phenotype (Fig. 14), the additional point mutation revealed in the *TPC1* gene of these *ouf* mutants could have impaired the expression of the TPC1 gene. To examine this possibility, the number of TPC1 transcripts were quantified with qRT-PCR. As shown in Figure 16, the number of TPC1 transcripts were comparable for WT and *fou2* plants ranging between three to four thousand transcripts per 10.000 actin molecules and exhibiting a significant difference to the *tpc1-2* knock-out mutant (131±81 transcripts per 10.000 actin) (Fig. 16). The further analysis of *TPC1* gene expression in the *ouf* mutants revealed similar amounts of transcripts in the mutants compared to WT and *fou2* (Fig. 16). Thus, in contrast to the *tpc1-2* knock-out mutant, the *ouf* mutations did not result in strong changes in the *TPC1* expression.

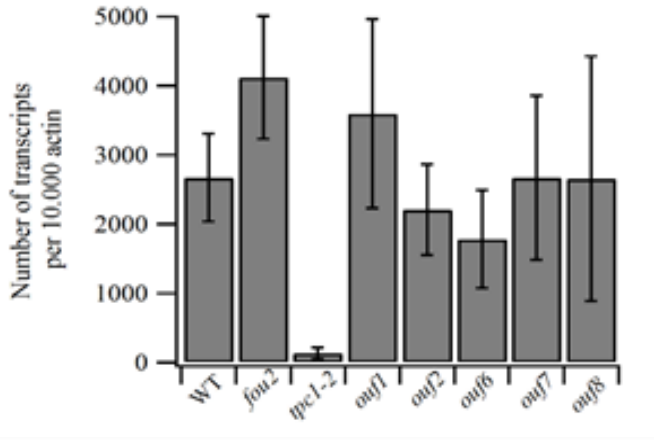

Figure 16. Expression level of TPC1 gene in ouf mutants. qRT-PCR of TPC1 transcripts of unwounded leaves from different plant lines as indicated. TPC1 transcripts were normalized to those of actin 2/8. Bars represent the mean of three to five biological replicates (± SD).

4.3. Patch-clamp characterization of the various *ouf* mutants

To better understand the underlying mechanism of the reversed *fou2* phenotype in the different *ouf* mutants, in the present doctoral thesis the electrical features of the corresponding *TPC1* channels were electrophysiologically studied. For this, the patch clamp technique was applied to mesophyll vacuoles, which have been isolated from the stable *ouf* mutant lines and for comparison from *fou2* mutant and WT plants, as well (chapter 3.1.1.2). Macroscopic or single-channel currents were measured in response to vacuolar depolarized membrane voltages in the whole-vacuole configuration or in excised membrane patches under symmetrical K^+ conditions.

4.3.1. TPC1 channel functionality in the *ouf1, ouf2* and *ouf7* mutants

In order to quantify the TPC1 channel activity, patch-clamp measurements on *Arabidopsis thaliana* vacuoles were conducted in the whole-vacuole configuration. Experiments were performed in the presence of 150 mM K^+ at both sides of the vacuolar membrane and absence of inhibitory calcium in the vacuolar lumen. Additionally, 1 mM Ca^{2+} were present at the cytosolic side of the vacuolar membrane to enable voltage-dependent TPC1 channel activation. When voltage pulses in the range of -80 mV to +110 mV were applied in +10 mV steps, WT vacuoles showed no time-dependent current responses in the negative voltage range. Instead, increasing, slowly activating outward potassium currents were measured with further membrane depolarisation at positive membrane voltages (Figure 17A). When the steady-state current responses were normalized to C_m as a measure for the vacuole size and plotted against respective voltages, the well-known voltage-dependent gating behaviour of TPC1 channels becomes even more visible (Fig. 17B). Under symmetrical K^+ condition outward-rectifying TPC1 currents were only evoked from WT vacuoles at voltages positive of a voltage threshold of about 0 mV. In comparison, in the *fou2* mutant the slow current activation, the most obvious attribute of the TPC1 channel, was drastically speed up (Fig. 17A; Bonaventura et al. 2007a). Furthermore, TPC1 current responses were observed in a much broader voltage range in the *fou2* mutant than in WT because minor inward currents were additionally recorded at low negative voltages, i.e. positive of -30 mV. As illustrated by the

current/voltage relationship ($I_{ss}/C_m(V)$; Fig. 17B), both WT and *fou2* vacuoles showed comparable outward current densities while inward potassium currents directed into the cytosol were measured only with *fou2* but not with WT vacuoles. Thus, the mutation D454N in the *fou2* TPC1 channel protein altered the voltage dependency of the TPC1 channel (Fig. 17B; Beyhl et al., 2009). In the *tpc1-2* null mutant TPC1 currents were not evoked upon voltage pulses in the entire voltage range from -80 mV to +110. Due to the lack of TPC1 in vacuolar membrane, we only observed leak currents which resulted in a linear, ohmic-like shape of the current/voltage curve (Fig. 17B).

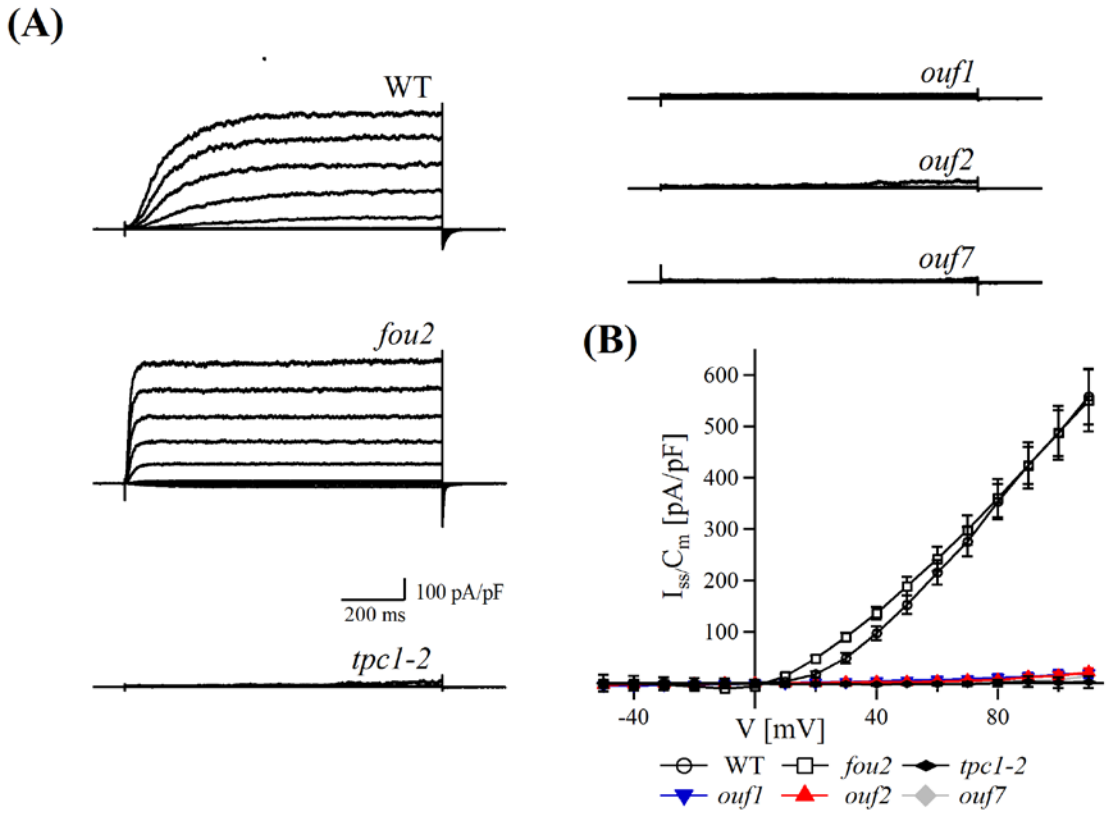

Figure 17. Macroscopic current responses of ouf1, ouf2 and ouf7 vacuoles to voltage depolarization.

(A) Representative current responses of WT, *ouf1,2,*7, *tpc1-2* and *fou2* to voltage pulses in the range of -80 mV to +110 mV applied in 20 mV increments from a holding voltage of -60 mV. (B) Steady-state current density (I_{ss}/C_m) plotted against respective voltages for mutants *ouf1,2,7*, *tpc1-2*, *fou2* and WT. Data points represent mean of 3-5 experiments, error bars give SEM. Measurements in (A, B) were performed in the whole-vacuole configuration in the absence of vacuolar Ca^{2+}.

ouf1 and *ouf7* mutants harbor TPC1 channel variants with a nonsense mutation (Fig. 15; chapter 4.1). In line with the TPC1-loss-of-function mutant *tpc1-2,* vacuolar membrane depolarization from mutant lines *ouf1* and *ouf7* did not lead to the activation of TPC1 currents. The deduced steady-state current/voltage curve (I_{ss}/C_m (V)) exhibited neither outward nor inward currents which were characteristic for *fou2* and/or WT under symmetrical K^+ condition (Fig. 17A). Similarly to *ouf1*, *ouf7* and *tpc1-2*, the *ouf2* mutant did not exhibit any TPC1 currents in the recording voltage range of -80 to +110 mV, (Fig. 17A). Accordingly, for *ouf2* mutant the related current/voltage relationship also revealed only minor background currents which were characterized by an ohmic behaviour (Fig. 17B). Thus, not only *ouf1* and *ouf7* mutants but also *ouf2* lost the TPC1 channel activity (Fig.17A,B).

4.3.2. TPC1 channel functionality in *ouf6* (A669V D454N) mutant

In order to evaluate TPC1 function in the *ouf6* mutant, TPC1 channel activity was also quantified by current recordings in the whole vacuole configuration. In contrast to *ouf1*, *ouf2* and *ouf7*, depolarizing voltage pulses applied in the range of -80 mV to +110 mV evoked time-dependent outward current responses from *ouf6* vacuoles (Fig. 18A). These currents were characterized by the same rapid activation kinetics, which are typical for the hyperactive TPC1 channels of the *fou2* mutant (Fig. 18B). For both, the *ouf6* and *fou2* mutant, TPC1 half-activation times $t_{1/2}$ around 15-20 ms were determined in the voltage range of +40 mV to +110 mV (Fig. 18C). Thus, in comparison to wild-type TPC1 currents with $t_{1/2}$ = 110 - 140 ms, 7-fold faster half-activation times of TPC1 currents were deduced in *ouf6* and *fou2* (Fig. 18C). However, current densities (I_{ss}/C_m) determined from *ouf6* vacuoles at positive voltages in the absence of vacuolar calcium, were much smaller than those from *fou2* and WT (Fig. 18A,D). For instance, the currents were reduced by about 80% at +100 mV (Fig. 18A,D).

Due to the *fou2* mutation D454N, the susceptibility of the TPC1 channel to the inhibitory effect of luminal calcium is largely eliminated (Beyhl et al., 2009). In the presence of 10 mM luminal Ca^{2+} the TPC1 currents were suppressed by about 45% at +100 mV in *fou2*, while the WT TPC1 currents were completely inhibited (Fig. 18A,D,E). In comparison, the minor TPC1 currents observed at 0 luminal Ca^{2+} with *ouf6* vacuoles were reduced by about 75% at +100 mV in the presence of 10 mM luminal Ca^{2+}.

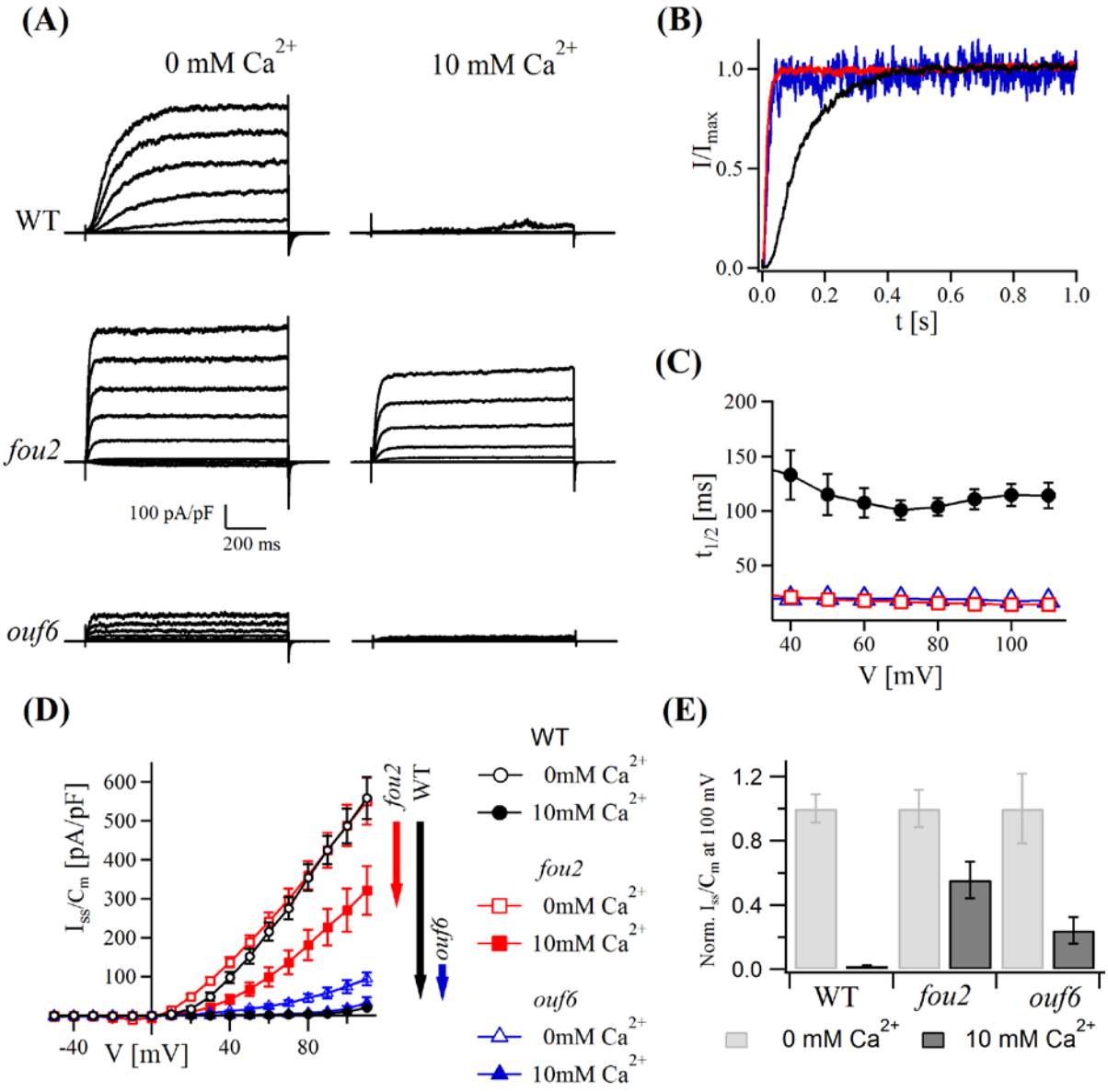

Figure 18. Voltage-dependent ouf6 current responses under different vacuolar calcium concentration.

(A) Current responses of WT, *ouf6* and *fou2* to voltage pulses applied from -80 mV to +110 mV in 20 mV increments steps. Whole vacuole experiments were performed at either 0 mM or 10 mM luminal calcium concentration as indicated. (B) Current responses of *ouf6, fou2* and WT vacuoles to +100 mV normalized to the maximal current amplitude. Experiments were carried out at 0 mM vacuolar Ca^{2+}. (C) Comparison of TPC1 half-activation times deduced from *ouf6, fou2* and WT vacuoles in the voltage range of +40 mV to +110 mV at 0 mM Ca^{2+}. Mean of 4-6 experiments with SEM. (D) Plotted current density (I_{ss}/C_m) against respective voltage pulses (V) for *fou2*, *ouf6* and WT at 0 mM and 10 mM luminal Ca^{2+}. Arrows indicate a difference in current reduction upon increased Ca^{2+}. (E) Bar diagram shows the current densities for WT, *fou2* and *ouf6* which were measured at +100 mV under 10 mM vacuolar Ca^{2+} and normalized to the current density determined at 0 mM vacuolar Ca^{2+}. Mean of 3-5 experiments with SEM.

Thus, as previously reported by Beyhl et al. (2009), the *fou2* mutation reduced susceptibility to inhibition of TPC1 channel by luminal calcium leaving about 55% of the currents unblocked. This effect is partly preserved in *ouf6* mutant because 25% of currents were still present (Fig. 18A,D,E). As a result of the alanine-to-valine change at position 669 in TPC1 channel protein, the TPC1 outward current density in the *ouf6* mutant was extremely low and comparable to WT TPC1 currents at high luminal Ca^{2+} loads. To evaluate the mechanism causing the reduced current density in the *ouf6* mutant at 0 mM vacuolar calcium, tail currents from *ouf6*, *fou2* and WT were examined. Tail currents were achieved by instantaneous jump from different potentials in the range of -80 mV to +110 mV to the negative potential of -60 mV causing the deactivation of the TPC1 channel to stabilize the close state. Due to the unified driving force for the ion movement at -60 mV, the instantaneous tail current amplitude only depends on the number of open channels activated upon the previous voltage pulse and therefore was used to determine the relative voltage-dependent open-channel probability ($G/G_{max}(V)$) (Jaslan et al., 2016). The slope of G/G_{max} data points derived for WT and *fou2* were described with a double Boltzmann equation according to Pottosin et al. (2004). Thereby, a three-state model for channel gating consisting of two closed state and one open channel state ($C_2 \leftrightarrows C_1 \leftrightarrows O$) was assumed. Former studies with *fou2* have demonstrated that the voltage threshold for TPC1 channel activation in the *fou2* mutant shifted toward negative potentials by about 30 mV compared to WT (Beyhl et al., 2009). In the present work, the conductance-voltage curves revealed the same effect of the *fou2* mutation on TPC1 voltage gating compared to WT. The V_2 midpoint voltage reflecting the $C_2 \leftrightarrows C_1$ transition was V_2= 26 ± 5 mV for WT and V_2= 2 ± 5 mV for *fou2* (Supplement table 1; Fig. 19) In comparison to WT and *fou2*, the G/Gmax(V) curve of *ouf6*, however, was strongly shifted to positive membrane potentials. *ouf6* mutant exhibited the first channel activity by stimulation at 50-mV (Fig. 19). Furthermore, the *ouf6* G/Gmax(V) curve could not be fitted with a double but only with a single Boltzmann equation. Thus, the state model applied to describe *ouf6* channel gating was simpler considering the transition between only the close and the open channel state ($C \leftrightarrows O$). This analysis revealed a pronounced shift of midpoint voltage V_{half} = 147 ±15 mV towards positive potentials (Fig. 19). Accordingly, the relative open channel probability was largely reduced (≈ 80 % at 110 mV) in the observed voltage range (Fig. 19), leading in turn to the reduced macroscopic current density (Fig. 18A,D).

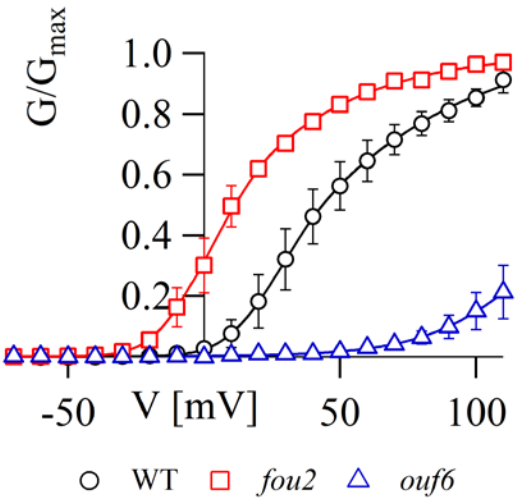

Figure 19. Relative voltage-dependent open channel probability of ouf6, WT and fou2.

Conductance-voltage curves ($G/G_{max}(V)$ were determined via instantaneous tail current responses to -60 mV after voltage pre-pulses ranging from -80 mV to +110 mV were applied. After normalization to maximum predicted tail current density the data points were plotted as means (±SEM) of 3 experiments against respective voltage. Solid lines give the fits of the data points with double Boltzmann (WT and *fou2*) equation according to Pottosin et al. (2004) or single Boltzmann equation for *ouf6*. Whole vacuole experiments were performed in absence of vacuolar calcium.

However, the decreased macroscopic current density in *ouf6* mutant could additionally be caused by an altered single channel conductance. The close neighbourhood of the *ouf6* mutation and TPC1 pore region supports this possibility (Fig. 15). To examine this aspect, Katrin Trageser, a former bachelor student in our group, was trained to perform single channel measurements with membrane patches excised from *ouf6*, *fou2* and WT vacuoles under symmetrical potassium condition in the absence of vacuolar calcium (Fig. 20A). These recordings revealed more frequent transitions into the open conductive channel state in WT and *fou2*, while in *ouf6* TPC1 openings were much rarer (Fig. 20B). Nevertheless, I was able to determine the single-channel current amplitudes from these single channel fluctuations recorded at different membrane voltages (Fig. 8, chapter 3.2.7.2). After plotting the individual single-channel current amplitudes against respective voltages, the single channel conductance were derived from the slope of the global regression line fit (Fig. 20C). In case of *ouf6* the single channel conductance was reduced by about 50% compared to WT and *fou2* [γ_{WT} = 81 pS (n= 6), γ_{fou2} = 82 pS (n= 4), γ_{ouf6} = 43 pS (n=4)] (Fig. 20D). Thus, TPC1 channels from *fou2* and WT exhibited the same conductivity as those measured at negative membrane potentials by Beyhl et al. (2009).

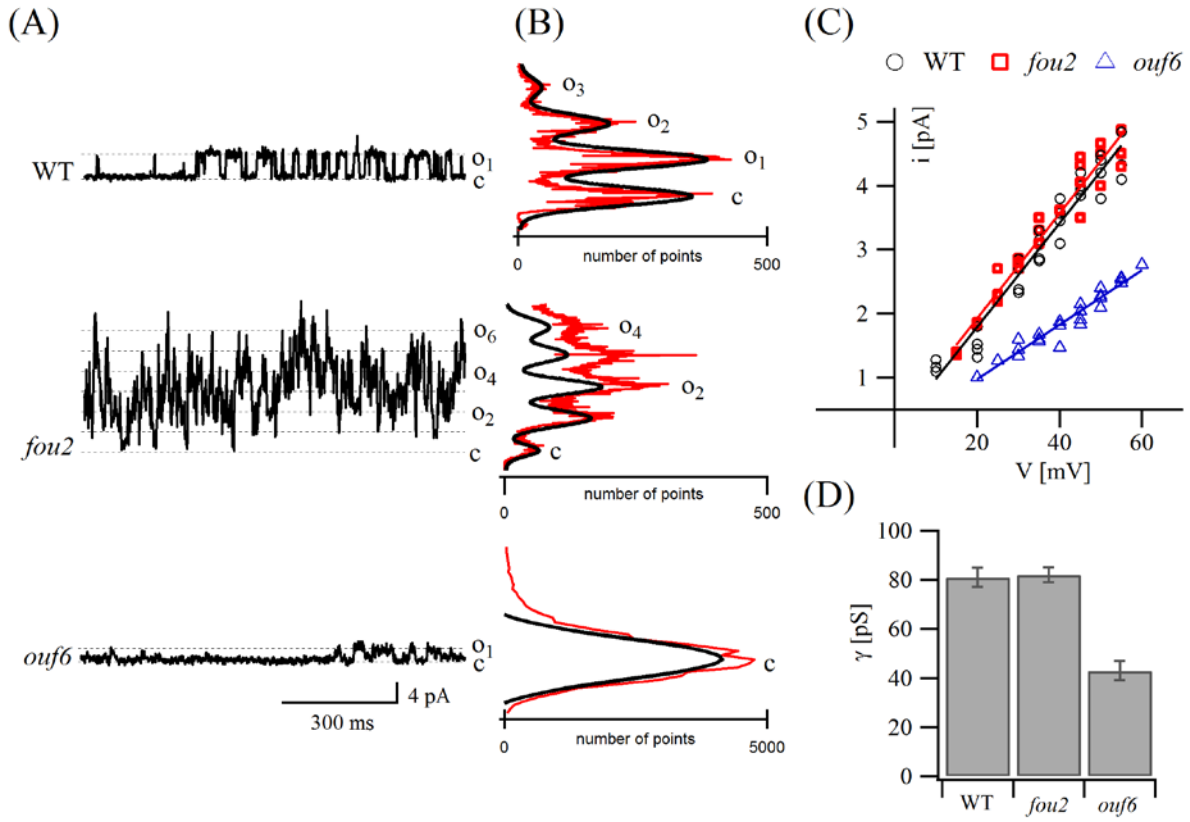

Figure 20. Single channel recordings of ouf6 mutant.

(A) Single channel fluctuations of *ouf6, fou2* and WT channels evoked at +45 mV. (B) All-point histograms of single-channel current fluctuations of *ouf6, fou2* and WT TPC1 channels shown in A. (C) Single channel current amplitudes of *ouf6, fou2* and WT plotted against the respective depolarizing voltage pulses. Solid lines reflect global regression fit for each plant line. Symbols for each plant line comprises 4-6 individual experiments. (D) Bar diagram gives the calculated unitary conductance of *ouf6, fou2* and WT. Means (±SD) of 4-6 measurements for each plant line are shown.

4.3.3. TPC1 channel functionality in *ouf8* (M629I D454N) mutant

In the previous chapter the characteristic features of *fou2* mutant such as fast activation kinetics, altered voltage threshold of channel activation and luminal calcium insensitivity have been presented and compared with those of the *ouf6* channels. In analogy, these features were also examined for the *ouf8* mutant to unravel the mechanism underlying the reversion of the *fou2* phenotype.

Likewise to *ouf6*, activation kinetics of *ouf8* TPC1 channels at 0 mM vacuolar calcium was similar with *fou2* mutant at positive voltages. Accordingly, *ouf8* also activated 10-fold faster than WT (Fig. 21A,B). During macroscopic current recordings at 0 mM vacuolar calcium, depolarizing voltage pulses to *ouf8* vacuoles resulted in outward current densities which were comparable to those of WT and *fou2* (Fig. 21C). Likewise, inward currents directed into the cytosol, which were typical for *fou2* under these solute condition, were preserved in *ouf8,* but exhibited higher current densities (Fig. 21C;$_{magn.}$). Also, the voltage threshold of these inward currents appeared to be slightly altered to more negative membrane potentials. This deviation suggested us to quantify the relative open channel probability over the applied voltage range via tail current analysis and double Boltzmann fits. From the latter the midpoint voltage V_2 was derived as descriptive parameter for the $C_2 \leftrightarrows C_1$ transition on which the voltage threshold for channel activation mostly depends. In case of *ouf8,* midpoint voltage V_2= -14 mV ±5 was shifted by 40 mV towards more negative potentials compared to WT (V_2= 26 mV ±5). The conductance-voltage curves revealed also a shift in voltage-dependent activation of *ouf8* towards negative voltages compared to *fou2* (V_2= 2 ±7 mV) (Supplement table 1; Fig. 21D). A 16-mV difference in the midpoint voltage V2 of activation between *ouf8* mutant and *fou2* was calculated. Thus, due to these 16 to 30 mV differences in the midpoint voltage V_2, the TPC1 channel in the *ouf8* mutant has an increased relative probability for channel opening in the observed voltage range, compared to WT and *fou2* (Fig. 21D).

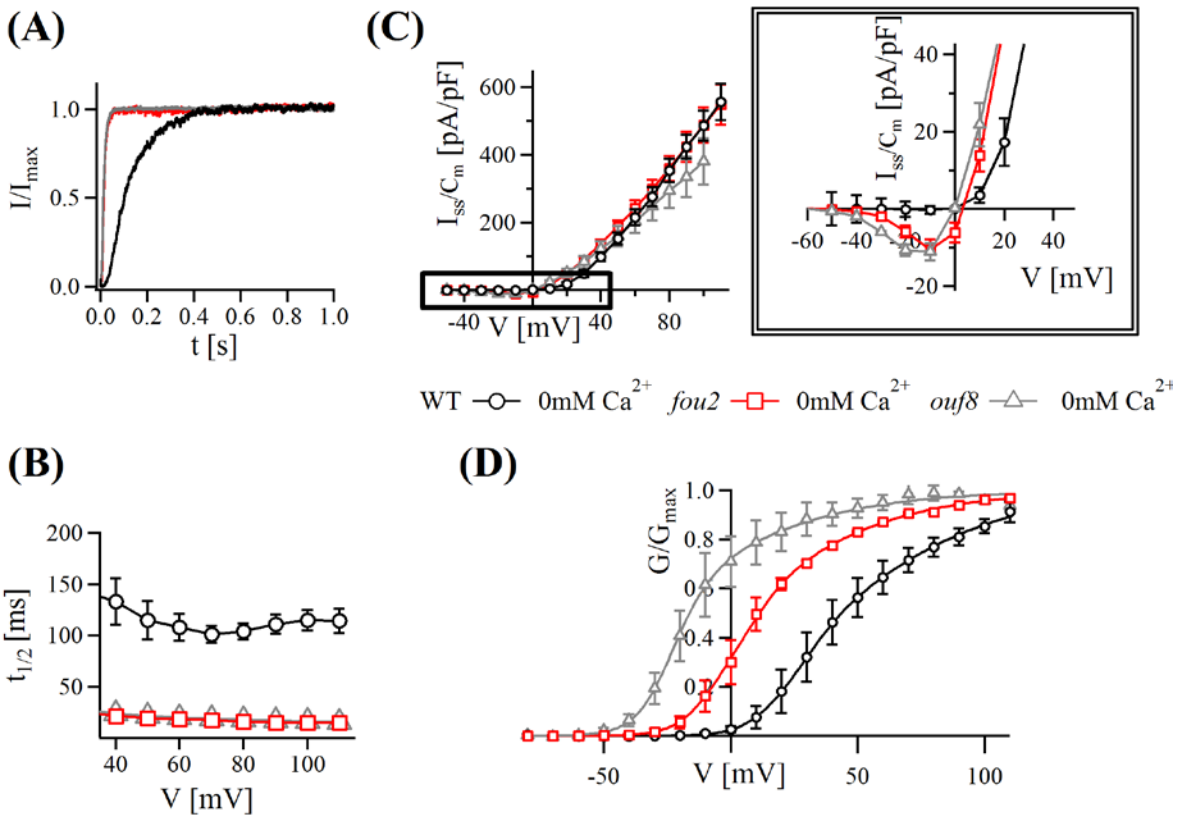

Figure 21. ouf8 current responses to membrane depolarization in the absence of vacuolar Ca^{2+}.

(A) Current responses of *ouf8, fou2* and WT to +100 mV normalized to the maximal current amplitude. Experiments were carried out at 0 mM vacuolar Ca^{2+}. (B) Comparison of TPC1 half-activation time deduced from *ouf8, fou2* and WT vacuoles in the voltage range of +40 mV to +110 mV at 0 mM Ca^{2+}. Mean of 4-6 experiments with SEM. (C) Current density (I_{ss} /C_m) plotted against respective voltages (V) for *ouf8* and WT. Mean of 3-5 experiments with SEM. The selected region in the left current/voltage graph (I_{ss}/C_m (V)) is shown enlarged in the right framed one. (D) Conductance-voltage curves (G/G_{max}(V) were determined via instantaneous tail current responses to -60 mV after voltage pre-pulses ranging from -80 mV to +110 mV were applied. After normalization to maximum predicted tail current density the data points were plotted as means (±SEM) of 3 experiments against respective pre-pulse voltage. Solid lines give the fits of the data points with double Boltzmann equation according to Pottosin et al. (2004). Whole vacuole experiments were performed in absence of vacuolar calcium.

This higher relative open channel probability of the TPC1 channel in mutant *ouf8* compared to *fou2* should be also reflected in higher TPC1 current densities in *ouf8* (Fig. 21C,D). However, current densities of these two mutants were comparable under identical solute conditions (Fig. 21D). This discrepancy could be explained by possible differences in single channel conductance. Therefore, our bachelor student, Katrin Trageser, also performed single channel recordings with the *ouf8* mutant enabling me to analyse and to determine its single channel conductance. As illustrated in Figure 22, the single-channel current amplitudes of the *ouf8* mutant was much smaller than that of WT and *fou2* not only at +45 mV but also at all other applied positive voltages. This fact becomes visible when the single-channel currents were

plotted against the respective membrane voltages (Fig. 22B). The global regression line fit of the data points revealed an unitary conductance of 40 pS for *ouf8* mutant at the positive voltage range (Fig. 22B). Thus, the single-channel conductance of *ouf8* was half of that of WT and *fou2* (Fig. 22b, bar diagram).

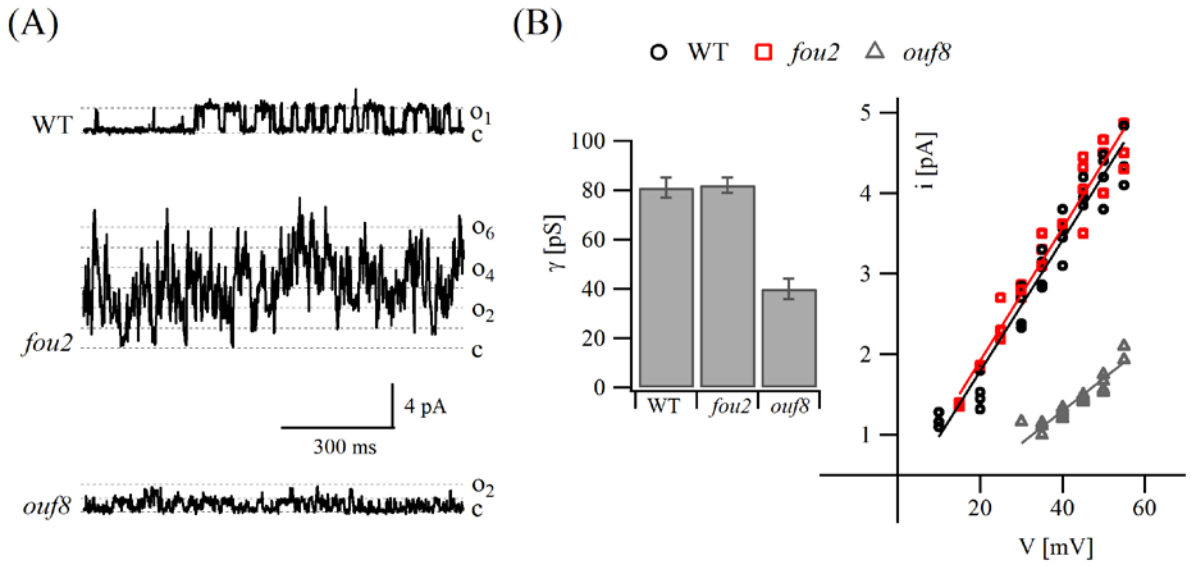

Figure 22. TPC1 single channel fluctuations of ouf8 mutant.

(A) Single channel fluctuations of *ouf8, fou2* and WT TPC1 channels evoked at +45 mV. (B) Single-channel current amplitudes of *ouf8, fou2* and WT plotted against the respective depolarizing voltage pulses. Solid lines reflect global regression fit for each plant line. Symbols for each plant line comprises 4-6 individual experiments. Bar diagram gives the calculated unitary conductance of *ouf8, fou2* and WT. Means (±SD) of 4-6 measurements for each plant line are shown.

The third *fou2* feature, the luminal calcium insensitivity, was examined in the whole vacuole configuration under increased vacuolar calcium conditions. For this, the TPC1 current density of the *ouf8* mutant was recorded at 10 mM vacuolar calcium and compared with those of WT and *fou2*. In contrast to WT, TPC1 outward currents were still elicited upon depolarization with the *ouf8* mutant even in the presence of 10 mM luminal calcium (Fig. 23A,B,C). Despite this similarity to *fou2*, some deviation in the TPC1 channel behaviour between *fou2* mutant and *ouf8* reverting mutant was observed (Fig. 23B,C). The absolute *ouf8* outward current density was about two times smaller than for *fou2* at +100 mV (Fig. 23C). So high luminal Ca^{2+} load caused an about 20% higher reduction in the outward current density of *ouf8* mutant, compared to *fou2* (Fig. 23B).

Taken together, the introduction of the *M629I* mutation into *fou2* allele did not drastically change the characteristic *fou2* features like fast activation, vacuolar calcium insensitivity and hyperactivity of the TPC1 channel. The lower unitary conductance of *ouf8* TPC1 channels also does not explain the reversion of the *fou2* phenotype in the *ouf8* mutant, because the ability to import potassium cations into the vacuole was not impaired at low luminal calcium concentration – as indicated by the similar outward current densities in *fou2* and *ouf8* - and only slightly deviated at high vacuolar Ca^{2+} level.

As mentioned above, the difference in current density between *ouf8* and *fou2* at high luminal Ca^{2+} load (10 mM) and revealed difference in channel conductance (Fig. 22B) led us to perform tail current analysis for gaining insights in effect of luminal Ca^{2+} on K^+ release from vacuole. Superimposition of tail currents, evoked by an instantaneous jump from +100 mV to -60 mV, revealed differences in the instantaneous tail current amplitudes of WT, *fou2* and *ouf8* recorded at 0 mM and 10 mM vacuolar Ca^{2+} (Fig. 23D). The instantaneous tail current density of all three plant lines was in a similar range at 0 mM vacuolar Ca^{2+} but differentially affected by 10 mM luminal Ca^{2+}. Thereby, the tail current density was almost completely reduced in WT from 162±43 to 4±1 pA/pF by 97% and in *ouf8* from 197±36 to 16±5 pA/pF by 92% in response to the high luminal Ca^{2+} level (Fig. 23D,E). Residual tail currents observed in WT and *ouf8* at 10 mM Ca^{2+} were ignored as an effect of membrane capacitance associated with fast voltage jumps (e.g. +100 mV to -60 mV) (Fig. 23D; upper). Unlike *fou2* the tail current density was still around 100 pA/pF in the presence of 10 mM luminal Ca^{2+} (Fig. 23E). Thus, *fou2* mutant showed a decrease in the tail current density in range of 55% and was much lower than WT and *ouf8*.

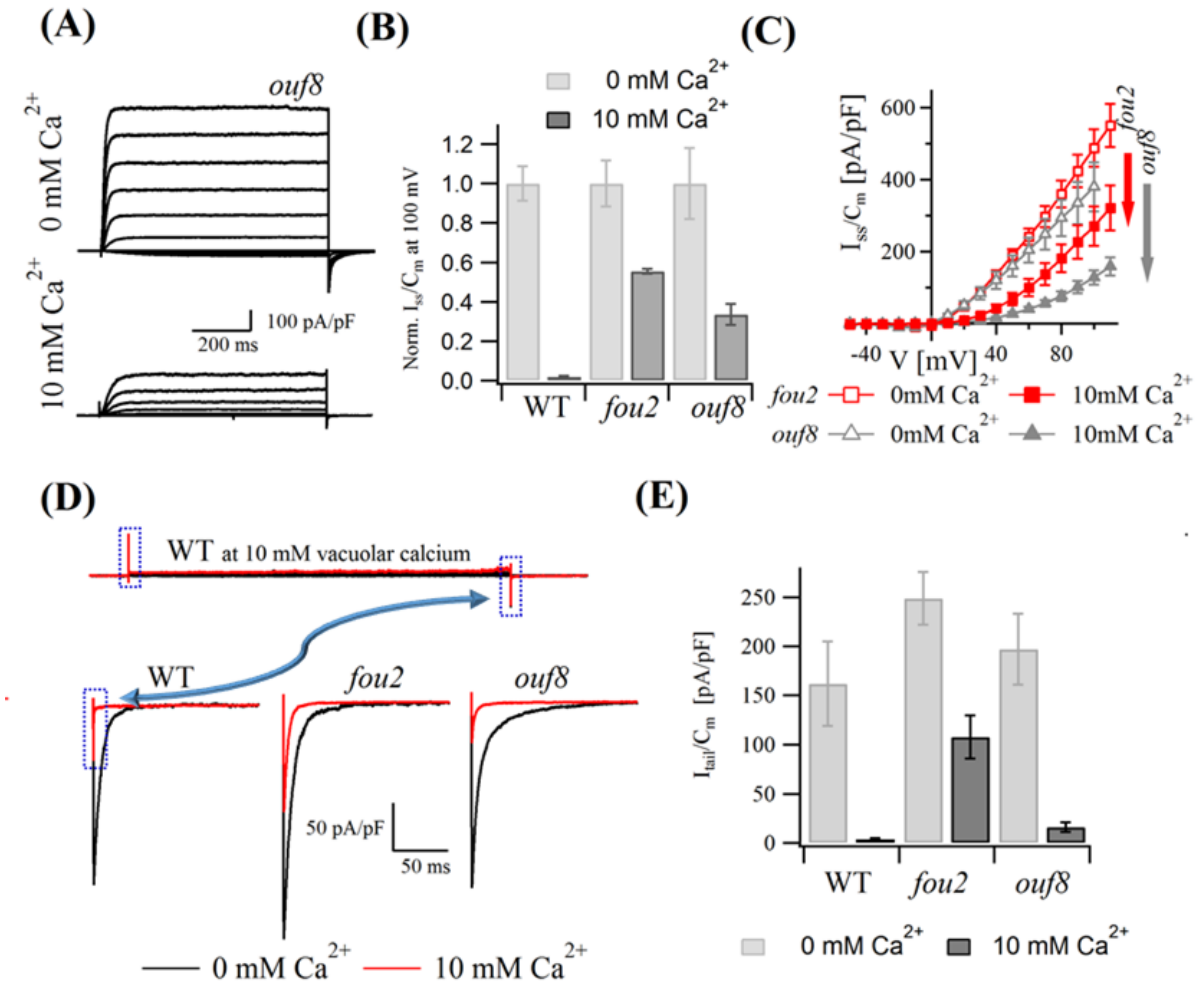

Figure 23. Ca2+ effect on voltage-dependent outward and inward TPC1 currents of ouf8 mutant.

(A) TPC1 current responses of WT, *ouf8* and *fou2* to voltage pulses applied from -80 mV to +110 mV in 20 mV increments. Whole vacuole experiments were performed at either 0 mM or 10 mM luminal calcium concentration as indicated. (B) Bar diagram with the current density for WT, *fou2* and *ouf8* measured at +100 mV under 10 mM vacuolar Ca^{2+} and normalized to current density determined at 0 mM vacuolar Ca^{2+}. Mean (±SEM) of 3-5 experiments. (C) Current density (I_{ss} /C_m) plotted against respective voltage pulses (V) for *fou2, ouf8* and WT at 0 mM and 10 mM luminal Ca^{2+}. Arrows indicate reduction in the current density upon increased Ca^{2+} level. (D) Representative tail currents normalized to the vacuole size (I_{tail}/C_m) recorded for WT, *fou2* and *ouf8* at -60 mV after a pre-pulse voltage of +100 mV in the absence and presence of 10 mM vacuolar calcium. Upper trace indicates localization of capacitive current transients on the example of voltage-induced WT current responses (blue dotted rectangles) (E) Bar diagram of the tail current densities determined for WT, *fou2* and *ouf8* at 0 or 10 mM vacuolar Ca^{2+}. Tail currents were recorded after jump from +100 mV to -60 mV. Values include partly current capacitive current transients clearly observed for WT and *ouf8* at 10mM vacuolar calcium (cf. D) . Mean (±SEM) of 3-5 experiments.

4.3.3.1. Influence of M629I mutation on TPC1 function

Pronounced macroscopic current density (Fig. 21C; 23A) and altered single-channel conductance (Fig. 22B) of the *ouf8* mutant arise the question about the role of Met629 in TPC1 channel function. This aspect was further examined with two additional mutant lines kindly provided by Prof. E.E. Farmer and called *ouf8ko* and *ouf8WT*. In these stable lines the single TPC1 mutant M629I was expressed either in the background of *Col0* (*ouf8WT* = $TPC1^{WT}$ + $TPC1^{M629I}$) or in the background of the *tpc1-2* knock out line (*ouf8ko* = $TPC1^{M629I}$). Phenotypic appearance of the plant rosettes both of these mutants was very similar to WT plants (Fig. 24A). In analogy to the previous patch clamp studies on the different *ouf* mutants (chapter 4.3.1- 4.3.3), macroscopic currents were recorded under symmetrical 150 mM K^+ conditions (Fig. 24B). Surprisingly, even in the absence of luminal Ca^{2+} no TPC1 currents were recorded upon depolarizing voltages in the mutant line harboring solely the TPC1 channel mutant M629I (*ouf8ko*) (Fig. 24B).

Functional TPC1 channel protein represents a dimer of polypeptides encoded by the *TPC1* gene (chapter 4, Fig. 3). Thus, TPC1 pore region is built by two P1 (pore region 1) and two P2 regions. To obtain a broader view about the contribution of sulphur present in the amino acid methionine 629 and localized within the P2 region on TPC1 channel conductance, possible heteromeric TPC1 channels ($TPC1^{WT/M629I}$) were used. For this, the mutant line *ouf8WT*, which contained not only the allele for the TPC1 WT channel but also for the TPC1 mutant channel M629I was examined. Voltage-induced current responses from this mutant *ouf8WT* revealed slow time-dependent current activation kinetics which are typical for the TPC1 WT channels (Fig. 24B,C,D). However, the plot of the steady-state current density against the respective voltages revealed a 40% lower current density for *ouf8WT* mutant compared to WT vacuoles. For example, at +100 mV the outward currents were ≈300 pA/pF and ≈500 mV/pA for *ouf8WT* and WT, respectively (Fig. 24E). When the vacuolar calcium concentration was increased to 10 mM, the depolarization-triggered TPC1 outward currents completely disappeared for both plant lines, WT and the mutant *ouf8WT* (Fig. 24E).

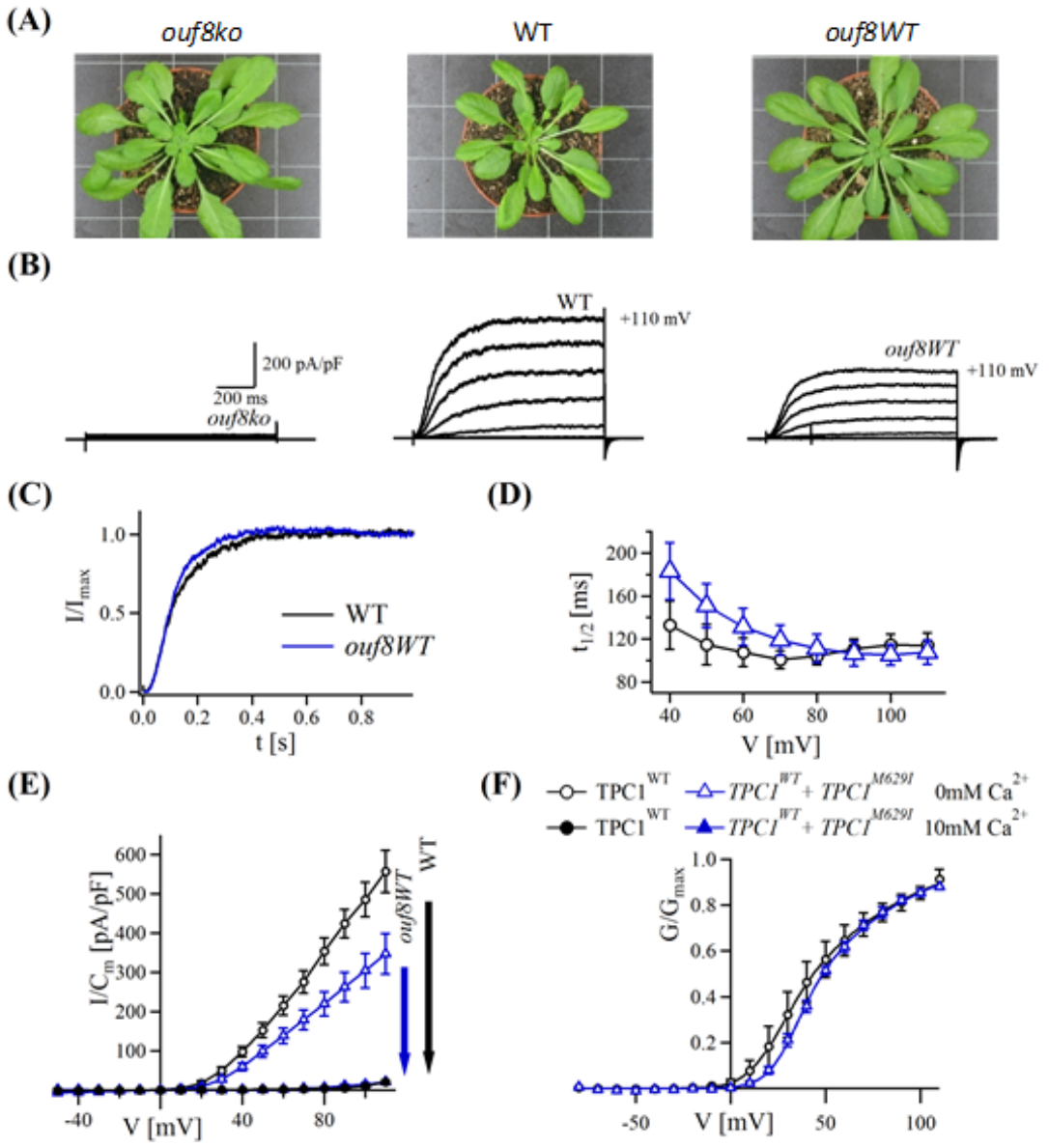

Figure 24. Voltage-dependent current responses of vacuoles from two plant lines ouf8WT (= TPC1WT + TPC1M629I) and ouf8ko (= TPC1M629I) harbouring the single TPC1 channel mutant M629I alone or together with TPC1 WT channels.

(A) Phenotype of ouf8WT, ouf8ko mutants and WT. Scaling of each square in the background = 3 cm. (B) Current responses of WT, *ouf8ko* and *ouf8WT* to voltage pulses applied from -80 mV to +110 mV in 20 mV increments. (C) Current responses of *ouf8WT* and WT to +100 mV normalized to the maximal steady-state current amplitude. (D) Comparison of half-activation time of ouf8WT and WT in voltage range of 40 mV to +110 mV at 0 mM Ca^{2+}. Mean of 4-6 experiments with SEM. (E) Current density (I_{ss} /C_m) plotted against respective voltage pulses (V) for ouf8WT and WT at 0 mM and 10 mM luminal Ca^{2+}. Arrows indicate a difference in current reduction upon increased Ca^{2+}. (F) Relative voltage-dependent open channel probability of WT and *ouf8WT*. Conductance-voltage curves (G/Gmax(V)) were determined via instantaneous tail current responses from voltages ranging from -80 mV to +110 mV to the negative voltage of -60 mV. After normalization to maximum predicted tail current density the data points were plotted as means (±SEM) of 3-4 experiments against respective voltage. Solid lines give the fits of the data points with double Boltzmann (WT and ouf8WT) equation according to Pottosin et al. (2004). Whole vacuole experiments in B, C, D, F were performed in absence of vacuolar calcium.

To examine the voltage-dependent gating of the TPC1 channels (i.e. the relative voltage-dependent open channel probability) in the *ouf8WT* mutant, tail currents were analysed via the relative conductance-voltage curves ($G/G_{max}(V)$). As illustrated in Figure 24F, similar conductance-voltage curves were deduced for WT and *ouf8WT.* Accordingly, their analysis showed similar midpoint voltages for the $C_2 \leftrightarrows C_1$ transition of TPC1 channels in the *ouf8WT* mutant (V_2= 35 mV ±2) and in WT (V_2= 26 mV ±5) at 0 mM vacuolar calcium condition (Fig. 24F). Thus, taken together, in the stable mutant line *ouf8ko* the TPC1 channel activity was silenced. When the two TPC1 channel variants, i.e. $TPC1^{WT}$ *and* $TPC1^{M629I}$, were co-existing/expressed in the *ouf8WT* mutant line, the exhibited current density was decreased by 40%. Other features of TPC1 channel like slow activation, inhibition by luminal Ca^{2+} and voltage-dependent activation remained unaffected.

4.3.3.2. Role of individual amino acid in TPC1 channel conductance

In the *ouf8* mutant (M629I D454N) the single-channel conductance was reduced (Fig. 22B). According to the crystal structure of AtTPC1 channel (Guo et al., 2016), amino acid Met629 is localized in the pore region P2 of the *A. thaliana* TPC1 channel (Fig. 3). To further investigate the role of this amino acid in channel conductivity, amino acid sequences of the pore region P2 within the second Shaker-like domain from TPC1 channel of different species were aligned (Fig. 25A). As depicted in Figure 25A, Met629 represents a highly conserved amino acid within the pore region P2. However, in some species the amino acid sequence is altered at the homologous site. For instance, in *L. japonicas* and *P. patens* the TPC1 channel contains a serine or threonine, respectively, instead of methionine. Therefore, I measured the LjTPC1 channel activity at the single-channel level and quantified its conductivity as described above (chapter 3.2.8.2 and 4.3.2). The analysis revealed a huge (3.5-fold) difference in the transport capacity between A. *thaliana* (≈80 pS) and *Lotus japonicus* (≈280 pS) (Fig. 25B). This result turned out to be not an exceptional case, because similar values for the unitary TPC1 conductance was found for *Vicia faba* as well (Fig. $25C_{\text{bar diagram}}$).

In the following, the master student Jan Rathje transiently transformed mesophyll protoplasts from *A. thaliana tpc1-2* null mutant plants with three AtTPC1 channel variants (M629I, M629T, M629S) to examine the effect of this polymorphic amino acid from *Lotus japonicus* and

Physcomitrella patens on the single channel conductance with the patch clamp technique. All three channel constructs were localized in the vacuolar membrane as confirmed by visualizing the fluorescence of the eGFP protein connected to the C-terminus of the TPC1 channel protein (Fig. 25C).

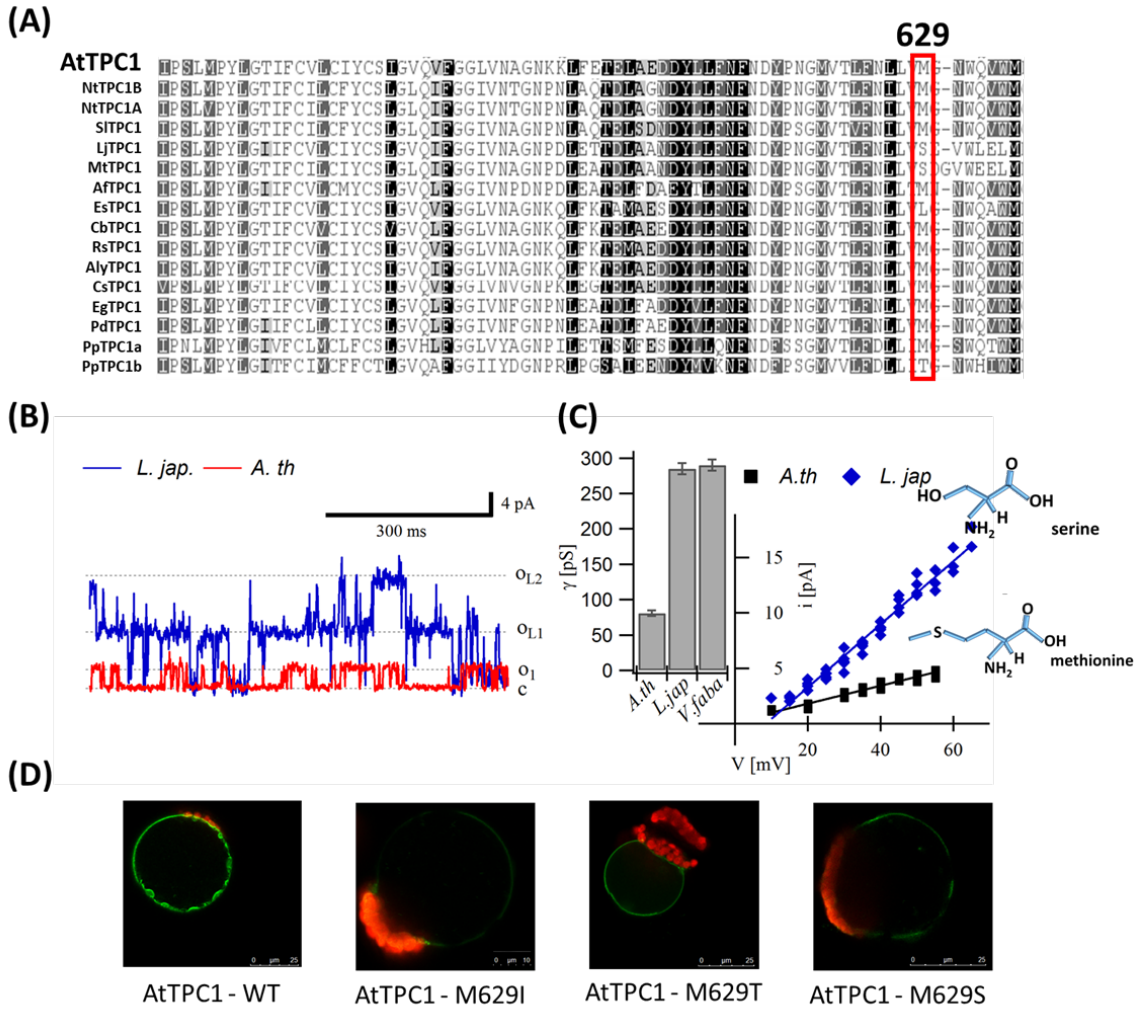

Figure 25. Amino acid alignment of TPC1 channel protein from chosen plant species in the pore region P2 between the transmembrane domains S5 and S6.

Physcomitrella patens (Pp), *Nicotiana tabacum* (Nt), *Lotus japonicus* (Lj), *Arabidopsis thaliana* (At), *Arabidopsis lyrata* (Aly), *Cucumis sativus* (Cs), *Solanum lycopersicum* (Sl), *Medicargo truncatula* (Mt), *Allium fistolosum (Af), Eutrema salsugineum (Es), Chorispora bungeana (Cb), Rophonus sativus (Rs), Elaeis guineensis (Eg), Phoenix dactylifera* (Pd). Red framed marked polymorphic amino acids for AtTPC1 position 629 in different species. (B) Superimposed TPC1 single-channel fluctuations from WT *Arabidopsis thaliana* (*A. tha.,* Col0) and *Lotus japonicus* (*L. jap.,* MG20) plants. c – close state, o_1- open state *A.th* $o_{L1/L2}$ – open state 1 and 2 for *Lotus japonicus* (C) Right: Single-channel current amplitudes for *Arabidopsis thaliana* (Col0) and *Lotus japonicus* (MG-20) plotted against the respective voltages. Solid lines reflect global linear regression fits of the data points for each mutant line. Left: Single-channel conductance of *Arabidopsis thaliana, Lotus japonicus* and *Vicia faba*. Means (±SD) of 5-6 measurements are shown. (D) Vacuolar localization of transiently expressed AtTPC1 channel variants with respective mutations. Green colour – TPC1 protein labelled with eGFP. Red – autofluorescence of chloroplasts.

The master student performed the patch-clamp measurements with excised membrane patches under symmetrical K^+ conditions (100 mM) in the absence of vacuolar Ca^{2+}. When the WT TPC1 channel was transiently expressed in the mutant line *tpc1-2*, similar single channel fluctuations were recorded as with the WT *A. thaliana* plants (Fig. 25C, Fig. 26B). The plot of derived single-channel current amplitudes against the respective voltages allowed us to calculate the unitary conductance of 79±4 pS for the transiently expressed TPC1 WT channel (Fig. 26B). Since the single-channel conductance of the WT TPC1 channel in plants was estimated to be 81±4 pS (Fig. 20D), the transient expression of the TPC1 channel in the *tpc1-2* mutant did not influence the TPC1 ion transport capacity. When the M629S channel mutant harbouring the polymorphic amino acid serine of *Lotus japonicus* at this position in the AtTPC1 channel was studied in excised membrane patches, distinct single-channel opening/closing events were not monitored (Fig. 26A). Therefore, it was impossible to determine the single-channel conductance for M629S. In contrast, single-channel fluctuations could be still resolved when Met629 was substituted by either isoleucine or threonine. Their analysis further revealed that both point mutations led to smaller single-channel current amplitudes at all applied positive voltages compared to the WT channel. Accordingly, when the slope of the current-voltage curve (i(V)) was determined via a linear regression fit, a decrease in the single-channel conductance of $AtTPC1^{M629T}$ by about 15 pS (= 19%) and of $AtTPC1^{M629I}$ by about 30 pS (=38%) was revealed compared to the WT TPC1 channel (Fig. 26B). Due to closer inspection of the M629I single-channel fluctuations, semi-open channel states were even detected which were not observed with the WT channel (Fig. $26C_{superimposion}$). As indicated by the all-point histogram derived for the 60-s-lasting single channel recordings at +45 mV (Fig. $26C_{histograms}$), the mutant channel M629I could reside in two separate conductive channel states: a low- and a high-conductive ones. In the high-conductive state ion currents of 2.4 pA passed M629I, while in the low-conductive state the single-channel current amplitudes were with 1.3 pA about 2-fold lower (Fig. 26C). The all-point-histograms further confirmed a presence of the semi-open state of the M629I mutant, which is not observed in WT TPC1 (Fig. 26C). A unitary conductance of 26±1 pS for this semi-open state was determined (Fig. 26D) which was half of the single channel conductance of the full M629I channel opening and three times smaller than the WT one.

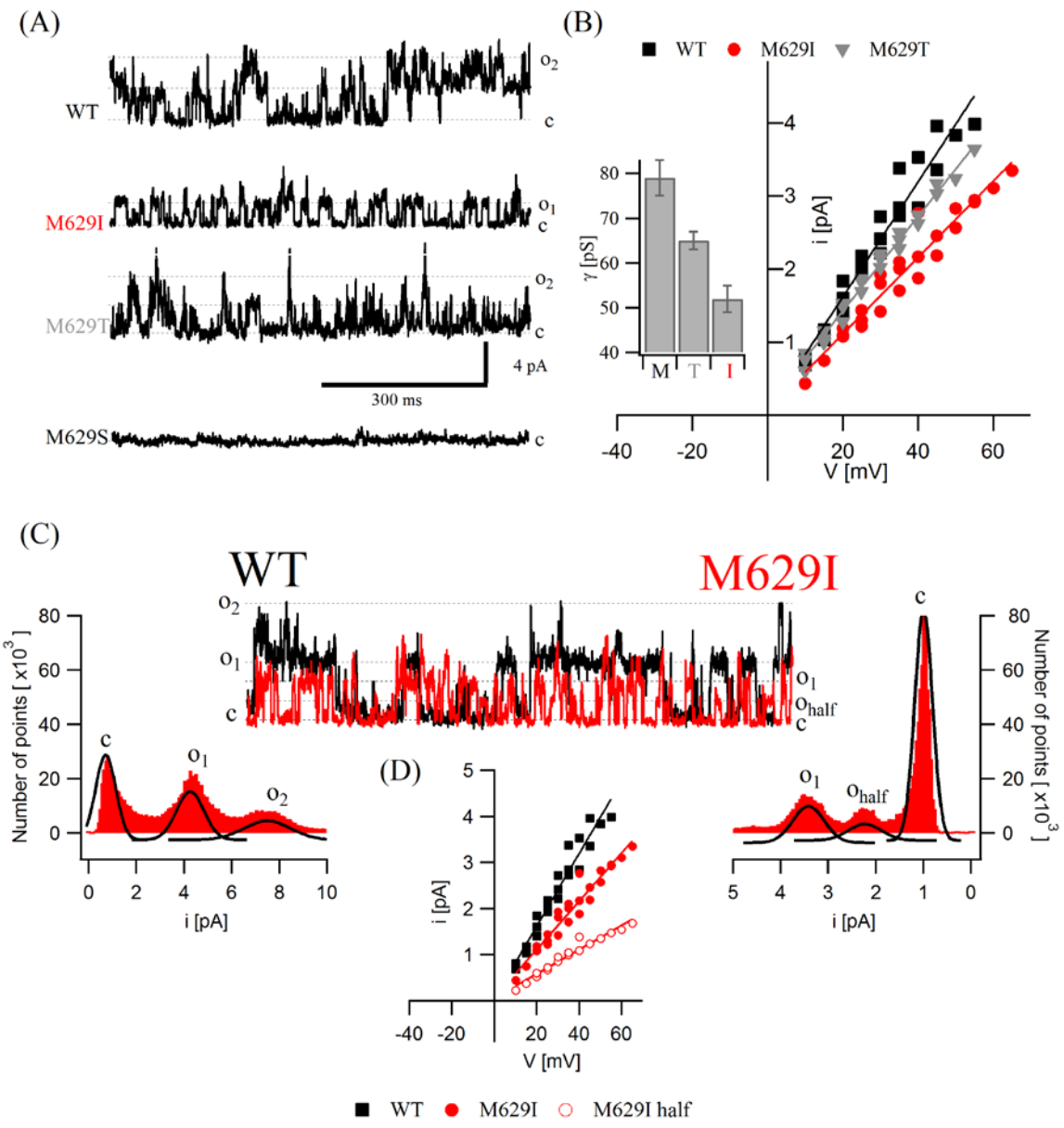

Figure 26. Unitary conductance of different TPC1 channel variants.

(A) Single channel fluctuations of transiently expressed AtTPC1^{WT}, AtTPC1^{M629I}, AtTPC1^{M629T}, AtTPC1^{M629S} channels at +35 mV. (B) Right: Single channel current amplitudes for WT, M629I and M629T plotted against the respective voltages. Solid lines reflect global linear regression fits of the data points for each mutant line. Left insert: Single channel conductance derived from the right i(V) curve for the indicated channel variants are depicted in the bar diagram. Means (±SD) of 3 measurements with SD. (C) In the middle superimposed single channel fluctuations from AtTPC1^{WT} (black) and AtTPC1^{M629I} (red) recorded at +45 mV were displayed. On both sides of the single channel traces, all-point histograms including the respective Gaussian equation fits (black) derived for WT (left) and M629I (right) are shown. The peaks indicate the current level at which TPC1 channels were closed (c) or one or two TPC1 channels were open (O_1, O_2)., (D) Single-channel current amplitudes for WT, M629I and M629I$_{half\ state}$ plotted against the respective voltages. Solid lines reflect global linear regression fits of the data points for each mutant line. Means (±SD) of 3 experiments are given.

4.3.4. TPC1 channel electrical properties in the *ouf4* mutant

ouf4 mutant is exhibiting a more WT-like than *fou2*-like phenotype (Fig. 14, chapter 4.1). In contrast to the *ouf1/2/3/6-8* mutants, the *TPC1* gene in *ouf4* does not contain any other point mutation than the *fou2* mutation D454N. To elucidate a potential effect of the mutated but unknown gene product on TPC1 channel function, patch clamp experiments were performed with *ouf4* vacuoles in the whole vacuole configuration. To allow the comparison of the results with those obtained with the other *ouf* mutants, the electrophysiological measurements were also conducted under symmetrical potassium (150 mM) conditions in the absence of inhibitory vacuolar Ca^{2+}.

Time-dependent outward currents appeared with depolarizing voltage pulses in positive voltage range (Fig.27A). Analysis of the macroscopic current recordings revealed that fast activation kinetics of the *fou2 TPC1* currents was still preserved in the *ouf4* TPC1 channels (Fig. 27B). Similar half-activation times of *fou2* (≈20-30 ms) and *ouf4* (30-40 ms) outward currents were determined at positive voltages, thus both being much faster than the one of WT (≈100-140 ms) (Fig.27C). However, the TPC1 current density was significantly reduced in the *ouf4* mutant in the absence of vacuolar calcium, compared to WT and *fou2* (e.g. at +110 mV by ≈80%; Fig. 27A,D). In analogy to the other active *ouf* mutants, *ouf4* TPC1 tail currents were also analysed to elucidate whether the altered current density could be caused by a change in the voltage-dependent TPC1 channel gating behaviour. Likewise to *fou2*, the normalized conductance-voltage curves ($G/G_{max}(V)$) of the *ouf4* TPC1 channel appeared to be shifted to negative potentials, compared to WT TPC1 channels (Fig. 27E). The midpoint voltage for the $C_2 \leftrightarrows C_1$ transition was V_2= 2 ± 7 mV for *fou2*, V_2= 2 ± 4 mV for *ouf4* and V_2= 26 ±5 mV for WT (Supplemental table 1). Despite the similar midpoint voltages V_2 , the midpoint voltage V_1 for the $C_1 \leftrightarrows O$ transition of *ouf4* and *fou2* TPC1 channels was found to be different (V_1^{ouf4} = 29 ±10 mV and V_1^{fou2} = -2 ±2 mV; Supplemental table 1).

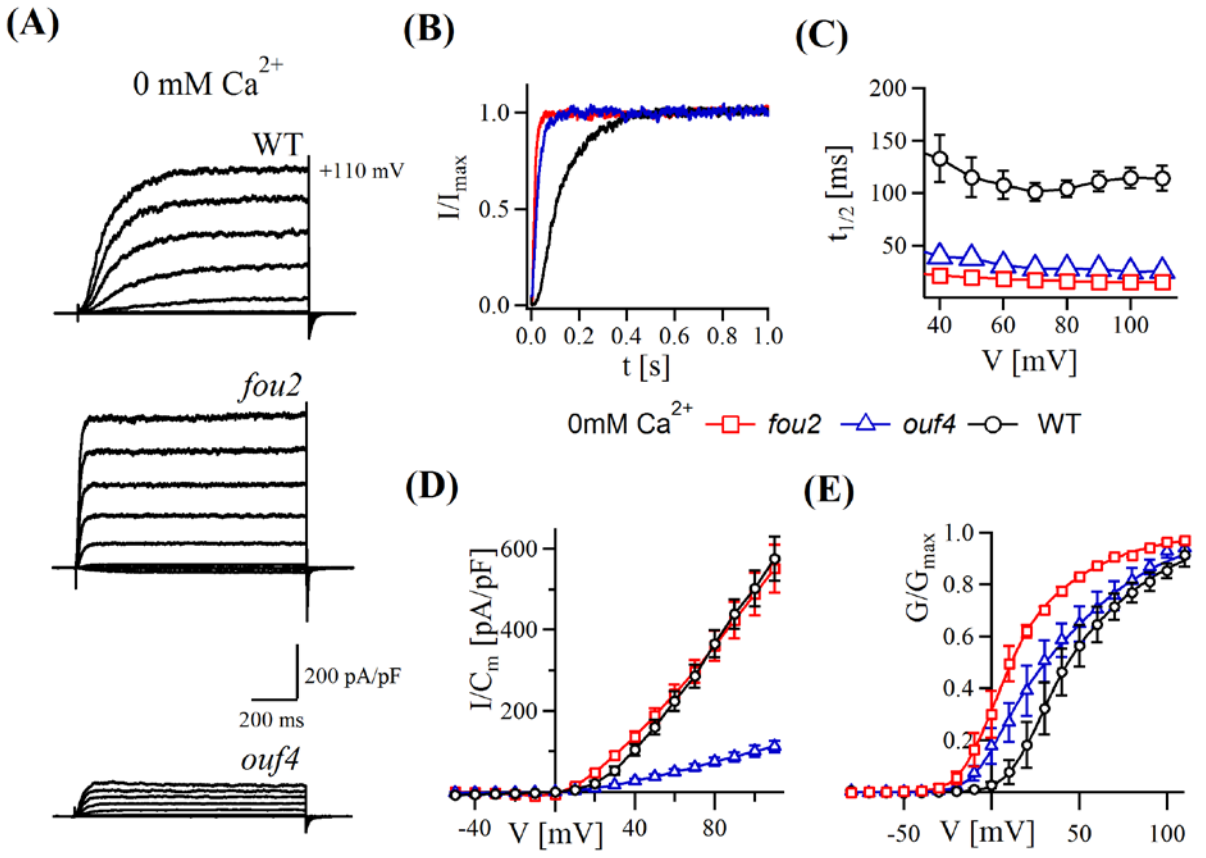

Figure 27. Voltage-dependent ouf4 current responses under 0 mM vacuolar calcium concentration.

(A) Current responses of WT, *ouf4* and *fou2* to depolarising voltage pulses in the range of -80 mV to +110 mV in 20 mV increments. (B) Current responses of *ouf4, fou2* and WT at +100 mV normalized to the maximal current amplitude. (C) Comparison of half-activation time of *ouf4, fou2* and WT in the voltage range of +40 mV to +110 mV. Mean of 4-6 experiments with SEM. (D) Current density (I_{ss} /C_m) plotted against respective voltage pulses (V) for *ouf4*, *fou2* and WT. Mean of 3-5 experiments with SEM. (E) Conductance-voltage curves (G/Gmax(V)) were determined via instantaneous tail current responses from voltages ranging from -80 mV to +110 mV to the negative voltage of 60 mV. After normalization to maximum predicted tail current density, the data points were plotted as means (±SEM) of 3 experiments against respective voltage. Solid lines give the fits of the data points with double Boltzmann equation according to Pottosin et al. (2004). Measurements were performed in whole vacuole configuration in the absence of vacuolar calcium.

Furthermore, the possibility of an altered ion transport capacity of the TPC1 channels in the *ouf4* mutant was examined. Therefore, to determine the *ouf4* TPC1 unitary channel conductance, the bachelor student Katrin Trageser performed current recordings at the single channel level. As shown in Figure 28A, the single current amplitudes recorded at +45 mV were similar for WT, *fou2* and *ouf4* channels. Based on the derived current-voltage curve (Fig. 28B), a single channel conductance of about 80 pS was estimated for the *ouf4* TPC1 channel and therefore remained at the same level as WT and *fou2* TPC1 channels (Fig. 28B). Thus, the reduced TPC1 current density of *ouf4* vacuoles is not linked to dramatic changes in the voltage-dependent gating behaviour or ion transport capacity of the *ouf4* TPC1 channels.

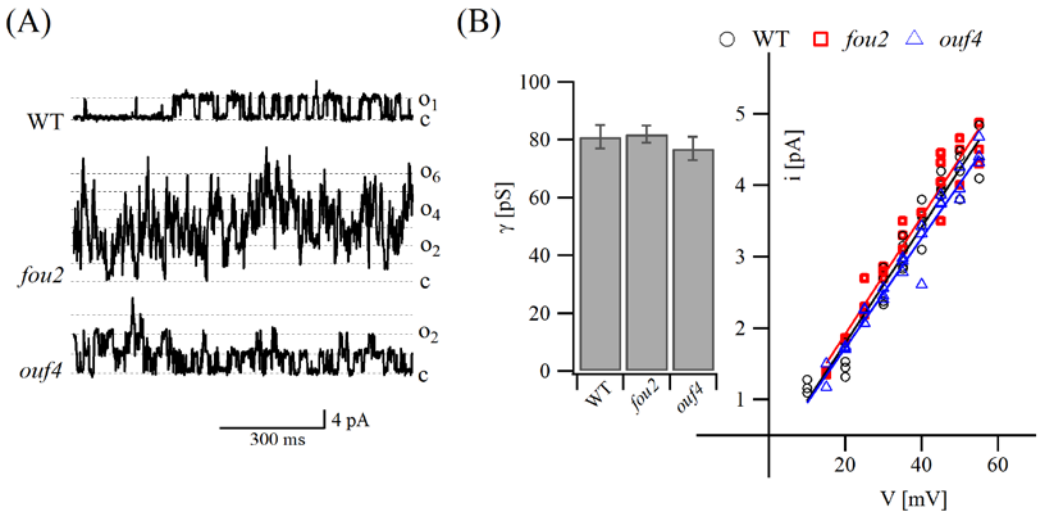

Figure 28. Single channel analysis of ouf4 mutant.

(A) Single channel fluctuations of *ouf4, fou2* and WT channels evoked at +45 mV. (B) Single channel current amplitudes *of ouf4, fou2* and WT plotted against the respective depolarizing voltage pulses. Lines reflect global regression fit for each plant line. Symbols for each plant line comprises 4-6 individual experiments. Bar diagram gives the calculated unitary conductance of *ouf4, fou2* and WT. Means (±SD) of 4-6 measurements for each plant line are shown.

4.4. Role of TPC1 in control of vacuolar membrane voltage

The TPC1 hyperactivity in the *fou2* mutant may affect the vacuolar membrane voltage and in turn influence the JA signalling pathway. To evaluate such a possible role of TPC1, the membrane voltage of mesophyll vacuoles was monitored in response to currents electrically injected in the range of 10 pA to 150 pA in the whole-vacuole current-clamp mode. These current-clamp experiments were performed with vacuoles isolated from different *A. thaliana* plant lines like WT, *fou2 and tpc1-2*. When the membrane voltage of the vacuole was maintained at -60 mV, the electrical currents were injected (Fig. 29A). Irrespective of the extent of the applied current injections, the membrane voltage of vacuoles from the TPC1-loss-of-function mutant *tpc1-2* did not alter (Fig. 29A). In contrast, current injections in particular above 10 pA resulted in transient depolarisation of WT vacuoles (Fig. 29A). These membrane depolarisations lasted longer with increasing current injections (Fig. 29A); or in other words the membrane repolarization time was prolonged with increasing current injections (Fig. 29A). In comparison to WT vacuoles, *fou2* vacuoles responded to the applied current injections with prolonged depolarisation of the vacuolar membrane (Fig. 29A). The lack of current-induced membrane depolarisation with *tpc1-2* vacuoles on the one hand and the persistence of current-induced membrane depolarisation with *fou2* vacuoles on the other hand suggest that the TPC1 channel may be involved in membrane voltage control. To underpin this view, the current-induced membrane depolarisation was studied in the presence of 1 mM luminal Ca^{2+}, a negative regulator of the TPC1 channel activity (Fig 29B). Under these high luminal Ca^{2+} conditions, the injection of 150 pA caused a tiny short-term depolarisation of WT vacuole membrane. Further increase of current injection did not cause a significant increase in the duration of vacuolar membrane depolarization (Fig. 29B). To evaluate whether vacuolar K^+-selective ion channels might be involved in the depolarisation of the membrane voltage, Cs^+ which is non-permeable for K^+-selective ion channels was applied instead of K^+ to both sides of the vacuolar membrane. As a result, the TPC1-dependent depolarization phase appeared to be changed compared to the voltage membrane response recorded in the presence of K^+ (Fig. 29C). Furthermore, the time span of vacuolar membrane depolarization phase was stable with $\geq$300 pA current injections under Cs^+-based solute conditions while prolonged membrane repolarization phases were recorded with current injections above 150 pA under K^+-based solute conditions.

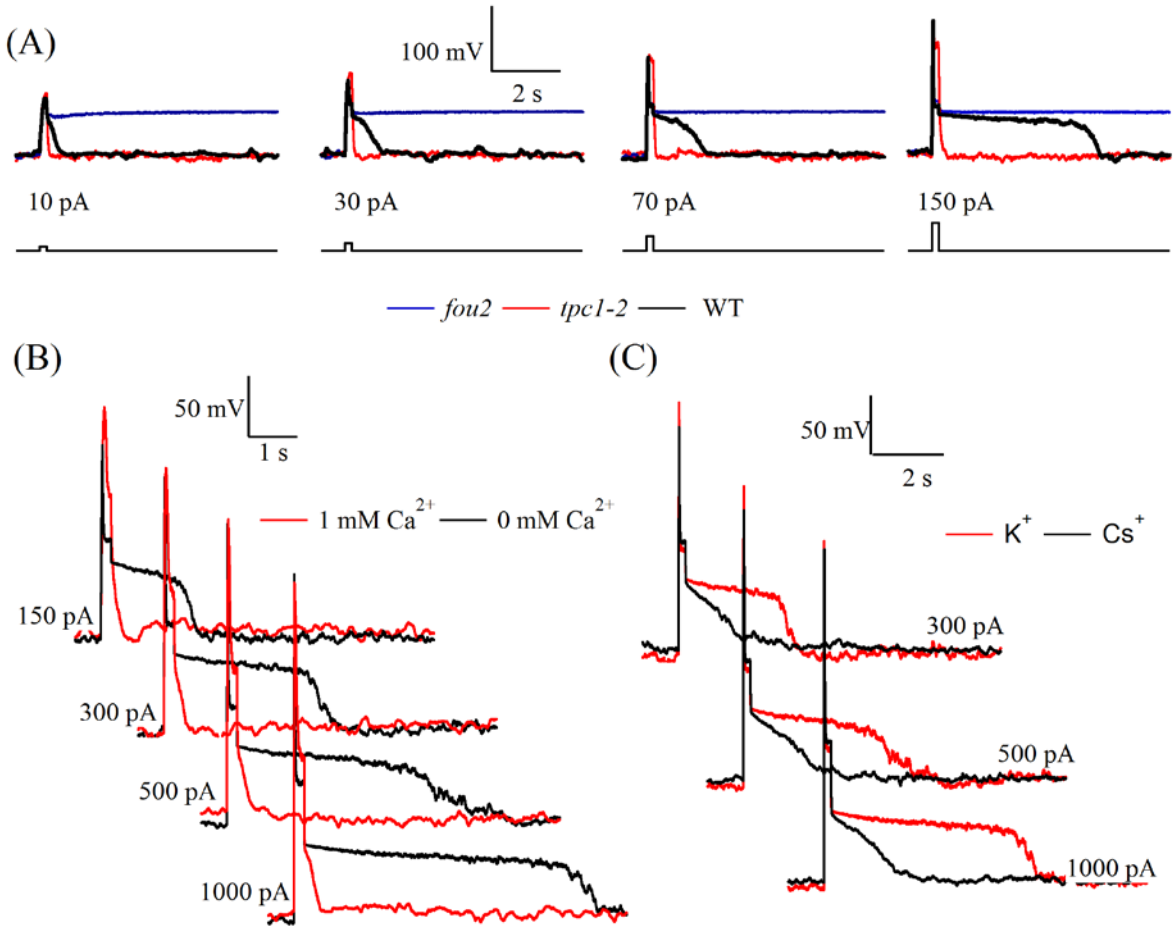

Figure 29. Changes in membrane voltage of Arabidopsis thaliana vacuoles.

(A) Vacuolar membrane voltage responses to different current injections (0 pA - 150 pA) recorded from WT (black), *fou2* (blue) and *tpc1-2* (red) vacuoles. Measurements were conducted in the absence of vacuolar calcium. (B) Comparison of vacuolar WT membrane voltage recordings performed after injection of indicated current amplitudes under 0 mM and 1 mM vacuolar free calcium. The voltage response was confirmed for each plant line in at least 3 separate experiments. (C) Vacuolar WT membrane voltage responses to injection of indicated current amplitudes were monitored in the presence of potassium- or cesium-composed solutions in three or two individual experiments, respectively.

5. Discussion

5.1. *ouf* mutants resemble very closely WT-like phenotype

The vacuolar SV/TPC1 channel is strictly controlled by changes in the vacuolar and cytoplasmic calcium concentration (Ivashikina et al., 2005; Beyhl et al., 2009; Hedrich and Neher, 1987; Pottosin et al., 1997, 2004). The lack of TPC1 vacuolar calcium-dependence in the *Arabidopsis thaliana* mutant *fou2* (fatty acid oxygenation upregulated 2) causes that, this non-selective cation channel acts in a hyperactive manner (Bonaventura et al. 2007a; Beyhl et al., 2009). A notable effect of the *fou2* mutation in the TPC1 protein is a strong phenotype, appearing after the *Arabidopsis thaliana* plant reaches the adult stage (Fig. 14). This phenotype manifests itself in reduced rosette diameter, epinastic leaves with short petioles and anthocyanin accumulation (Bonaventure et al., 2007a; 2007b). One of the most interesting feature of *fou2* mutant is an increased production of jasmonate, which becomes even more expressive in response to injury. The JA overproduction effect can be reversed through the cross of *fou2* with the *coi1-1* null mutant for the jasmonate co-receptor gene (Bonaventure et al., 2007a; 2007b). This double mutant *fou2 coi1-1* did not exhibit anymore the typical *fou2* phenotype like short petioles or anthocyanin accumulation, which has been identified as derivatives of the JA overproduction (Bonaventure et al., 2007a). Similar to *fou2 coi1-1,* a null mutation for ALLENE OXIDE SYNTHASE resulted in partial suppression of the *fou2-like* rosette morphology (Bonaventure et al., 2007b). Although the first 4–6 leaves of *fou2 aos* were morphologically similar to those of WT plants, minor differences between WT and *fou2* aos were still noticed. In conclusion, suppression of the *fou2* phenotype via *aos* null mutation is more extensive than *coi1-1* null mutation, but it is still not complete implicating a strong influence of the TPC1 hyperactivity on the cellular network (Bonaventure et al., 2007b).

However, morphology of the *ouf* mutants and WT plants resembled each other very closely. In our paper (Lenglet and Jaslan, 2017) three different phenotypes (I, II and III) were described which were found during plant cultivation under short and long-day growth conditions. The *ouf2*, *ouf7* and *ouf8* (class I) mutants shared a visual phenotype similar to WT independently of the day length. The second class (II) contains *ouf1* and *ouf3,* which resembled WT when grown under short-day conditions, but under long-day conditions flowering was delayed by

about one week compared to WT. The last class III was reserved for the *ouf6* mutant, because their leaf edges were more serrated than those of WT and additionally weakly epinastic under short-day conditions. However, such an *ouf6* phenotype was not observed during plant cultivation for patch clamp experiments, possibly due to slightly different short-day conditions and plant cultivation times. In the Lenglet and Jaslan (2017) paper, the phenotype characterization was carried out with five-week-old plants cultivated under a light intensity of 100 µE m^{-2} s^{-1} (1 µE = 1 µmol of photon energy) for 10/14 h and a constant temperature of 21°C. However, the electrophysiological measurements were performed with plants growing for 6.5 weeks under a day/night regime of 8/16 h with a light intensity of 150 µmol m^{-2} s^{-1} and a temperature of 22/16°C. Thus, difference in the plant appearance of *ouf6* seems to be lost at later developmental stages where the phenotype unified with WT-like. In the present doctoral thesis I examined three additional *Arabidopsis thaliana* TPC1 *ouf* mutants compare to Lenglet and Jaslan (2017) paper. I also created a different plant group classification. *Ouf8WT* (= $TPC1^{WT}$ + $TPC1^{M629I}$) and *ouf8ko* ($TPC1^{M629I}$), were not showing phenotypical differences to WT under short-day condition. Thus, they belong to group I, according to the classification presented in the present thesis together with WT and other *ouf* mutants (*ouf1/2/6/7/8*) (Fig. 14, 24A). At a 6.5 weeks-old cultivation stage under short day regime, the *ouf4* mutant exhibited a different morphology compared to *fou2* and group I-like plants. This plant line was characterized by a rosette size comparable to *fou2,* but did not manifest epinastic leaves with short petioles and anthocyanin accumulation. Therefore, based on the phenotype developed under the short-day conditions in the present work the available *ouf* mutants were classified into two groups: *ouf1/2/6/7/8/8WT/8ko* into group I and *ouf4* into group II.

The almost imperceptible differences between *ouf* and WT phenotypes already suggest that EMS-based mutagenesis had a high direct impact on *fou2*-related dysregulated TPC1 channel function. This notion was confirmed by *TPC1* gene sequencing in six out of eight *ouf* mutants (Fig. 15). The foregoing notwithstanding, the question arises why there are still some minor differences in the phenotype between WT and the *ouf* mutants? It is known that 273 genes in the *fou2* mutant were either subjected to the process of up-regulation (246 genes) or down-regulation (27 genes) compared to WT (Bonaventure et al., 2007b). There is the possibility that in the *ouf* mutant TPC1 channel activity is not regained to exactly the WT level (chapter 5.3), what could result in an altered stimulation of TPC1-dependent genes. Mutation restoring

WT phenotype in *ouf* plants could also directly have impacted other genes. Since the *ouf4* mutant does not contain a second mutation in the *TPC*1 gene (Fig. 15), the reversion of the *fou2* TPC1-channel-hyperactivity in the *ouf4* mutant is very likely related to the dysfunction of some other gene product which feeds back on the TPC1 channel activity possibly on the transcriptional and/or post-translational level. This notion is supported by the not fully recovered *fou2* phenotype in the *ouf*4 mutant, i.e. rosette size was still reduced in *ouf4* like in *fou2* compared to WT (Fig. 14). On the post-translational level one could speculate about regulatory proteins with either a positive or negative effect on the TPC1 channel activity, which then need to be either impaired or accelerated in the *ouf4* mutant, respectively (chapter 5.3). Furthermore, one cannot yet exclude that the *ouf* mutant plants could have additional few mutations in the genome, which may have some effects on the WT phenotype independent of the TPC1 channel.

5.2. Impact of altered TPC1 channel structure for the loss of *fou2*-like phenotype

In comparison to *fou2* and WT, all *ouf* mutants exhibited altered electrical SV/TPC1 channel properties (Fig. 17A, 18A, 23A, 27A). Due to the known crystal structure of TPC1 in *Arabidopsis* (Guo et al., 2016; Kinzer et al, 2016), we were able to connect the altered amino acid sequence in the TPC1 channel protein with different channel properties of the *ouf* mutants (Fig. 15; Lenglet, Jaslan et al., 2017). These considerations will be outlined in the present chapter.

***ouf1/2/3/7* mutants.** The SV/TPC1 channel activity was silenced not only in the *ouf1/3* and *ouf7* mutants by expressing truncated TPC1 channel protein versions, but also in the *ouf2* mutant by an additional point mutation (G583D) in the vacuolar part of transmembrane domain S11 of TPC1. Thus, these changes in the TPC1 amino acid sequence were sufficient to erase the hyperactivity of TPC1 channel originally caused by the D454N mutation (Fig. 17). Since these *ouf* mutants (*ouf1/3, ouf*2 and *ouf7*) did not exhibit any SV channel activity in the recorded voltage range of -80 to 110 mV, they imitate the TPC1-loss-of-function mutant *tpc1-2* characterized by a WT-like phenotype (Fig. 14; Peiter et al., 2005). The introduction of a stop codon into the gene sequence results in the lack of three (*ouf1/3*, W529X) or four (*ouf7*, W492X) transmembrane domains which very likely affected the integrity of the total channel

protein and in turn proper channel function. It may even cause the total absence of the protein in the vacuolar membrane (Fig. 15). With respect to *ouf2*, the molecular/structural mechanism leading to the TPC1 inactivity in the *ouf2* mutant (G583D), however, is hard to explain. One may consider that the absence of TPC1 currents in the *ouf2* mutant could be related to a shift of the TPC1-channel activation threshold to much more positive voltages (i.e. more than +110 mV) or to channel blockage. The hydrophobic glycine at position 583 is spatially located in the luminal part of the S11 helix, near the helices responsible for the construction of the TPC1 channel pore (Fig. 15). Structural differences and the polar nature of aspartate may cause local conformational changes, affecting adversely the geometry and function of the pore (Prof. Thomas Müller, *University Würzburg, personal communication).*

***ouf6* mutant.** The point mutation **A669V** together with the *fou2* (D454N) mutation created in the *ouf6* mutant new SV/TPC1 channel features (Fig. 15)**.** Replacement of alanine to valine at position 669 seems to be rather conservative due to its nonpolar character. The spatial localization in 6th turn of helix S12 ranks the amino acid in a tightly packed structure of the channel gates (Prof. Thomas Müller, University Würzburg, personal communication; Fig. 15). The larger size and the branched structure of valine may change the probable location of the nearby helices S6 and S12, affecting the flow of ions. Patch clamp recordings revealed drastic reductions of TPC1 current density already at 0 mM vacuolar calcium (Fig. 18). Further analysis showed that three factors contribute to this change: reduced relative and absolute open channel probability plus decreased single channel conductivity (Figs. 19, 20). Deviations in both relative and absolute open channel probabilities could also explain the lack of channel activity in the voltage range -30 mV to +40 mV. However, fast activation kinetics and reduced sensitivity to inhibitory luminal calcium (10 mM) of the TPC1 channels in *ouf6* (A669V D454N) were similar to *fou2*, suggesting a selective influence of Val669 on *fou2*-like SV channel features (Fig. 18). Interestingly, the high susceptibility of the WT channels to vacuolar calcium inhibition was not fully restored by the A669V mutation in the *ouf6* mutant. This higher vacuolar calcium susceptibility (≈30%) of *ouf6* TPC1 channels points to a possible interaction between the cytosolic entrance to the pore (A669V mutation) and the vacuolar calcium sensor (D454N mutation). Higher vacuolar calcium susceptibility together with the already reduced current density at 0 mM vacuolar calcium are likely able to keep channel activity low at high

luminal calcium concentration. As a result, the outward current density in *ouf6* was comparable to WT TPC1 currents at high luminal Ca^{2+} loads.

***ouf4* mutant** carries TPC1 channels containing solely the D454N mutation. Nevertheless, *ouf4* still shows a WT-like phenotype and WT-like response to wounding (Fig. 14). Thus, these results indicate that a change in a gene within the *ouf4* genome must have taken place, whose gene product is involved in regulation of the SV channel activity. The o*uf4* mutation did not change the *fou2* TPC1-channel features like fast channel activation (Fig. 27) and single channel conductance (Fig. 28). There was also no significant shift of the voltage activation threshold compared to *fou2* (Fig. 27). However, small differences in half-activation voltages V_1 and V_2 describing the voltage-dependent gating of the transitions between the different channel states (C1, C2, O) were noticed. $V_{1/2}$ values of *ouf4* seems to be a mixture of those values determined for WT and *fou2* (V_1: WT= 39 ± 9 mV, *ouf4*= 29 ± 10 mV, *fou2* = -2 ±2 mV ; V_2: WT = 26 ±5 mV, *fou2*= 2 ±7 mV, *ouf4*= 2 ± 4 mV; Supplemental table 1). This means that the voltage-dependent transition $C_1 \leftrightarrows O$ for *ouf4* were slowed down to the WT range. Nevertheless, in *ouf4* the TPC1 current density was 80% less than for *fou2* (Fig. 27). The underlying mechanism is yet unknown. However, one could guess a mutation in a protein, which can modulate the channel activity in a manner, for instance via the cytosolic calcium sensitivity in TPC1, that leads to the decreased SV/TPC1 current density. In the context of cytosolic Ca^{2+}, the fact is interesting that the cytosolic calcium sensitivity of TPC1 channel appears to be not similar in all cell types. Even though TPC1 is encoded in *A. thaliana* by a single-copy gene and no alternative splicing takes place, the cytosolic calcium sensitivity of TPC1 channel was lower in mesophyll cells than in guard cells (Rienmüller et al., 2010). Furthermore, the TPC1 current density level in guard cell protoplasts of *Arabidopsis thaliana* was much higher than in mesophyll protoplast (Rienmüller et al., 2010). It was proposed that these cell-type specific differences in TPC1 features and current density may be linked to cell-type specific modulation via external yet unknown factors. Similarly, such regulatory factors could be affected in the *ouf4* mutant leading to a change in the TPC1 channel activity.

Such a regulation could take place via the involvement of TPC1 C-terminus, which has a great impact for the channel functionality (Larisch et al., 2012). It forms a secondary structure, enabling the functional dimerization of the two monomers in TPC1 protein (Larisch et al., 2016). The C-terminus carries a number of motifs, which may play a structural role via

connections to other functional domains of the TPC1 channel (Kintzer & Stroud, 2016 and 2017). It was also postulated that the C-terminus harbours regulatory binding sites (poly-R motif, calcium coordination site, possible phosphorylation sites) for lipids, second messengers or kinases/phosphatases (Kintzer & Stroud, 2016). Mutations impairing the conformational intermolecular interaction of TPC1 C-terminus with regulatory factors resulted in a strong decrease in the current density without changing the voltage-dependent gating behaviour of TPC1 (Larisch et al., 2016). For instance, after mutation of a possible phosphorylation site (Ser706) (Larisch et al., 2016), or of Arg552 likely involved in linking the C-terminus with the voltage sensor (Jaslan et al., 2016), a drastic decrease in the macroscopic current density and unaltered voltage dependency compared to WT was observed. Taking into consideration the electrical characteristics of the *ouf4* mutant such as decreased current density and *fou2*-like channel activation (Fig. 27) and the multitude of regulatory binding sites within the C-terminus of TPC1, one could speculate that the decrease in the TPC1 current density in the *ouf4* mutant could be mediated via conformational changes induced by phosphorylation or interaction with another protein, destabilizing the C-terminal part of TPC1. A further plausible reason for the TPC1 current decrease in the *ouf4* mutant could be a change in the transcriptional control. A decreased transcript level compared to WT could lead to a lower amount of channel proteins in the vacuolar membrane and hence decrease in current density of *ouf4* mutant.

***ouf8* mutant.** The 1st pore loop (S5-pore loop-S6) and the 2nd pore loop (S11-pore loop-S12) is part of a heterodimeric TPC1 pore structure which is convergent towards the vacuolar lumen (Fig. 3; Guo et al., 2016;. Kinzer et al, 2016). In the *ouf8* mutant a strongly conservative methionine located at position 629 in the N-terminal part of second pore loop (S11-pore loop-S12) is substituted by isoleucine (Fig. 15). When the methionine is substituted with the branched isoleucine in the *ouf8* mutant, it leads to narrowing the pore diameter. Removal of the sulphur atom, present in methionine, could electrically affect the cations or their hydration shell resulting in disorder of ion transport capacity (Prof. Thomas Müller, University Würzburg, personal communication). M629I mutation within the selectivity filter II (Fig. 15) affected the TPC1 unitary conductance, reducing it by one half (Fig. 22). However, the slightly increased relative open probability of the *ouf8* mutant appeared to be sufficient to compensate the reduced transport capacity of individual TPC1 channels, leading to a similar macroscopic outward current density of *ouf8* and *fou2* in the absence of vacuolar Ca^{2+} (Fig.

21). Furthermore, the *ouf8* mutation did not drastically change *fou2* feature such as fast activation, vacuolar calcium insensitivity and voltage-dependent gating behaviour (Fig. 21). Thus, the ability of *ouf8* channels to import and export cations from the vacuole under luminal Ca^{2+}-free solute condition was not impaired (Fig. 21, 23). Since the vacuole is a plant calcium store, high luminal calcium loads provides for a more physiological condition for studies of *ouf8* mutant. Such patch clamp experiments conducted at a higher vacuolar calcium level revealed deviations in TPC1 current densities between WT, *fou2* and *ouf8*. No outward currents were observed in WT, while pronounced outward currents were still recorded for *ouf8* and *fou2* being about two times larger for *fou2* compared to *ouf8* (Fig. 23). One could consider, that the 50% reduction in the *ouf8* current density at 10 mM vacuolar Ca^{2+} at the respective voltages compared to *fou2* and the 50%-decrease in the single channel conductance of *ouf8* mutant at 0 mM vacuolar calcium is not a coincidence. Then, one could claim that these two mutants in the range of positive voltages and high vacuolar calcium have similar relative voltage-dependent open probabilities. However, tail current experiments revealed one TPC1 channel property that was very similar for *ouf8* and WT and significantly different to *fou2*, namely, the ability to release cations from the vacuolar lumen into the cytosol at high vacuolar Ca^{2+} level. For *ouf8 and* WT, we observed a decrease in the tail current density by 92% and 97%, respectively, with increasing vacuolar calcium level from 0 mM to 10 mM. Nonetheless, for *fou2* a 55% reduction in tail current density was determined after a rise of the vacuolar calcium level from 0 mM to 10 mM; i.e. an inward cation flux was still noticed for the *fou2* mutant but absent in WT and *ouf8* (Fig. 23). Thus, the similar lack of cation inward currents in *ouf8* and WT at high vacuolar calcium loads seems to cause the reverted *fou2* phenotype in the *ouf8* mutant, even though the underlying mechanism is apparently different in these plant lines. In WT vacuoles the ion efflux from the vacuole into the cytosol via TPC1 channel under high vacuolar calcium is most likely suppressed under normal growth conditions by negative regulatory effect of luminal Ca^{2+} on the vacuolar calcium sensor of TPC1. In contrast, for *ouf8* mutant we could observe that a vacuolar calcium-dependent block inhibits the cation inward currents; i.e. Ca^{2+} seems to got stuck in the channel pore. Irrespective of the underlying reason, the inability to release cation into the cytosol has obviously the same effect as the complete loss of TPC1 function in the *tpc1-2* mutant. As a result, the stressed *fou2*-like phenotype disappeared in *ouf8*. Thus, this finding suggest a key role of the TPC1 channel in the cation release from the vacuole into the cytosol. Furthermore,

ouf8 reverting mutation allow a reversible block of SV channel pore region in presence of high vacuolar calcium (Fig. 23). This feature could be used to dissect the impact of outward and inward currents on plant in wounding/defence responses as well in other stress responses as e.g. salt stress.

5.3. Amino acid involved in AtTPC1 channel conductivity

Until now, comparison of TPC1 unitary conductance from different plant species was difficult, mainly caused by the heterogeneity of the experimental conditions used by researchers (pH, ion concentrations, buffers) (Schulz-Lessdorf and Hedrich, 1995; Dobrovinskaya et al., 1999; Pottosin et al., 2001). Nevertheless, former studies already pointed to some species-dependent differences in the TPC1 unitary conductance (Schulz-Lessdorf and Hedrich, 1995). Results about the TPC1 channels from *Lotus japonicus*, *Vicia faba* and *Arabidopsis thaliana* provided in the present work further underpin this view. LjTPC1 and VfTPC1 showed a 3.5-fold higher conductance than AtTPC1 (Fig. 25B,C). The alignment of the TPC1 amino acid sequences from different species including AtTPC1 and LjTPC1 provided some insights in possible underlying molecular mechanism (Fig. 25A). A protein polymorphic amino acids in the P2 region of the TPC1 channel from *Arabidopsis thaliana* ^{629}**M**GNWQVW^{636} and *Lotus japonicus* ^{632}**S**EVWLEL^{636} was revealed (Fig. 25A). Unfortunately, *A. thaliana* SV/TPC1 channel with M629S mutation mimicking the homologous amino acid of *L. japonicus* and *V. faba* at this position exhibited unstable single channel fluctuations, preventing the determination of the single channel conductance so far (Fig. 26A,B). Instead, a 35% and 18% reduction of single channel conductance was observed for transiently expressed TPC1 channel mutants carrying M629I and M629T single mutation, respectively (Fig. 26A,B). Thus, Met629 in AtTPC1 was proven to have a high impact for the single channel conductance. But the results also suggest, that the unitary conductance of AtTPC1 does not depend only on Met629 but probably on some other amino acids located in pore region of the TPC1 channel. Additionally, it is also possible that the amino acid background of the LjTPC1 is also important to generate a pore region with a higher transport capacity. Furthermore, single channel fluctuations of transiently expressed M629I mutant channels showed side by side not only openings to the full-open channel state but frequently also to a semi-open channel state (Fig. 26C). This observation

leads to the assumption that Met629 in AtTPC1 might be crucial for synchronized opening movements of both polypeptides building a functional pore in the TPC1 protein. Experiments with the stable *ouf8* (M629I D454N) plant line confirmed a decrease in its unitary conductance due to the M629I mutation, compared to the *fou2* TPC1 channel (D454N). In contrast to the transiently expressed single channel mutant M629I, the semi-open channel states, however, were not recorded with the stable *ouf8* (M629I D454N). One could suspect that the *fou2* mutation causing channel hyperactivity may decrease the probability to undergo the transition into the stable intermediate open-channel-state (O_{half}) and shift it to the full open-channel-state. It is interesting, that the coexistence of the two mutations D454N and M629I in one channel protein creates a new SV/TPC1 channel feature: Ca^{2+}-dependent block of ion release from the vacuole into the cytosol. This result suggests a general and important role of Met629 in modulation of AtTPC1 ion transport pathway. However, the structurally very similar substitution of Met629 to valine (M629V) did not seem to influence the channel filter size and the ion permeation when the crystal structure was inspected (Guo et all. 2017). Furthermore, electrophysiological experiments with M629V-expressing HEK cells did not reveal changes in the K^+/Na^+ selectivity of TPC1 channel (Guo et all. 2017). The unitary conductance of M629V mutant channel still needs to be examined. A crucial role of this amino acid in formation of protein packing surrounding the channel filter was postulated by Guo et al. (2017). These interactions seems to be responsible for the stability of the channel selectivity filter and may also support the ion transport capacity.

5.4. The luminal calcium sensor of TPC1 could be functionally linked to the pore region

SV/TPC1 channel activity is modulated by many factors, underlying its complex structure and regulatory network (chapter 1.4). For instance, it is already known for two decades, that an increased vacuolar Ca^{2+} concentration is preventing SV channel activation or in other words forcing the TPC1 pore region to reside in the closed position (Pottosin et al., 1997, 2004). Stimuli recognized by TPC1 are converted to cumulative physiological cellular response, which is mediated via vacuolar membrane depolarization or hyperpolarization (chapter 5.7). These statements may suggest, that key amino acids forming functional channel domains, such as

vacuolar calcium sensor, voltage sensing domain or pore region, can affect each other directly or indirectly and modulate channel responses. The crystal structure of AtTPC1 (Guo et al., 2016; Kintzer & Stroud, 2016) suggests a distance of about 35Å between the vacuolar Ca^{2+} sensor (VCS) and the pore region, excluding any direct interaction between them (Guo et al., 2016). However, indirect influence of VCS on the pore region seems to be possible. Theoretically, one can track chain of functionally linked amino acids from vacuolar Ca^{2+} sensor to the pore region. The amino acids building the VCS in the loop between S7 and S8 helices are localized near the major voltage sensing domain (VSD) in S10 helix. Structure-function studies showed that D454N (*fou2)* lost its sensitivity toward luminal calcium, promoting voltage-dependent channel opening via shifting the activation threshold to more negative potentials (Beyhl et al., 2009). Same results were obtained for other mutated amino acids (Asp240, Glu528, Glu239, Glu457) predicted to structurally contribute to the vacuolar calcium sensor (Dadacz-Narloch et al., 2011; Guo et al., 2016: Jaslan et al., 2016). Parallel changes in voltage and vacuolar calcium sensing strongly suggest the functional link and interactions between the VCS and the VSD of TPC1 channel. Moreover, replacement of Arg531 located in the upper half of the voltage sensor helix S10 (Guo et al., 2016; Kintzer & Stroud, 2016) to methionine resulted in *fou2*-like vacuolar calcium insensitivity (Jaslan et al., 2016). This effect indicates that at least in one conformational state Arg531 provides a link between the major voltage-sensing helix S10 and the luminal calcium sensor (Jaslan et al., 2016). It is also indisputable that cytoplasmic Ca^{2+} ions are required for voltage-dependent activation of plant TPC1 (Hedrich and Neher, 1987). This fact indicates that cooperation between the voltage sensor domain and the cytosolic calcium sensor (EF-hands) is necessary to force channel opening. Electrophysiological studies in the native membrane environment (Jaslan et al., 2016) indicate that in line with the crystal structures (Guo et al. 2016; Kintzer & Stroud 2016) Arg537, Arg540 and Arg543 are part of the voltage-sensing domain of TPC1. They are separated by two hydrophobic residues following the conserved motif of a voltage sensor (Noda et al., 1984; Catterall, 2010). These three core arginine in S10 (R537, R540 and R543) serve as gating charges which re-orientate in response to changes in the electrical field of the vacuolar membrane. They are followed by two conserved arginines at position 550 and 552, located in the S10–S11 linker, which transfers vertical movements of the voltage sensor helix S10 to C-terminal domain of TPC1 (CTD) via ion pairing (Jaslan et al., 2016). This statement is supported by electrophysiological studies showing the lack of a voltage shift in TPC1 channel

mutants R550M and R552M (Jaslan et al., 2016). It can be further assumed that the amino acid residues Glu682 and Glu685 in the C-terminus creates hydrogen-bonds to Arg552 and thereby directly link the C-terminus, which is an extension of the pore region, to the major voltage-sensing S10 domain (Kintzer & Stroud, 2016). These interactions provide for voltage-dependent modulation of TPC1 channel opening (Jaslan et al., 2016). There are also hints in the channel structure, which can structurally facilitate voltage-dependent channel activation in presence of cytoplasmic Ca^{2+} ions. Ca^{2+} seems to be crucial for creation an intramolecular complex between EF-hands and the C-terminal domain via a salt-bridge to Asp376 and Arg700 in the C-terminus. The C-terminal amino acid residue Ser701 additionally appears to coordinate the activating Ca^{2+} ion together with Glu374 and Asp377 (Kintzer & Stroud, 2017). So, lack of cytosolic Ca^{2+} could result in no EF2-CTD interaction, increased dynamics in the CTD, and may disrupt conformational coupling to VSD2 (Kintzer & Stroud, 2017). One could conclude, that *fou2* mutation (D454AN), which is part of the luminal calcium sensor, is functionally connected to pore region via the voltage sensor and C-terminus and thereby might be able to modulate the spatial position of pore amino acid residue like e.g. Met629 in channel selectivity filter SF2. So structural changes in the area of the vacuolar calcium sensor could lead to spatial rearrangements within the TPC1 channel pore.

Accordingly, deviation in single channel conductance of *ouf8* stable line (M629I D454N: 40 pS versus WT and *fou*2 (D454N): 80 pS; Fig. 22B) and lack of functionality of TPC1 channels in the *ouf8ko* stabile line (M629I*)* could suggest that the D454N mutations is simultaneously necessary to obtain the channel activity in the presence of isoleucine at position 629 in AtTPC1 protein. The assumption that isoleucine at amino acid position 629 might be responsible for the TPC1 channel inactivity is supported via the decreased current density in *ouf8WT* mutant line (*ouf8WT = $TPC1^{WT}$ + $TPC1^{M629I}$*) compared to WT, indirectly pointing to the presence of non-functional TPC1 channel proteins in the vacuolar membrane. Thus, the *fou2* mutation may influence the isoleucine localization in the pore region of TPC1 channels of stable M629I mutants. However, transiently expressed M629I channels in *tpc1-2* null mutant were functional and exhibited a 30% higher conductance (52 pS) than the transiently expressed M629I D454N TPC1 mutant channels (*ouf8*, 40 pS*)* (Fig. 26B). Comparison of WT-TPC1 unitary conductance in stable line and transiently expressed in *tpc1-2* were not showing any significant deviation (Fig. 22B, 25C). A putative effect of the transient expression on the

unitary conductance of TPC1 channels in the *fou2* remains to be examined. Furthermore, the loss of channel activity in the stable M629I mutant line is still very hard to explain and might be related to some unknown posttranscriptional modifications, such as when enormous quantities of channel proteins are produced during transient expression, they might be not properly processed.

5.5. TPC1-dependent K^+ release from vacuole occurs during wound-induced JA response

Jasmonate (JA), as a key player in systemic plant stress response, is participating in signalling cascade associated with cytosolic calcium signatures, and spreading a wound signal (Farmer et al., 2014; Choi et al., 2014; Maffei et al., 2004; Munemassa et al., 2011; Yang et al., 2012; Vadassery et al., 2012; Sholz et al., 2014; Kiep et al., 2015). However, it is not yet clear what causes the initiation of JA synthesis. Highly upregulated JA production in *fou2* mutant connects TPC1 channel with JA signalling. So far, only the potassium starvation transcriptome can be directly connected to the D454N mutation in the AtTPC1 channel protein (Bonaventure et al., 2007b). Interestingly, it was proposed that JA plays a central role in the control of K^+ homeostasis in *Arabidopsis* plants (Armengaud et al., 2004). Thanks to vacuolar localization of nonselective SV channel, one can correlate vacuolar potassium management with up-regulation of jasmonate synthesis (Hedrich and Marten, 2011; Beyhl et al., 2009). Is it now possible that K^+ fluxes may trigger JA responses? While the nature of the cation(s) responsible for the *fou2* phenotype is still a mystery, it is known that Ca^{2+} plays a critical role in the K^+ starvation response (Xu et al. 2006). So one could assume that the activation of JA biosynthesis in *fou2* could be caused by deregulated intracellular K^+ fluxes and perhaps also by indirectly activated Ca^{2+} signalling. To expand our knowledge about the involvement of the TPC1 channel in activation of the JA pathway, electrophysiological characterization of six *ouf* mutants as restorer of WT-like plant morphology and JA synthesis was performed in this thesis. Among these *ouf* mutants, M629I mutation in the *ouf8* mutant turned out to be the most interesting, because it affected the TPC1 channel pore region. Isoleucine at position 629 not only reduced the unitary conductance of the TPC1 channel, but also led to a very rapid and efficient block of cation flux into the cytosol under high luminal calcium loads. The *ouf8* reverting mutation

selectively abolished the inward cation currents rather the outward cation currents in 10 mM luminal Ca^{2+} condition. Therefore, the vacuolar localization of TPC1 channel (Peiter et al., 2005) suggests a connection of TPC1-mediated K^+ efflux from the vacuole into the cytosol with the activation of jasmonate synthesis (Bonaventure et al., 2007a). This view is supported by several findings: (i) the high ability of TPC1 to conduct potassium ions (Schulz-Lessdorf and Hedrich, 1995; Ivashikina and Hedrich, 2005), (ii) 50% lower vacuolar K^+ level in the vacuoles of the *fou2* mutant harbouring the hyperactive TPC1 channel (Beyhl et al., 2009), and (iii) the selective Ca^{2+} block of K^+ release in the *ouf8* mutant, sufficient to reverse the *fou2* phenotype characteristic for the hyperactive jasmonate signalling pathway (Fig. 14, chapter 4.3.3). Vacuolar calcium-induced block of TPC1 channels in the *ouf8* mutant obviously mimics the lack of potassium release from the vacuole into the cytoplasm, which seems to be the key to the initiation of *fou2*-phenotype creation. All *ouf* mutants share this *ouf8* feature with WT and *tpc1-2*. With regard to *ouf4*, it even seems that a decrease of inward potassium fluxes with *fou2*-like voltage dependency is sufficient to remove *fou2* phenotype (Fig. 14; Fig. 27). Under potassium gradient (high $[K^+]_{lumen}$/low $[K^+]_{cytosol}$), inward currents for *fou2* are about five times higher compared to WT (Beyhl et al., 2009). Therefore, one could assume that *ouf4*, which has all *fou2* attributes but 5 times lower current density will mimic WT-like inward currents under asymmetrical potassium condition and in turn the WT phenotype. To sum up, potassium release from vacuole via TPC1 is strongly correlated with jasmonate signalling. With respect to TPC1 activity of the *fou2* and *ouf4* mutant, one could now assume that quantity of released K^+ ions is important. This is in line with *fou2* plant phenotype, which is appearing only in older plants or after injury and supports an idea of dosage effect of *fou2* allele postulated by Bonaventure et al. (2007a). Thus, after a wounding signal, TPC1 channel activity likely has to reach a certain threshold to turn on JA biogenesis. It is also worth to mention the phenomenon of an increased expression of JAZ10 or VSP2 genes in response to injury which is still observed in the TPC1 loss-of-function mutant as well as in the *ouf* mutants (Lenglet and Jaslan, 2017). These findings suggests that potassium ions flowing out of vacuole are important for initiation the activation of the jasmonate pathway, but TPC1 seems not to be the only channel, which participate in this process.

5.6. Is TPC1 involved in vacuolar Ca^{2+} management?

It was mentioned in chapter 5.4, that Ca^{2+} signatures are related to wound signalling in plants. However, till now a big debate is ongoing about the question which plant ion channel is responsible for the calcium release from the vacuole store. In the present chapter I would like to discuss a TPC1 participation in this process.

Experiments performed with guard cell vacuoles from *Arabidopsis thaliana* in the presence of 15 mM Ca^{2+} at the cytosolic side and 150 mM K^+ at vacuolar side of the tonoplast with symmetrical pH 7.5, showed a Ca^{2+} current directed towards the vacuolar lumen (Rienmüller et al., 2010). Due to acidification of the vacuolar lumen a further increase in the Ca^{2+} current density was found in this cell type (Rienmüller et al., 2010). Similar transport feature of TPC1 channels were recorded from vacuoles derived from *Arabidopsis thaliana* suspension cell culture and mesophyll cells under physiological pH conditions (vacuolar pH 5.6, cytosolic pH 7.4) and similar solute conditions (Ivashikina and Hedrich, 2005; Rienmüller et al., 2010). These data suggest that under artificial solute conditions in principle TPC1 could provide for a transport pathway for Ca^{2+} across the vacuole membrane. However, *in vivo* the extremely large Ca^{2+} gradient is directed in the cytosol and not into the vacuole. Therefore, calcium sequestration in the vacuolar lumen can only take place upon active or secondary active Ca^{2+} transport, mediated by P-type Ca^{2+} pumps (Geisler et al., 2000; Sze et al., 2000) or H^+/Ca^{2+} antiporter (Shigaki and Hirschi et al., 2006) but not by TPC1 channels.

But the crucial question is: Is the TPC1/SV channel from *Arabidopsis thaliana* able to mediate a calcium efflux and directly participate in calcium signalling? TPC1 contribution in cytosolic Ca^{2+} signal generation was proposed by Ward and Schroeder (1994) hypothesizing a calcium-induced calcium efflux from the vacuoles into the cytosol (CICR: calcium induced calcium release). Based on patch clamp measurements on *Vicia faba* guard cell vacuoles, authors showed that in the presence of 5 mM $[Ca^{2+}]_{cyt}$ and 50 mM $[Ca^{2+}]_{vac}$, the SV channel is capable to release calcium from the vacuole (Ward and Schroeder, 1994). Subsequently, a permeability ratio P_{Ca}/P_K of 3:1 was calculated for the SV channels from *V. faba* guard cells. Unfortunately, the ionic condition used in this publication was also far away from physiological conditions for Ca^{2+} and K^+ in native cellular environment which is more in the range of 0.01-1 µM $[Ca^{2+}]_{cyt.}$/ 0.2-2 µM $[Ca^{2+}]_{vac.}$ and close to symmetrical 100 mM K^+ (Felle, 1988; Bethke

and Jones, 1994; Pérez et al., 2008). Furthermore, quantification of the impact of luminal and cytosolic Ca^{2+} on SV channel activity from barley performed by Pottosin and co-workers (1997) demonstrated that the inhibitory effect of vacuolar Ca^{2+} dominated channel stimulation by cytosolic Ca^{2+} (Pottosin et al., 1997). Similar inhibitory luminal Ca^{2+} effect was found for AtTPC1 activity, where a shift in voltage activation toward more positive membrane voltage was observed during rising calcium concentration (Dadacz-Narloch et al., 2011). To sum up, cytosol-directed (inward) steady-state calcium currents in *A. thaliana* TPC1 were not yet recorded (Ivashikina and Hedrich, 2005). Therefore, the activity of VfTPC1 in the presence of 50 mM luminal calcium concentration is surprising at first glance but could be explained by deviations in the structure of the vacuolar calcium sensor. A negative charged amino acid homologous to AtTPC1 Glu457 and crucial for vacuolar calcium sensing in AtTPC1 is not present in VfTPC1 and replaced by asparagine (Prof. Dirk Becker, University Würzburg, personal communication). This amino acid polymorphism probably results in hyperactivity and a lack of negative regulation by vacuolar calcium similar to D454N (*fou2*) and other vacuolar calcium-sensor mutations in AtTPC1 (Dadacz-Narloch et al. 2011; Beyhl et al., 2009; Guo et al. 2017). Other parameter which could be responsible for differences between *A. thaliana* and *V. faba*, is the structure of the pore region. The differences in unitary conductance and selectivity filter sequences of second pore region P2 between *Arabidopsis thaliana* (^{629}MGNWQVW^{636}) and *Vicia faba* (^{631}SGIWGEL^{638}) are possibly correlated, thereby revealing the different functions of the SV channel in both plants.

In light of mentioned differences between AtTPC1 and VfTPC1, **CICR** was already widely studied and discussed in numerous publications, causing doubts about general TPC1 function as a vacuolar Ca^{2+}-release channel and initiator of CICR (Allen and Sanders, 1996; Pottosin et al., 1999; Carpaneto et al., 2001; Ivashikina and Hedrich, 2005; Ranf et al., 2008). According to the CICR hypothesis, physiological stimuli cause an increase in cytoplasmic Ca^{2+}, which together with TPKs will depolarize the vacuolar membrane voltage, leading to SV/TPC1 channel activation. Activated TPC1 channel can release Ca^{2+} ions from the vacuole and thereby the Ca^{2+} signal will be self-reinforced (Ward and Schroeder, 1994). But, in practice electrochemical Ca^{2+} gradients present in physiological ionic condition across the tonoplast that favour Ca^{2+} release from the vacuole, allow only a tiny fraction of SV channels to stay active (Pérez et al., 2008). *fou2* mutant plants harbouring a hyperactive TPC1 channel variant

(D454N) show an increased vacuolar calcium content compared to WT, what is surprising if TPC1 would release calcium under physiological condition *in vivo* (Beyhl et al., 2009). The *fou2* mutant has also a slightly lower resting cytosolic Ca^{2+} level compared to WT, and cytosolic Ca^{2+} increases after wounding stays similar in both plants (Lenglet and Jaslan, 2017). According to CICR, one would expect a decrease in the Ca^{2+} level in the plant vacuole and a rise in the cytosol. These three facts does not seem to support the CICR hypothesis, i.e. that TPC1 is vacuolar calcium channel capable to release calcium ions into the cytoplasm. This statement is reinforced by the same cytosolic Ca^{2+} signals still recorded in different native plant lines such as *A. thaliana* WT, *tpc1-2* null mutant ($TPC1_{ko}$) and TPC1-overexpressor ($TPC1_{ox}$) when exposed to various biotic and abiotic stimuli (cold, salt stress, oxidation stress, mannitol) (Ranf et al., 2008). For both $TPC1_{ox}$ and $TPC1_{ko}$ plants calcium responses were just as in WT plants (Ranf et al., 2008). This result suggests that the SV channel is not involved in the generation of global Ca^{2+} signals in response to stimuli mentioned above, and does not directly affect the cytoplasmic calcium homeostasis (Ranf et al., 2008). In well agreement, Choi and co-workers (2014) reported that there is no difference between the Ca^{2+} rise in WT and *tpc1-2* after salt stress, although they did exhibit a slightly delayed onset. This observation led to the assumption that TPC1 is involved in generation/modulation of the Ca^{2+} wave (Choi et al., 2014). However, long-distance Ca^{2+} waves seem to be TPC1-dependent and contribute to stress tolerance. It is possible that TPC1 takes part in generation of electrical signal, spreading during the salt stress and important to generate the Ca^{2+} signal (Choi et al., 2014; Kiep et al., 2015; chapter 5.7).

Due to similarity of plant amino acid sequences of SV/TPC1 channel to the animal Ca^{2+} and Na^{+} channels (Ishibashi et al., 2000), it was assumed that the TPC1/SV could play a role in Ca^{2+} transport through the vacuolar membrane and therefore involved in calcium signalling (Pottosin et al., 2009). However, this seems to be an over-simplification, i.e. Ca^{2+} release directly mediated via AtTPC1 is highly unlikely but one cannot exclude an indirect TPC1 participation in calcium signalling. Furthermore, amino acid polymorphism in channel structures like vacuole calcium sensor and pore region could also result in calcium-permeable TPC1 channels even under physiological condition.

5.7. TPC1-controlled membrane voltage involved in jasmonate signalling

As a lipid mediator of defence responses in plants, jasmonate is rapidly produced upon wounding. It could stimulate its own production via a positive feedback circuit (Bonaventure et al., 2007a). Moreover, metabolic labelling experiments in *N. attenuate* provided evidence that JA-Ile (active form) is synthesized *de novo* in leaves distal to the wound site (Wang et al., 2008). Activation of the jasmonate production in locations distant from harm involves the presence of a mobile signal induced during injury. In plants, these signals may include peptide or cell wall-derived oligosaccharide fragments (Narvaez-Vasquez et al., 2007), as well as wound-induced hydraulic or electrical signals (Malone, 1994; Zimmermann et al., 2009). There are few events recognized in initiation phase of jasmonate production: (i) Wound-induced ion fluxes (Schaller and Oecking, 1999; Bonaventure et al., 2007a), (ii) plasma membrane depolarization followed by a phase of slow repolarization (Stahlberg et al., 2006; Mousavi et al., 2013), (iii) well known cytosolic calcium signatures (Kiep et al., 2015). But, what is the key to the activation of JA synthesis and signalling? The discovery of the *fou2* mutant revealed the TPC1 channel as one key player in JA production (Bayle et al., 2009, Bonaventure et al., 2007). Its high ability to release potassium from the vacuole is directly linked to JA production as already discussed in chapter 5.5. Moreover, a TPC1-independent pathway of JA signalling initiation must exist because JA production can be still observed in TPC1 loss-of-function mutant *tpc1-2* or the *ouf* mutants during injury (chapter 5.5) (Lenglet and Jaslan, 2017). TPC1 channel participates also in indirect generation/modulation of the Ca^{2+} wave, but thereby very unlikely in direct generation of a calcium conductance itself as discussed in chapter 5.6. Thus, it seems to be reasonable to suggest a supreme trigger, which can regulate calcium and potassium fluxes .

Vacuolar membrane depolarization may be one of the missing early triggers for JA production and signalling. This statement is supported, by the prolonged depolarization of the vacuolar membrane in the *fou2* mutant compared to WT (Fig. 29). Since WT-TPC1 is negatively regulated via rising vacuolar calcium, this effect is reflected by shortened membrane depolarization at high vacuolar Ca^{2+} (Fig. 29). One could now further assume that the defective vacuolar calcium sensor in *fou2* will cause a vacuolar calcium-independent membrane depolarization. The application of cesium as a conductive ion for TPC1 also result in shortening of vacuolar membrane depolarization time. This effect could be explained by possible

participation of TPK channels in modulation of vacuolar membrane voltage (Fig. 29). Cesium is a conductive ion for TPC1 channels but not for TPK channels. Second possible reason is the different selectivity of TPC1 for cesium and potassium (Guo et all. 2016). However, lack of WT-like response in *tpc1-2* null mutant showed that TPC1 is a key player in vacuolar membrane voltage control (Fig. 29). Thus, TPC1 is important but not the only component involved in vacuolar membrane depolarization what seems to be in line with the facts that (i) TPC1 is probably active only during stress responses and (ii) a clear/pronounced *tpc1-2* phenotype is not observed/missing under normal growth conditions. One could now assume that the vacuolar membrane voltage is regulated, by the concerted action of potassium-permeable channels and proton pumps (Hedrich, 2012) linking the collective ion flow with the generation of physiological responses.

Looking over for all features of TPC1 hyperactivity, one can speculate about a chain of events stimulated in response to injury. When the high-conductive TPC1 channel is activated upon wounding, K^+ will be released into the cytosol and depolarize the vacuolar membrane, resulting in activation of JA synthesis. Consequently, the proton pump activity should be increased to restore the tonoplast membrane voltage. Increased proton pumping into the vacuole would in turn provide a higher driving force for H^+-coupled Ca^{2+} uptake into the vacuole via up-regulated CAX antiporters (Armengaud et al., 2004). This notion is well in line with (i) the increased Ca^{2+} level detected in the vacuolar lumen of *fou2* plants, (ii) higher ratio of potassium to calcium level in *fou2* vacuoles compared to WT plants (Beyhl et al., 2009), and (iii) the decreased cytosolic Ca^{2+} level in *fou2* (Lenglet and Jaslan, 2017). The lack of a proper feedback regulation of TPC1 channel by vacuolar calcium in *fou2* mutant in response to stimuli possibly results in a preserved state of membrane depolarization due to the lower ability to restore the vacuolar resting voltage via proton pumps, resulting in turn in constant jasmonate production.

6. Summary

In the framework of the presented doctoral thesis, the plant ubiquitous, non-selective vacuolar cation channel TPC1/SV was electrophysiologically studied in *Arabidopsis thaliana* mesophyll vacuoles to further enlighten its physiological role in plant stress responses. For this, the hyperactive channel version *fou2* (D454N), gaining a non-functional vacuolar calcium sensor, strong retarded growth phenotype and upregulated JA signalling pathway, and eight *fou2* reverting WT-like *ouf* mutants were used. Except of *ouf4*, all other seven *ouf* mutants carried a 2nd mutation in the *TPC1* gene. Therefore, the TPC1 electrical features of all *ouf* mutants were electrophysiologically characterized with the patch clamp method and compared with *fou2* and WT.

Due to a missense mutation, ***ouf1*** and ***ouf7*** mutants harboured a truncated TPC1 channel protein, resulting in an impaired protein integrity and in turn loss of TPC1 channel activity. Accordingly, *ouf1* and *ouf7* mimicked the *tpc1-2* null mutant with a WT- rather *fou2*-like phenotype. The ***ouf2*** (G583D D454N) mutant exhibited inactive TPC1 channels, probably because the G583D mutation located in luminal part of the S11 helix caused (i) a shift of the activation threshold to much more positive voltages (i.e. to more than +110 mV) (ii) or channel blockage. As a result of the TPC1 channel inactivity, the *ouf2* mutant also imitates the WT-like phenotype of the *tpc1-2* null mutant. In the ***ouf6*** mutant (A669V D454N) the 2nd reverting mutation selectively influenced *fou2*-like SV channel features. Both, the fast activation kinetics and reduced luminal calcium sensitivity were similar in *ouf6* and *fou2*. However, deviations in both, the relative and absolute open channel probability, resulted in strongly reduced (80 %) current density at 0 mM and channel inactivity in the voltage range between -30 mV to +40 mV compared to *fou2* and WT. Furthermore, the TPC1 channels in *ouf6* exhibited a higher susceptibility to inhibitory luminal Ca^{2+} than *fou2*. As a result of these different effects, the TPC1 channel activity almost vanished at high luminal Ca^{2+} loads, what is very likely the reason that *ouf6* lost the *fou2*-like phenotype. The ***ouf4*** mutation did not change the *fou2* TPC1-channel features like fast channel activation, single channel conductance and voltage-dependent gating behaviour. Nevertheless, the TPC1 current density was 80% less in *ouf4* than in *fou2.* Since the *TPC1* gene was not the target of the 2nd mutation, it can be assumed that it is modulated via external, yet unknown factor. In the ***ouf8*** mutant the TPC1 channels

additionally possess M629I mutation within the selectivity filter II resulting in a 50% decrease in the TPC1 unitary conductance. However, the slightly increased relative open channel probability of the TPC1 channels in *ouf8* compared to *fou2* appeared to be sufficient to compensate the reduced transport capacity of individual TPC1 channels. As a result, a similar macroscopic outward current density of *ouf8* and *fou2* was detected in the absence of vacuolar Ca^{2+}. Furthermore, *ouf8* mutation did not drastically change the typical *fou2* TPC1 channel features such as fast activation, vacuolar calcium insensitivity and voltage dependency. However, a reversible block of the cytosol-directed potassium efflux at increased vacuolar calcium concentration in *ouf8* mutant was found. Further inspection of transiently expressed TPC1 channel variants (M629I, M629T) on the single channel level suggest that Met629 of AtTPC1 in the channel pore region is crucial for the unitary channel conductance.

Taken together, current membrane recordings from *ouf* mutants revealed one common feature: All of them lacked or showed a strongly impaired ability for TPC1-mediated potassium release from the vacuole into the cytosol. Additionally, considering the detected dependence of the vacuolar membrane voltage on TPC1 activity, it thus seems that the TPC1-triggered vacuolar membrane depolarization caused by vacuolar K^+ release plays a key role in generation of the *fou2*-like phenotype. Accordingly, one can conclude that TPC1-dependent vacuolar membrane depolarization and initiation of jasmonate production are likely linked. This statement is supported also by the complete restoration of WT-like plant phenotype and JA signalling in the *ouf* mutants. Finally, as a control element of the vacuolar membrane voltage TPC1 is probably upstream located in JA signalling pathway and therefore a perfect junction for linking multiple physiological stimuli and response to them.

7. Zusammenfassung

Im Rahmen der vorgelegten Doktorarbeit wurde der in Pflanzen ubiquitär exprimierte, nicht-selektive vakuoläre Kationenkanal TPC1/SV elektrophysiologisch in *Arabidopsis thaliana* Mesophyllvakuolen untersucht, um seine physiologische Rolle in der pflanzlichen Stressantwort weiter aufzuklären. Hierfür wurde die hyperaktive Kanalvariante *fou2* (D454N), die einen nicht-funktionalen vakuolären Calciumsensor, ein stark verzögertes Pflanzenwachstum und einen hochregulierten Jasmonsäure-Signalweg aufweist, sowie acht *ouf* Mutanten mit *fou2*-umkehrenden Phänotyp benutzt. Mit Ausnahme von *ouf4* enthalten alle anderen *ouf* Mutanten eine weitere Mutation im *TPC1*-Gen. Daher wurden die elektrischen Eigenschaften von TPC1 in allen *ouf* Mutanten elektrophysiologisch mittels der Patch clamp Technik charakterisiert und mit *fou2* und dem Wildtyp verglichen.

Aufgrund einer Missense-Mutation beinhalten die Mutanten *ouf1* und *ouf7* ein verkürztes TPC1 Protein, woraus eine gestörte Proteinintegrität resultiert und daraus wiederum ein Fehlen der TCP1-Kanalaktivität. Dementsprechend ähneln *ouf1* und *ouf7* der *tpc1-2* Nullmutante mit einem WT- oder eher *fou2*-artigen Phänotyp. Wahrscheinlich weist die *ouf2* (G583D D454N) Mutante einen inaktiven TPC1-Kanal auf, weil die G583D Mutation, die in einem luminalen Teil der S11 Helix sitzt, eine Verschiebung der Aktivierungsschwelle hin zu einer höheren Spannung (z. B. mehr als +110 mV) oder einen Kanalblock verursacht. Als Folge der TPC1 Kanal Inaktivität, ahmt die *ouf2* Mutante auch den WT-ähnlichen Phänotyp der *tpc1-2* Nullmutante nach. In der *ouf6* Mutante (A669V D454N) beeinflusst die zweite Mutation selektiv die *fou2*-ähnlichen SV-Kanaleigenschaften. Sowohl die schnelle Aktivierungskinetik als auch die verringerte luminale Calciumsensitivität waren denen von *ouf6* und *fou2* ähnlich. Die Abweichungen in der relativen sowie der absoluten Offenwahrscheinlichkeit resultierten jedoch in einer stark reduzierten (80 %) Stromdichte bei 0 mM luminalem Calcium verglichen mit *fou2* und dem WT, sowie einer Kanalinaktivität bei Spannungen zwischen -30 mV und +40 mV. Darüber hinaus zeigten die TPC1 Kanäle in *ouf6* eine höhere Anfälligkeit für inhibitorisches, luminales Calcium als die in *fou2*. Das Ergebnis der beiden unterschiedlichen Effekte ist, dass die TPC1 Kanalaktivität bei einer hohen luminalen Calciumkonzentration fast verschwindet, woraus zu schließen ist, dass *ouf6* den *fou2*-ähnlichen Phänotyp verlor. Die *ouf4* Mutation veränderte nicht die *fou2* TPC1 Kanaleigenschaften, wie die schnelle

Kanalaktivierung, die Einzelkanalleitfähigkeit und das spannungsabhängige Verhalten. Nichtsdestotrotz war die TCP1 Stromdichte in *ouf4* um 80 % geringer als in *fou2*. Da das TPC1 Gen nicht das Ziel der zweiten Mutation war, kann angenommen werden, dass es durch äußere, bisher noch unbekannte Faktoren, reguliert wird. In der *ouf8* Mutante haben die TPC1 Kanäle zusätzlich eine M629I Mutation innerhalb des zweiten Selektivitätsfilters, welche in einem 50 % Rückgang der TCP1 Einzelkanalleitfähigkeit resultiert. Jedoch scheint die leicht erhöhte Offenwahrscheinlichkeit der TCP1 Kanäle in *ouf8*, verglichen mit *fou2*, ausreichend zu sein, um die reduzierte Transportkapazität der individuellen TPC1 Kanäle zu kompensieren. Schlussfolgernd wurde eine ähnliche makroskopische auswärts gerichtete Stromdichte des *ouf8* und des *fou2* in Abwesenheit vakuolären Calciums entdeckt. Des Weiteren änderte eine *ouf8* Mutation die *fou2* TPC1 Kanaleigenschaften wie eine schnelle Aktivierung, vakuoläre Calciuminsensitivität und die Spannungsabhängigkeit nicht drastisch. Jedoch wurde ein reversibler Block des Zytosol-gerichteten Kalium Ausstroms bei erhöhten vakuolären Calcium Konzentrationen in ouf8 gefunden. Eine weitere Betrachtung transient exprimierter TPC1 Kanalvarianten (M629I, M629T) auf Einzelkanalebene weist darauf hin, dass das Met629 des AtTPC1 in der Kanalporenregion entscheidend ist für die Einzelkanalleitfähigkeit.

Zusammengefasst zeigt der über die Membran von ouf Mutanten gemessene Strom eine Gemeinsamkeit: Alle zeigten keinen oder einen stark beeinträchtigten TPC1-vermittelten Kaliumausstrom aus der Vakuole ins Zytosol. Unter Berücksichtigung der beobachteten Abhängigkeit der vakuolären Membranspannung von der TPC1 Aktivität, scheint es, als ob die durch TPC1 angeregte Depolarisation der Vakuolenmembran, welche durch die vakuoläre Kaliumfreisetzung bedingt wird, in der Ausbildung des *fou2* Phänotyps eine Rolle spielt. Daraus lässt sich ableiten, dass die TPC1-abhängige Depolarisation der Vakuolenmembran und die Jasmonat Bildung vermutlich verbunden sind. Diese Behauptung wird auch gestützt durch die komplette Wiederherstellung des WT-ähnlichen Pflanzenphänotyps und des Jasmonsäure Signalwegs in den ouf Mutanten. Letztendlich ist TPC1 als kontrollierendes Element der vakuolären Membranspannung wahrscheinlich dem Jasmonsäure Signalweg vorgeschaltet und deswegen ein perfekter Knotenpunkt, der verschiedene physiologische Stimuli und ihre Antworten verbindet.

8. Table list

9. Figure list

10. References

Allen, G., & Sanders, D. (1995). **Calcineurin, a Type 2B Protein Phosphatase, Modulates the Ca^{2+}-Permeable Slow Vacuolar Ion Channel of Stomatal Guard Cells.** *Plant Cell*, 7(9):1473-1483.

Allen, G., & Sanders, D. (1996). **Control of ionic currents in guard cell vacuoles by cytosolic and luminal calcium**. *The Plant Journal*, 10(6):1055-1069.

Amodeo, G., Escobar, A., & Zeiger, E. (1994). **A Cationic Channel in the Guard Cell Tonoplast of *Allium cepa***. *Plant Physiol.*, 105(3):999-1006.

Angeli, A. D., Zhang, J., Meyer, S., & Martinoia, E. (2013). **AtALMT9 is a malate-activated vacuolar chloride channel required for stomatal opening in *Arabidopsis***. *Nature Commun.*, 4: 1804.

Aprile, A., Federici, C., Close, T., De, B., Cattivelli, L., & Roose, M. (2011). **Expression of the H+-ATPase AHA10 proton pump is associated with citric acid accumulation in lemon juice sac cells**. *Funct. Integr. Genomics*, 11:551–563.

Armengaud, P., Breitling, R., & Amtmann, A. (2004). **The potassium-dependent transcriptome of *Arabidopsis* reveals a prominent role of jasmonic acid in nutrient signaling.** *Plant Physiol.*, 136(1):2556-76.

Bagnéris, C., Decaen, P., Hall, B., Naylor, C., Clapham, D., Kay, C., & Wallace, B. (2013). **Role of the C-terminal domain in the structure and function of tetrameric sodium channels.** *Nature Commun.*, 4:2465.

Balbi, V., & Devoto, A. (2008). **Jasmonate signalling network in *Arabidopsis thaliana*: crucial regulatory nodes and new physiological scenarios.** *New Phytol.*, 177(2):301-18.

Becker, B. (2007). **Function and evolution of the vacuolar compartment in green algae and land plants (*Viridiplantae*).** *International review of cytology*, 264:1-24.

Becker, D., Geiger, D., Dunkel, M., Roller, A., Bertl, A., Latz, A., Carpaneto A., Dietrich P., Roelfsema MR., Voelker C., Schmidt D., Mueller-Roeber B., Czempinski K., Hedrich, R. (2004). **AtTPK4, an *Arabidopsis* tandem-pore K^+ channel, poised to control the pollen**

membrane voltage in a pH- and Ca^{2+}-dependent manner. *Proceedings of the National Academy of Sciences*,, 101(44):15621-6.

Bertl, A., Blumwald, E., Coronado, R., Eisenberg, R., Findlay, G., Gradmann, D., . . . MacRobbie, E. (1992). **Electrical measurements on endomembranes**. *Science*, 258(5084):873-4.

Bethke, P., & Jones, R. (1994). **Ca^{2+}-Calmodulin Modulates Ion Channel Activity in Storage Protein Vacuoles of Barley Aleurone Cells**. *Plant Cell.*, 6(2):277-285.

Bethke, P., & Jones, R. (1997). **Reversible protein phosphorylation regulates the activity of the slow-vacuolar ion channel**. *The Plant Journal*, 11: 1227-1235.

Bethmann, B., Thaler, M., Simonis, W., & Schonknecht, G. (1995). **Electrochemical Potential Gradients of H^+, K^+, Ca^{2+}, and Cl^- across the Tonoplast of the Green Alga *Eremosphaera Viridis***. *Plant Physiol.*, 109(4):1317-1326.

Beyhl, D., Hörtensteiner, S., Martinoia, E., Farmer, E., Fromm, J., Marten, I., & Hedrich, R. (2009). **The *fou2* mutation in the major vacuolar cation channel TPC1 confers tolerance to inhibitory luminal calcium**. The *Plant Journal*, 58: 715-23.

Biemelt, S., Tschiersch, H., & Sonnewald, U. (2004). **Impact of altered gibberellin metabolism on biomass accumulation, lignin biosynthesis, and photosynthesis in transgenic tobacco plants.** *Plant Physiol.*, 135(1):254-65.

Bihler, H., Eing, C., Hebeisen, S., Roller, A., Czempinski, K., & Bertl, A. (2005). **TPK1 is a vacuolar ion channel different from the slow-vacuolar cation channel.** *Plant Physiol.*, 139(1):417-24.

Blée, E. (2002). **Impact of phyto-oxylipins in plant defense.** *Trends Plant Sci.* , 7(7):315-22.

Bonaventure, G., Gfeller, A., Proebsting, W., Hörtensteiner, S., Chételat, A., Martinoia, E., & Farmer, E. (2007a). **A gain-of-function allele of TPC1 activates oxylipin bio-genesis after leaf wounding in Arabidopsis.** *The Plant Journal*, 49: 889-898.

Bonaventure, G., Gfeller, A., Rodriguez, V., Armand, F., & Farmer, E. (2007b). **The *fou2* gain-of-function allele and the wildtype allele of Two Pore Channel 1 contribute to different extents or by different mechanisms to defense gene expression in Arabidopsis.** *Plant Cell Physiol.*, 48: 1775-1789.

Brailoiu, E., Rahman, T., Churamani, D., Prole, D., Brailoiu, G., Hooper, R., Taylor CW., Patel, S. (2010). **An NAADP-gated two-pore channel targeted to the plasma membrane uncouples triggering from amplifying Ca^{2+} signals.** *Jurnal of Biol. Chem.*, 285(49):38511-6.

Browse, J. (2009). **The power of mutants for investigating jasmonate biosynthesis and signaling.** *Phytochemistry*, 70:1539–1546.

Calcraft, P., Ruas, M., Pan, Z., Cheng, X., Arredouani, A., Hao, X., Tang J., Rietdorf K., Teboul L., Chuang KT., Lin P., Xiao R., Wang C., Zhu Y., Lin Y., Wyatt CN., Parrington J., Ma J., Evans AM., Galione A., Zhu M. (2009). **NAADP mobilizes calcium from acidic organelles through two-pore channels.** *Nature*, 459(7246):596-600.

Carpaneto, A. (2003). **Nickel inhibits the slowly activating channels of radish vacuoles**. *Eur Biophys J.*, 32(1):60-6.

Carpaneto, A., Cantu, A., & Gambale, F. (1999). **Redox agents regulate ion channel ac-tivity in vacuoles from higher plant cells.** *FEBS Letters*, 442: 129-132.

Carpaneto, A., Cantu, A., & Gambale, F. (2001). **Effects of cytoplasmic Mg^{2+} on slowly activating channels in isolated vacuoles of *Beta vulgaris***. *Planta* , 213: 457-468.

Carpaneto, A., Cantu, A., Busch, H., & Gambale, F. (1997). **Ion channels in the vacuoles of the seagrass *Posidonia oceanica*.** *FEBS Lett.*, 412(1):236-40.

Carter, C. J., Bednarek, S. Y., & Raikhel, N. V. (2004). **Membrane trafficking in plants: new discoveries and approaches.** *Current Opinion in Plant Biology*, 7:701–707.

Catterall, W. (2010). **Ion channel voltage sensors: structure, function, and pathophysiology.** *Neuron*, 67(6):915-28.

Chini, A., Fonseca, S., Fernández, G., Adie, B., Chico, J., Lorenzo, O., García-Casado G., López-Vidriero I., Lozano FM., Ponce MR., Micol JL., Solano, R. (2007). **The JAZ family of repressors is the missing link in jasmonate signalling.** *Nature*, 448: 666–671.

Choi, W.-G., Toyota, M., Kim, S.-H., Hilleary, R., & Gilroy, S. (2014). **Salt stress-induced Ca^{2+} waves are associated with rapid, long-distance root-to-shoot signaling.** *Proceedings of the National Academy of Sciences*, 111, 6497–6502.

Chung, H., & Howe, G. (2009). A **critical role for the TIFY motif in repression of jasmonate signaling by a stabilized splice variant of the JASMONATE ZIM-domain protein JAZ10 in Arabidopsis**. *Plant Cell*, 21(1):131-45.

Conn, S., & Gilliham, M. (2010). **Comparative physiology of elemental distributions in plants.** *Ann. Bot.*, 105, 1081–1102.

Czempinski, K., Zimmermann, S., Ehrhardt, T., & Müller-Röber, B. (1997). **New structure and function in plant K^+ channels: KCO1, an outward rectifier with a steep Ca^{2+} dependency.** *EMBO Jurnal*, 16(10):2565-75.

Dadacz-Narloch, B., Beyhl, D., Larisch, C., Lopez-Sanjurjo, E. J., Reski, R., Kuchitsu, K., Müller TD., Becker D., Schönknecht G., Hedricha, R. (2011). **A Novel Calcium Binding Site in the Slow Vacuolar Cation Channel TPC1 Senses Luminal Calcium Levels.** *Plant Cell.* , 23(7):2696-707.

De Angeli, A., Moran, O., Wege, S., Filleur, S., Ephritikhine, G., Thomine, S., Barbier-Brygoo H., Gambale, F. (2009). **ATP binding to the C terminus of the Arabidopsis thaliana nitrate/proton antiporter, AtCLCa, regulates nitrate transport into plant vacuoles.** *J. Biol. Chem.*, 284(39):26526-32.

Deeken, R., Ivashikina, N., Czirjak, T., Philippar, K., Becker, D., Ache, P., & Hedrich, R. (2003). **Tumour development in Arabidopsis thaliana involves the Shaker-like K^+ channels** AKT1 and AKT2/3. *Plant Jurnal*, 34(6):778-87.

Dobrovinskaya, O., Muniz, J., & Pottosin, I. (1999a). **Asymmetric block of the plant vacuolar Ca^{2+}-permeable channel by organic cations**. *Eur Biophys J.*, 28: 552-563.

Dobrovinskaya, O., Muniz, J., & Pottosin, I. (1999b). **Inhibition of vacuolar ion channels by polyamines.** *J. Membr. Biol.*, 167(2):127-40.

Drozdowicz, Y., & Rea, P. (2001). **Vacuolar H(+) pyrophosphatases: from the evolutionary backwaters into the mainstream.** *Trends Plant Sci.*, 6(5):206-11.

Dunkel, M., Latz, A., Schumacher, K., Müller, T., Becker, D., & R.Hedrich. (2008). **Targeting of vacuolar membrane localized members of the TPK channel family.** *Mol. Plant.*, 6:938-49.

Echeverria, E., & Burns, J. (1989). **Vacuolar Acid hydrolysis as a physiological mechanism for sucrose breakdown.** *Plant Physiol.*, 90(2):530-3.

Faraco, M., Spelt, C., Bliek, M., Verweij, W., Hoshino, A., Espen, L., Prinsi B., Jaarsma R., Tarhan E., de Boer AH., Di Sansebastiano GP., Koes R., Quattrocchio, F. (2014). **Hyperacidification of vacuoles by the combined action of two different P-ATPases in the tonoplast determines flower color.** *Cell Rep.*, 6:32–43.

Farmer, E. (1994). **Fatty acid signalling in plants and their associated microorganisms.** *Plant Mol. Biol.* , 26(5):1423-37.

Farmer, E., Gasperini, D., & Acosta, I. (2014). **The squeeze cell hypothesis for the activation of jasmonate synthesis in response to wounding.** *New Phytol.*, 204(2):282-8.

Felle, H. (1988). **Cytoplasmic free calcium in Riccia fluitans L. and Zea mays L.: Interaction of Ca^{2+} and pH.** *Planta*, 176(2):248-55.

Fonseca, S., Chini, A., Hamberg, M., Adie, B., Porzel, A., Kramell, R., Miersch O., Wasternack C., Solano, R. (2009). **(+)-7-iso-Jasmonoyl-L-isoleucine is the endogenous bioactive jasmonate.** *Nat. Chem. Biol.*, 5(5):344-50.

Frigerio, L., Hinz, G., & Robinson, D. G. (2008). **Multiple Vacuoles in Plant Cells: Rule or Exception?** *Traffic*, 10 : 1564–1570.

Furuchi, T., Cunningham, K., & Muto, S. (2001). A **putative two pore channel AtTPC1 mediates Ca^{2+} flux in Arabidopsis leaf cells.** *Plant Cell Physiol.*, 42: 900-905.

Geisler, M., Axelsen, K., Harper, J., & Palmgren, M. (2000). **Molecular aspects of high-er plant P-type Ca^{2+}-ATPases.** Biochim Biophys. *Biochim Biophys Acta.*, 1465: 52-78.

Gfeller, A., Dubugnon, L., Liechti, R., & Farmer, E. E. (2010). **Jasmonate Biochemical Pathway.** *Science Signaling* , 3:109.

Glauser, G., Dubugnon, L., Mousavi, S., Rudaz, S., Wolfender, J., & Farmer, E. (2009). **Velocity estimates for signal propagation leading to systemic jasmonic acid accumulation in wounded Arabidopsis.** *Jurnal of Biol. Chem.*, 284(50):34506-13.

Glauser, G., Grata, E., Dubugnon, L., Rudaz, S., Farmer, E., & Wolfender, J. (2008). **Spatial and temporal dynamics of jasmonate synthesis and accumulation in Arabidopsis in response to wounding.** *Jurnal of Biol. Chem.*, 283(24):16400-7.

Gobert, A., Isayenkov, S., Voelker, C., Czempinski, K., & Maathuis, F. (2007). **The two-pore channel TPK1 gene encodes the vacuolar K^+ conductance and plays a role in K^+ homeostasis.** *Proceedings of the National Academy of Sciences*, 104(25):10726-3.

Grabarek, Z. (2006). **Structural basis for diversity of the EF-hand calcium-binding proteins**. *J. Mol. Biol.*, 359(3):509-25.

Guo, J., Zeng, W., & Jiang, Y. (2017). **Tuning the ion selectivity of two-pore channels.** *Proceedings of the National Academy of Sciences*, 114(5):1009-1014.

Guo, J., Zeng, W., Chen, Q., Lee, C., Chen, L., Yang, Y., Cang C., Ren D., Jiang, Y. (2016). **Structure of the voltage-gated two-pore channel TPC1 from *Arabidopsis thaliana*.** *Nature*, 531(7593):196-201.

Gustina, A., & Trudeau, M. (2011). **hERG potassium channel gating is mediated by N- and C-terminal region interactions.** *Jurnal of Geneneral Physiol.*, 137(3):315-25.

Hamill, O., Marty, A., Neher, E., Sakmann, B., & Sigworth, F. (1981). **Improved patch-clamp techniques for high-resolution current recording from cells and cell-free membrane patches.** *Pflugers Arch.*, 391(2):85-100.

Hatano, N., Ohya, S., Muraki, K., Clark, R., & Imaizumi, W. G. (2004). **Two arginines in the cytoplasmic C-terminal domain are essential for voltage-dependent regulation of A-type K^+ current in the Kv4 channel subfamily**. *Jurnal of Biol. Chem.*, 279(7):5450-9.

Hedrich, R. (2012). **Ion channels in plants.** *Physiol. Rev.* , 92(4):1777-811.

Hedrich, R., & Kurkdjian, A. (1988). **Characterization of an anion-permeable channel from sugar beet vacuoles: effect of inhibitors.** *EMBO J.*, 7(12):3661-6.

Hedrich, R., & Marten, I. (2011). **TPC1-SV channels gain shape.** *Molecular plants*, 428–41.

Hedrich, R., & Neher, E. (1987). **Cytoplasmic calcium regulates voltage-dependent ion channels in plant vacuoles.** *Nature*, 329: 833-835.

Hedrich, R., Flügge, U., & Fernandez, J. (1986). **Patch-clamp studies of ion transport in isolated plant vacuoles.** *FEBS Lett.*, 3910: 228-232.

Hedrich, R., Kurkdjian, A., Guern, J., & Flügge, U. (1989). **Comparative studies on the electrical properties of the H^+ translocating ATPase and pyrophosphatase of the vacuolar-lysosomal compartment.** *EMBO J.*, 8(10):2835-41.

Hedrich, R., Salvador-Recatalà, V., & Dreyer, I. (2016). **Electrical Wiring and Long-Distance Plant Communication.** *Trends Plant Sci.*, 21(5):376-87.

Hedrich, R., Sauer, N., & Neuhaus, E. (2015). **Sugar transport across the plant vacuolar membrane: nature and regulation of carrier proteins.** *Current Opinion in Plant Biology*, 25: 63–70.

Heil, M., & Bueno, J. (2007). **Within-plant signaling by volatiles leads to induction and priming of an indirect plant defense in nature.** *Proceedings of the National Academy of Sciences* , 104(13):5467-72. .

Heil, M., & Ton, J. (2008). **Long-distance signalling in plant defence**. *Trends Plant Sci.*, 13(6):264-72.

Herman, E., & Larkins, B. (1999). **Protein storage bodies and vacuoles.** *Plant Cell*, 11(4):601-14.

Hille, B. (1992). *Ionic channel of excitable membranes.* Sunderland, MA: Sinauer.

Hooper, R., & Patel, S. (2012). **NAADP on target.** *Adv. Exp. Med. Biol*, 325-347.

Howe, G., Lee, G., Itoh, A., Li, L., & DeRocher, A. (2000). **Cytochrome P450-dependent metabolism of oxylipins in tomato. Cloning and expression of allene oxide synthase and fatty acid hydroperoxide lyase.** *Plant Physiol.*, 123(2):711-24.

Isayenkov, S., Isner, J. C., & Maathuis, F. J. (2010). **Vacuolar ion channels: Roles in plant nutrition and signalling.** *FEBS Letters*, 584 :1982–1988.

Ivashikina, N., & Hedrich, R. (2005). **K^+ currents through SV-type vacuolar channels are sensitive to elevated luminal sodium levels.** *The Plant Jurnal.*, 606-14.

Ivashikina, N., Deeken, R., Ache, P., Kranz, E., Pommerrenig, B., Sauer, N., & Hedrich, R. (2003). **Isolation of AtSUC2 promoter-GFP-marked companion cells for patch-clamp studies and expression profiling.** *The Plant Jurnal.*, 36(6):931-45.

Jaquinod, M., F.Villiers, Kieffer-Jaquinod, S., Hugouvieux, V., Bruley, C., Garin, J., & Bourguignon, J. (2007). **A Proteomics Approach Highlights a Myriad of Transporters in the Arabidopsis thaliana Vacuolar Membrane.** *Plant Signal Behav.*, 2(5):413-5.

Jaślan, D., Mueller, T., Becker, D., Schultz, J., Cuin, T., Marten, I., Dreyer I., Schönknecht G., Hedrich, R. (2016). **Gating of the two-pore cation channel AtTPC1 in the plant vacuole is based on a single voltage-sensing domain.** *Plant Biol.*, 18(5):750-60.

Jauh, G., Phillips, T., & Rogers, J. (1999). **Tonoplast intrinsic protein isoforms as markers for vacuolar functions.** *Plant Cell*, 11: 1867–1882.

Kiep, V., Vadassery, J., Lattke, J., Maaß, J.-P., Boland, W., Peiter, E., & Mithoefer, A. (2015). **Systemic cytosolic Ca^{2+} elevation is activated upon wounding and herbivory in Arabidopsis.** *New Phytologist*, 207, 996–1004.

Kintzer, A., & Stroud, R. (2016). **Structure, inhibition and regulation of two-pore channel TPC1 from Arabidopsis thaliana.** *Nature*, 531(7593):258-62.

Kolb, H.-A., Kohler, K., & Martinoia, E. (1987). **Single potassium channels in membranes of isolated mesophyll barley vacuoles.** *J. Mem Biol.*, 95, 163–169.

Koo, A. J., & Howea, G. A. (2009). **The wound hormone jasmonate.** *Phytochemistry* , 70:1571–1580.

Kovermann, P., Meyer, S., Hörtensteiner, S., Picco, C., Scholz-Starke, J., Ravera, S., Lee Y., Martinoia, E. (2007). **The Arabidopsis vacuolar malate channel is a member of the ALMT family,** The *Plant Journal,*, 52, 1169 - 1180.

Krebs, M., Beyhl, D., Görlich, E., Al-Rasheid, K., Marten, I., Stierhof, Y., Hedrich R., Schumacher, K. (2010). **Arabidopsis V-ATPase activity at the tonoplast is required for efficient nutrient storage but not for sodium accumulation.** *Proceedings of the National Academy of Sciences* , 107(7):3251-6.

Larisch, N., Kirsch, S., Schambony, A., Studtrucker, T., Böckmann, R., & Dietrich, P. (2016). **The function of the two-pore channel TPC1 depends on dimerization of its carboxy-terminal helix.** *Cell molecular life Sci.*, 73(13):2565-81.

Larisch, N., Schulze, C., Galione, A., & Dietrich, P. (2012). **An N-terminal dileucine motif directs two-pore channels to the tonoplast of plant cells.** *Traffic*, 13(7):1012-22.

Latz, A., Becker, D., Hekman, M., Müller, T., Beyhl, D., Marten, I., Eing C., Fischer A., Dunkel M., Bertl A., Rapp UR., Hedrich R. (2007). **TPK1, a Ca^{2+}-regulated Arabidopsis vacuole two-pore K^+ channel is activated by 14-3-3 proteins.** *The Plant Jurnal*, 52: 449-59.

Loewus, F., & Murthy, P. (2000). **myo-Inositol metabolism in plants.** *Plant Science*, 150,1-19.

Logemann, J., Schell, J., & Willmitzer, L. (1987). **Improved method for the isolation of RNA from plant tissues.** *Anal Biochem.*, 163(1):16-20.

Maathuis, F., & Sanders, D. (1999). **Plasma membrane transport in context - making sense out of complexity.** *Current opinion in plant biol.*, 2(3):236-43.

Maeshima, M. (2000). **Vacuolar H^+-pyrophosphatase.** *Biochim Biophys Acta*, 1465: 37-51.

Maffei, M., Mithöfer, A., & Boland, W. (2007). **Before gene expression: early events in plant-insect interaction.** *Trends Plant Sci.*, 12(7):310-6.

Malone, M. (1994). **Wound-induced hydraulic signals and stimulus transmission in *Mimosa pudica L.*** *New Phytologist*, 128: 49-56.

Marchant, J., & Patel, S. (2013). **Questioning regulation of two-pore channels by NAADP.** *Messenger.*, 2(2):113-119.

Marchler-Bauer, A., Anderson, J., Chitsaz, F., Derbyshire, M., DeWeese-Scott, C., Fong, J., Geer LY., Geer RC., Gonzales NR., Gwadz M., He S., Hurwitz DI., Jackson JD., Ke Z., Lanczycki CJ., Liebert CA., Liu C., Lu F., Lu S., Marchler GH., Mullokandov M., Song JS., Tasneem A., Thanki N., Yamashita RA., Zhang D., Zhang N., Bryant S. (2009). **CDD: specific functional annotation with the Conserved Domain Database.** *Nucleic Acids Res.*, 37(Database issue):D205-10.

Marten, I., & Hoshi, T. (1997). **Voltage-dependent gating characteristics of the K^+ channel KAT1 depend on the N and C termini.** *Proceedings of the National Academy of Sciences*, 94(7):3448-53.

Martinoia, E., Maeshima, M., & Neuhaus, E. (2006). **Vacuolar transporters and their es-sential role in plant metabolism.** *Jurnal of experimantal botany*, 58: 83-102.

Martinoia, E., Meyer, S., Angeli, A. D., & Nagy, R. (2012). **Vacuolar Transporters in physiological context.** *Annual review in plant Biol.*, 63:183–213.

Matsui, K., Minami, A., Hornung, E., Shibata, H., Kishimoto, K., Ahnert, V., Kindl H., Kajiwara T., Feussner, I. (2006). **Biosynthesis of fatty acid derived aldehydes is induced upon mechanical wounding and its products show fungicidal activities in cucumber.** *Phytochemistry*, 67(7):649-57.

Meyer, S., Scholz-Starke, J., Angeli, A. D., Kovermann, P., Burla, B., Gambale, F., & Martinoia, E. (2011). **Malate transport by the vacuolar AtALMT6 channel in guard cells is subject to multiple regulation,**. *The Plant Journal,*, 67, 247 - 257.

Moran, N., Ehrenstein, G., Iwasa, K., Bare, C., & Mischke, C. (1984). **Ion channels in plasmalemma of wheat protoplasts.** *Science*, 226(4676):835-8.

Mousavi, S., Chauvin, A., Pascaud, F., Kellenberger, S., & Farmer, E. (2013). **GLUTAMATE RECEPTOR-LIKE genes mediate leaf-to-leaf wound signalling**. *Nature.*, 500(7463):422-6.

Müller, M., Irkens-Kiesecker, U., Rubinstein, B., & Taiz, L. (1996). **On the mechanism of hyperacidification in lemon. Comparison of the vacuolar H^+-ATPase activities of fruits and epicotyls.** *Jurnal of biol. chem.*, 271:1916–1924.

Munemasa, S., Hossain, M., Nakamura, Y., Mori, I., & Murata, Y. (2011). **The Arabidopsis calcium-dependent protein kinase, CPK6, functions as a positive regulator of methyl jasmonate signaling in guard cells.** *Plant Physiol.*, 155(1):553-61.

Narváez-Vásquez, J., Orozco-Cárdenas, M., & Ryan, C. (2007). **Systemic wound signaling in tomato leaves is cooperatively regulated by systemin and hydroxyproline-rich glycopeptide signals.** *Plant molecular biol.*, 65(6):711-8.

Neher, E. (1992). **Correction for liquid junction potentials in patch clamp experiments.** *Methods Enzymol.*, 207:123-31.

Neher, E., & Sakmann, B. (1976). **Single-channel currents recorded from membrane of denervated frog muscle fibres.** *Nature. 1976*, 260(5554):799-802.

Noda, M., Shimizu, S., Tanabe, T., Takai, T., Kayano, T., Ikeda, T., Takahashi H., Nakayama H., Kanaoka Y., Minamino, N. (1984). **Primary structure of Electrophorus electricus sodium channel deduced from cDNA sequence.** *Nature*, 121-7.

Nørholm, M. (2010). **A mutant Pfu DNA polymerase designed for advanced uracil-excision DNA engineering.** *BMC Biotechnol.*, 10:21.

Numberger, M., & Draguhn, A. (1996). *Patch clamp technik von Markus Numberger und Andreas Draguhn.* Spektrum Akademischer Verlag.

Otegui, M. S., Capp, R., & Staehelin, L. A. (2002). **Developing Seeds of Arabidopsis Store Different Minerals in Two Types of Vacuoles and in the Endoplasmic Reticulum.** *The Plant Cell*, 14; 1311–1327.

Ahmad, P. Rasool S., Gul A., Sheikh SA., Akram NA., Ashraf M., Kazi AM., Gucel S., (2016). **Jasmonates: Multifunctional Roles in Stress Tolerance.** *Front. Plant Sci.*, 7:813.

Pauwels, L., Inzé, D., & Goossens, A. (2009). Jasmonate-inducible gene: What does it mean? *Trends Plant Sci.*, 14(2):87-91.

Pei, Z., Ward, J., & Schroeder, J. (1999). **Magnesium sensitizes slow vacuolar channels to physiological cytosolic calcium and inhibits fast vacuolar channels in fava bean guard cell vacuoles.** *Plant Physiology*, 121: 977-986.

Peiter, E., Maathuis, F., Mills, L., Knight, H., Pelloux, J., Hetherington, A., & Sanders, D. (2005). **The vacuolar Ca^{2+}-activated channel TPC1 regulates germination and stomatal movement.** *Nature*, 434: 404-8.

Pérez, V., Wherrett, T., Shabala, S., Muñiz, J., Dobrovinskaya, O., & Pottosin, I. (2008). **Homeostatic control of slow vacuolar channels by luminal cations and evaluation of the channel-mediated tonoplast Ca^{2+} fluxes in situ.** *Jurnal of experimental botany*, 59(14):3845-55.

Pieterse, C., Leon-Reyes, A., Ent, S. V., & Wees, S. V. (2009). **Networking by small-molecule hormones in plant immunity.** *Nature chemical biol.*, 5(5):308-16.

Pitt, S., Funnell, T., Sitsapesan, M., Venturi, E., Rietdorf, K., Ruas, M., Ganesan A, Gosain R, Churchill GC., Zhu MX., Parrington J., Galione A., Sitsapesan, R. (2010). **TPC2 is a novel NAADP-sensitive Ca^{2+}-release channel, operating as a dual sensor of luminal pH and Ca^{2+}.** *Jurnal of Biol. Chem.*, 285(45):35039-46.

Pottosin, I., Dobrovinskaya, O., & Muniz, J. (2001). **Conduction of monovalent and diva-lent cations in the slow vacuolar channel.** *Journal of Membrane Biology*, 181: 55-65.

Pottosin, I., Martinez-Estevez, M., Dobrovinskaya, O., Miniz, J., & Schönknecht, G. (2004). **Mechanism of luminal Ca^{2+} and Mg^{2+} action on the vacuolar slowly activating channels.** *Planta*, 219: 1057-1070.

Pottosin, I., Tikhonova, L., Hedrich, R., & Schönknecht, G. (1997). **Slowly activating vacuolar channels cannot mediate Ca^{2+}-induced Ca^{2+} release.** *The Plant Journal*, 12:1387-1398.

Ranf, S., Wunnenberg, P., Lee, J., Becker, D., Dunkel, M., Hedrich, R., Scheel D, Dietrich, P. (2008). **Loss of the vacuolar cation channel, AtTPC1, does not impair Ca^{2+} signals induced by abiotic and biotic stresses.** *The Plant Jurnal.*, 53: 287–299.

Ratajczak, R., Hinz, G., & Robinson, D. (1999). **Localization of pyrophosphatase in membranes of cauliflower inflorescence cells.** *Planta.*, 208(2):205-211.

Rienmüller, F., Beyhl, D., Lautner, S., Fromm, J., Al-Rasheid, K., Ache, P., Farmer EE., Marten I., Hedrich, R. (2010). **Guard cell-specific calcium sensitivity of high density and activity SV/TPC1 channels.** *Plant Cell Physiol.*, 51: 1548-1554.

Robinson, D. G., Oliviusson, P., & Hinz, G. (2005). P**rotein Sorting to the Storage Vacuoles of Plants:**. *Traffic* , 6: 615–625.

Ruas, M., Rietdorf, K., Arredouani, A., Davis, L., Lloyd-Evans, E., Koegel, H., Funnell TM, Morgan AJ., Ward JA., Watanabe K., Cheng X., Churchill GC., Zhu MX., Platt FM., Wessel GM., Parrington J., Galione, A. (2010). **Purified TPC isoforms form NAADP receptors with distinct roles for Ca(2+) signaling and endolysosomal trafficking.** *Current Biology.*, 20(8):703-709.

Sanders, D., Pelloux, J., Brownlee, C., & Harper, J. F. (2002). **Calcium at the Crossroads of Signaling.** *The Plant Cell*, 401–S417.

Savatin, D. V., Gramegna, G., Modestiand, V., & FeliceCervone. (2014). Wounding in the plant tissue: the defense of a dangerous passage. *Front. Plant Sci.*, 5:470.

Schaller, A., & Oecking, C. (1999). **Modulation of plasma membrane H^+-ATPase activity differentially activates wound and pathogen defense responses in tomato plants.** *Plant Cell.*, 11(2):263-272.

Schieder, M., Rotzez, K., Bruggemann, A., Biel, M., & Wahl-Schott, C. (2010). **Characterization of two-pore channel 2 (TPCN2)-mediated Ca^{2+} currents in isolated lysosomes.** *Jurnal of biol. chem.*, 21219–21222.

Scholz, S., Vadassery, J., Heyer, M., Reichelt, M., Bender, K., Snedden, W., Boland W., Mithöfer, A. (2014). **Mutation of the Arabidopsis calmodulin-like protein CML37 deregulates the jasmonate pathway and enhances susceptibility to herbivory.** *Mol. Plant* , 7: 1712-1726.

Schönknecht, G. (2013). **Calcium Signals from the Vacuole.** *Plants*, 2(4), 589-614.

Schönknecht, G., Spoormaker, P., Steinmeyer, R., Brüggeman, L., Ache, P., Dutta, R., Reintanz B., Godde M., Hedrich R., Palme, K. (2002). **KCO1 is a component of the slow-vacuolar (SV) ion channel.** *FEBS Lett.*, 511(1-3):28-32.

Schroeder, J., Hedrich, R., & Fernandez, J. (1984). **Potassium-selective single channels in guard-cell protoplasts of Vicia faba.** *Nature*, 312: 361–362.

Schulze, C., Sticht, H., Meyerhoff, P., & Dietrich, P. (2011). **Differential contribution of EF-hands to the Ca^{2+}-dependent activation in the plant two-pore channel TPC1.** *The Plant Journal*, 68, 424–432.

Schulz-Lessdorf, B., & Hedrich, R. (1995). **Protons and calcium modulate SV-type channels in the vacuolar-lysosomal compartment: channel interaction with calmodulin inhibitors.** *Planta*, 197: 655-671.

Schumacher, K. (2014). **pH in the plant endomembrane system-an import and export business.** *Current opinion in plant biol.*, 22:71-76.

Shaul, O. (2002). **Magnesium transport and function in plants: the tip of the iceberg.** *Biometals.* , 15(3):309-23.

Shigaki, T., & Hirschi, K. (2006). **Diverse functions and molecular properties emerging for CAX cation/H+ exchangers in plants.** *Plant Biol.*, 8(4):419-29.

Stahlberg, R., Stephens, N., Cleland, R., & Volkenburgh, E. V. (2006). **Shade-Induced Action Potentials in Helianthus annuus L. Originate Primarily from the Epicotyl.** *Plant signaling and behaviour.*, 1(1):15-22.

Sun, Q., Guo, Y., Sun, Y., Sun, D., & Wang, X. (2006). **Influx of extracellular Ca^{2+} involved in jasmonic-acid-induced elevation of [Ca2+]cyt and JR1 expression in *Arabidopsis thaliana*.** *Jurnal of Plant Reserch.*, 119(4):343-50.

Szczegielniak, J., Klimecka, M., Liwosz, A., Ciesielski, A., Kaczanowski, S., Dobrowolska, G., Harmon AC., Muszyńska, G. (2005). **A Wound-Responsive and Phospholipid-Regulated Maize Calcium-Dependent Protein Kinase.** *Plant Physiol.* , 4:1970-1983.

Sze, H., Liang, F., Hwang, I., Curran, A., & Harper, J. (2000). **Diversity and regulation of plant Ca^{2+} pumps: insights from expression in yeast.** *Annual review of plant physiology and plant molecular Biol.*, 51:433-62.

Thines, B., Katsir, L., Melotto, M., Niu, Y., Mandaokar, A., Liu, G., Nomura K., He SY., Howe GA., Browse, J. (2007). **JAZ repressor proteins are targets of the SCF(COI1) complex during jasmonate signalling.** *Nature*, 448(7154):661-665.

Vadassery, J., Reichelt, M., Hause, B., Gershenzon, J., Boland, W., & Mithöfer, A. (2012). **CML42-mediated calcium signaling coordinates responses to Spodoptera herbivory and abiotic stresses in Arabidopsis.** *Plant Physiol.*, 159(3):1159-1175.

Vlot, A., Klessig, D., & Park, S. (2008). S**ystemic acquired resistance: the elusive signal(s).** *Current Opinion of Plant Biol.*, 11(4):436-442.

Voelker, C., Gomez-Porras, J. L., Becker, D., Hamamoto, S., Uozumi, N., Gambale, F., Mueller-Roeber B., Czempinski K., Dreyer, I. (2010). **Roles of tandem-pore K^+ channels in plants – a puzzle still to be solved.** *Plant Biol.* , 1:56-63.

Walker, D., Leigh, R., & Miller, A. (1996). **Potassium homeostasis in vacuolate plant cells.** *Proceedings of the National Academy of Sciences*, 10510-10514.

Walker, D., Smith, S., & Miller, A. (1995). **Simultaneous measurement of intracellular pH and K^+ or NO_3^- in Barley Root Cells Using Triple-Barreled, Ion-Selective Microelectrodes.** *Plant Physiol.*, 743-751.

Wang, L., Allmann, S., Wu, J., & Baldwin, I. (2008). **Comparisons of LIPOXYGENASE3- and JASMONATE-RESISTANT4/6-silenced plants reveal that jasmonic acid and jasmonic acid-amino acid conjugates play different roles in herbivore resistance of Nicotiana attenuata.** *Plant Physiol.*, 146(3):904-915.

Wang, X., Zhang, X., Dong, X., Samie, M., Li, X., Cheng, X., Goschka A., Shen D., Zhou Y., Harlow J., Zhu MX., Clapham DE., Ren D., Xu, H. (2012). **TPC proteins are phosphoinositide-activated sodium-selective ion channels in endosomes and lysosomes.** *Cell*, 151, 372–383.

Wang, Y., Dindas, J., Rienmüller, F., Krebs, M., Waadt, R., Schumacher, K., Wu WH., Hedrich R., Roelfsema, M. (2015). **Cytosolic Ca^{2+} Signals Enhance the Vacuolar Ion Conductivity of Bulging Arabidopsis Root Hair Cells.** *Molecular Plant.*, 8(11):1665-1674.

Wang, Y., Yu, J., Chen, T., Zhang, Z., Hao, Y., Zhang, J., & Chen, S. (2005). **Functional analysis of a putative Ca^{2+} channel gene TaTPC1 from wheat.** *Jurnal of Experimental Botany*, 56, 3051–3060.

Ward, J. M., & Schroeder, J. (1994). **Calcium-Activated K^+ Channels and Calcium-lnduced Calcium Release by Slow Vacuolar Ion Channels in Guard Cell Vacuoles lmplicated in the Control of Stomatal Closure.** *The Plant Cell*, 6: 669-683.

Wasternack, C., & Hause, B. (2013). **Jasmonates: biosynthesis, perception, signal transduction and action in plant.** *Annals of Botany*, 111: 1021–1058.

Wasternack, C., Stenzel, I., Hause, B., Hause, G., Kutter, C., Maucher, H., Neumerkel J., Feussner I., Miersch, O. (2006). **The wound response in tomato--role of jasmonic acid.** *Jurnal of Plant Physiol.*, 163(3):297-306.

Weber, H., Vick, B., & Farmer, E. (1997). **Dinor-oxo-phytodienoic acid: a new hexadecanoid signal in the jasmonate family.** *Proceedings of the National Academy of Sciences*, 10473-10478.

Weiser, T., Blum, W., & Bentrup, F. (1991). **Calmodulin regulates the Ca^{2+}-dependent slow-vacuolar ion channel in the tonoplast of Chenopodium rubrum suspension cells.** *Planta*, 185(3):440-442.

White, P., Bowen, H., Demidchik, V., Nichols, C., & Davies, J. (2002). **Genes for calcium-permeable channels in the plasmamembrane of plant root cells.** *Biochim. Biophys. Acta.*, 1564,299–309.

Yan, D., Duermeyer, L., Leoveanu, C., & Nambara, E. (2014). **The Functions of the Endosperm During Seed Germination.** *Plant Cell Physiol.*, 55(9):1521-1533.

Yan, Y., Stolz, S., Chételat, A., Reymond, P., Pagni, M., Dubugnon, L., & Farmer, E. (2007). **A downstream mediator in the growth repression limb of the jasmonate pathway.** *Plant Cell*, 19(8):2470-2483.

Yang, D., Hettenhausen, C., Baldwin, I., & Wu, J. (2012). **Silencing Nicotiana attenuata calcium-dependent protein kinases, CDPK4 and CDPK5, strongly up-regulates wound- and herbivory-induced jasmonic acid accumulations.** *Plant Physiol.*, 159(4):1591-1607.

Yoo, S., Cho, Y., & Sheen, J. (2007). **Arabidopsis mesophyll protoplasts: a versatile cell system for transient gene expression analysis.** *Nature Protoc.*, 2(7):1565-1572.

Zhu, M., Ma, J., Parrington, J., Calcraft, P., Galione, A., & Evans, A. (2010). **Calcium signaling via two-pore channels: local or global, that is the question.** *American jurnal of physiology. Cell Physiology*, 298(3):C430-441.

Zimmermann, M., Maischak, H., Mithöfer, A., Boland, W., & Felle, H. (2009). **System potentials, a novel electrical long-distance apoplastic signal in plants, induced by wounding.** *Plant Physiol.*, 149(3):1593-1600.

11. Glossary

°C	degree Celsius
µM	micro moll
ABA	abscisic acid
AD/DA	analog-to-digital
ADP	adenosine diphosphate
Ag	Silver
AgCl	silver chloride
Arg	arginine
Asp	aspartate
AtALMT	Arabidopsis thaliana Al^{3+}-activated malate transporters
ATP	adenosine triphosphate
bp	base par
BSA	Bovine serum albumin
C_1	Firs close state
C_2	Second close state
Ca^{2+}	Calcium ion
CAX	Calcium / proton Exchanger
cDNA	Complementary DNA
C_{fast}	Fast compensation
Cl^-	Chloride ion
C_m	Membrane capacitance
Cs^+	Cesium ion
CsCl	Cesium chloride
C_{slow}	Slow compensation
DEPC	Diethylpyrocarbonate
dNTPs	Deoxynucleotide
e^-	electron
e.g	exempli gratia
eGFP	Enhanced green fluorescent protein
EGTA	ethylene glycol-bis(β-aminoethyl ether)-N,N,N',N'-tetraacetic acid
E_N	Nernst potential
ER	Endoplasmic reticulum

exp	exponential
FV	Fast vacuolar
fwd	forward
g	gram
g	gravity acceleration
Glu	glutamate
h	hour
H^+	proton
Hepes	4-(2-hydroxyethyl)-1-piperazineethanesulfonic acid
I_{ss}	Steady state current
I_{ss} (V)	Steady state current in certain voltage
I_{ss}/C_m	Steady state current density
JA-	Jasmonic acid
JAZ	JASMONATE-ZIM DOMAIN
K^+	Potassium ion
kDa	Kilo Daltons (1/12 weight of carbon C^{12})
kHz	Kilo Hertz
K_m	Michalis constant
l	Litter
LB media	Luria-Bertani media
LSM	Laser scanning microscope
M	molar
MES	2-(N-morpholino)ethanesulfonic acid
Mg^{2+}	Magnesium ion
ml	millilitre
ml/min	Millilitre per minute
mm	millimetre
mM	milimolar
MMg	Mannitol magnesium buffer
Mohm	Mega ohm
mosmol kg^{-1}	Milliosmole per kilogram
mRNA	messenger RNA
ms	millisecond
mV	millivolt
MYC2	Transcription factor MYC2
MΩ	mega ohm
$N*P_o(V)$	Obsolete number of channel in vacuolar multiplied by open probability for certain voltage

Na^+	Sodium ion
nm	Nanometre
nM	nanomolar
NO_3^-	Nitrate ion
O	Open state
Ø	diameter
OD	optical density
pA	Picoampere
PEG	Polyetyloglicol
pH	Proton concentration
P_{max}	Maximal open probability
P_o (V)	Open probability in certain voltage
PP	pyrophosphate
qRT-PCR	Quantitative real time polychain reaction
rel.P_o (V)	Relative open probability in certain voltage
rev	revers
R_s	Resistant series
s	second
SCF complex	Skp, Cullin, F-box containing complex
sec	second
SV	Slow vacuolar
TaTPC1	*Triticum aestivum* TPC1
TGN	Trans Golgi network
TPC1	Two pore channel
tpc1-2	Two pore channel knock-out mutant
TPK1	tandem pore K^+ 1
Tris	(hydroxymethyl)aminomethane
Ub	ubiquitin
µg/ml	Microgram per millilitre
V	volt
v/v	Volume/volume
V_1	midpoint voltage reflecting the $C_1 \leftrightarrows O$ transition
V_2	midpoint voltage reflecting the $C_2 \leftrightarrows C_1$ transition
VK	Vacuolar potassium
w/v	Weight/volume
W5	Incubation buffer in protoplast transformation procedure

z1	Gating charge 1
z2	Gating charge 2
ΔT_m	Melting temperature
µl	microliter
µm	micrometre
µmol s^{-1} m^{-2}	Micromole per second and square meter
µs	microsecond
π	Osmotic pressure

12. Supplement

Table 1. V's values

Mutant name	Vacuolar free calcium concentration in [mM]	V_1 ±SEM [mV]	V_2 ±SEM [mV]
WT	0	38±9	26±5
WT	10	-	-
fou2	0	-2±2	2±7
fou2	10	65±9	23±7
ofu8	0	-46±26	-14±5
ouf8	10	65±2	14±2
ouf6	0	147±15	-
ouf8wt	0	42±3	35±2
ouf4	0	29±10	2±4

Picture 1. AtTPC1 in pSat1564 (p51) vector map

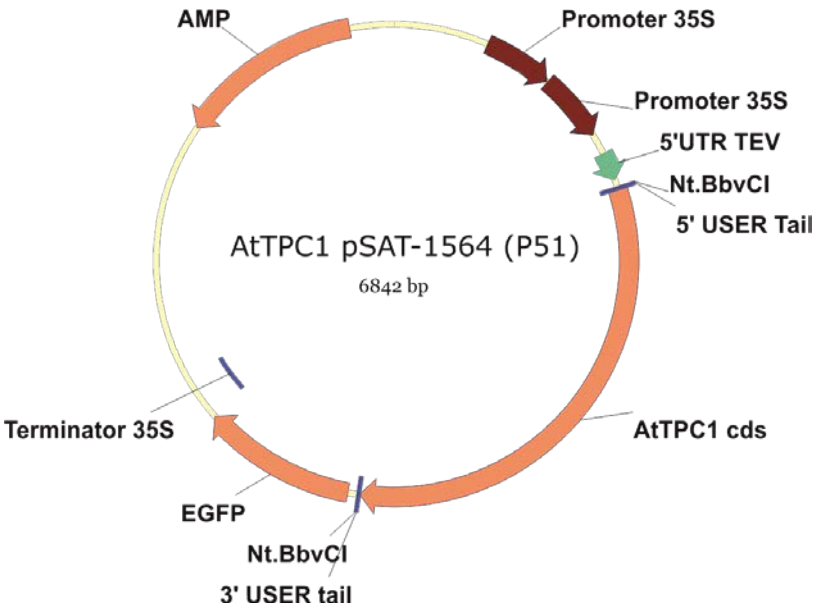

14. Publication list

1) Jaślan, D., Mueller, T., Becker, D., Schultz, J., Cuin, T., Marten, I., Dreyer, I., Schonknecht, G., Hedrich, R. (2016). Gating of the two-pore cation channel AtTPC1 in the plant vacuole is based on a single voltage-sensing domain. *Plant Biol.*, 18(5):750-60.

2) Lenglet*, A., Jaślan*, D., Toyota, M., Mueller, M., Muller, T., Schonknecht, G., Marten I., Gilroy S., Hedrich, R. and Farmer, E. E. (2017). Control of basal jasmonate signalling and defence through modulation of intracellular cation flux capacity. *New Phytologist, [Epub ahead of print]* * equal contribution

15. Acknowledgements

I would like to thanks everyone that supported me and contributed to make this work a success.

Especially, I would like to thank Prof. Dr. Rainer Hedrich for giving me the possibility to perform my dissertation under his guidance. I appreciated the interesting topic and the discussions, which helped me to develop my own scientific ideas.

I would also like to thank Prof. Dr. Erhard Wischmeyer for his interest in my work and evaluation process as a second referee.

Special acknowledgements I would like to send to Prof. Irene Marten for the incredible patience, all the scientific conversations, constructive criticism and never-ending proofreading. Without all these things, writing of this thesis would not have been possible.

Thanks goes out to all my colleagues and all other employees of the Botany I Institute, which have always offered me help and created a pleasant working atmosphere.

Pragnę podziękować moim rodzicom, za trud włożony w moje wychowanie. Bez nich nie byłbym w miejscu, w którym obecnie się znajduję.

Mojemu rodzeństwu: Agnieszce, Mateuszowi oraz Karolowi, dziękuje za pomoc której każdorazowo mi udzielali.

Pragnę podziękować również, najważniejszej dla mnie osobie, a mianowicie mojej żonie Justynie, będącej moim wsparciem, przyjacielem, a zarazem miłością.

16. Affidavit in English and German

I hereby confirm that my thesis entitled **The physiological secret of the TPC1 function - *ouf's* mutants** is the result of my own work. I did not receive any help or support from commercial consultants. All sources and / or materials applied are listed and specified in the thesis.

Furthermore, I confirm that the thesis has not yet been submitted as part of another examination process neither in identical nor in similar form.

…… ……

Place, date Signature (Dawid Jaślan)

Hiermit erkläre ich an Eides statt, die **Das physiologische Geheimnis der TPC1-Funktion - *ouf* Mutanten** Eigenständig, d.h. insbesondere selbstständig und ohne Hilfe eines kommerziellen Promotionsberaters, angefertigt und keine anderen als die von mir angegeben Quellen und Hilfsmittel verwendet zu haben.

Ich erkläre außerdem, dass die Dissertation weder in gleicher noch in ähnlicher Form bereits in einem anderen Pruefungsverfahren vorgelegen hat.

…… …….

Ort, Datum Unterschrift (Dawid Jaślan)